The PHILOSOPHICAL MAGAZINE

FIRST PUBLISHED IN 1798

OL. 46 SEVENTH SERIES No. 372 January 1955

A Journal of Theoretical Experimental and Applied Physics

PRICE 15s. 0d.
Annual Subscription £8 0s. 0d. payable in advance

ED AND PUBLISHED BY TAYLOR & FRANCIS LTD., RED LION COURT, FLEET ST., LONDON, E.C.4.

THE
PHILOSOPHICAL MAGAZINE
A JOURNAL OF THEORETICAL EXPERIMENTAL AND APPLIED PHYSICS
First published in 1798
[SEVENTH SERIES—VOL. 46]

I. *The Distribution of the Products of Heavy Ion Reactions with Aluminium*

By G. A. Chackett, K. F. Chackett and J. H. Fremlin
University of Birmingham *

[Received August 21, 1954]

Abstract

The distribution in depth of the radioactive products of heavy ion bombardments of aluminium has been studied by stacked foil techniques. The bombardments were mainly done with $^{14}N^{6+}$ ions of energies up to 125 Mev but a few were done with $^{16}O^{6+}$ ions. Some products were estimated from gross decay curves and some by radiochemical analysis. The results show that the products fall into two groups : ^{24}Na together with heavier nuclei on the one hand, and ^{18}F together with lighter nuclei on the other. In discussion it is shown that this can readily be explained if most products are derived from interaction of parts only of the nuclei concerned, in a way analogous to stripping reactions, rather than from breakdown of a compound nucleus.

§ 1. Introduction

In a previous paper (Chackett and Fremlin 1954) some experimental work was described on the production of ^{13}N when aluminium was bombarded by ^{14}N ions accelerated in the Birmingham cyclotron. It was shown that the greatest ^{13}N activity occurred 60 microns from the surface of a thick target, indicating that the ^{13}N nuclei produced retained a large part of the initial forward momentum of the ^{14}N ions. This result was consistent with the formation of ^{13}N by loss of a neutron to the ^{27}Al in a relatively weak interaction.

* Communicated by the Authors.

It was believed that a similar investigation of the distribution in depth in the target of other reaction products would give useful information as to their mode of formation and in this paper we present the main results of such an investigation.

§ 2. General Method of Experiment

In all experiments, stacks of aluminium foil were bombarded by the internal beam of the cyclotron at the radius at which the maximum beam of ions with energies over about 50 Mev was obtained. For ^{14}N ions this radius was 63·5 cm and for ^{16}O it was 60 cm. The target used, and the method of carrying out bombardments, have already been described (Chackett, Fremlin and Walker 1954, Chackett and Fremlin 1954). Since the earlier work the internal beams have been considerably improved, and measurable activities of the main products were observed down to a depth of 120 μ in the target, with a beam current of about 0·03 μA.

Concurrently with the present work, the cyclotron was often engaged in the production of very large activities by deuteron bombardment. Consequently there was a serious risk of irrelevant activities being picked up by the stack of foils and, to prevent contamination, a 5 μ thick aluminium foil was always used to cover the main stack. This ' cover foil ' was discarded when there was any risk of confusion.

The foils were separated immediately after bombardment, some being used for chemical separation of the isotope to be investigated, the activity of the rest being determined as a measure of the total effective bombardment. The strength of the bombardment could not be derived accurately from a current measurement as the total thickness of the stacks varied. Also small changes in the energy spectrum of the bombarding ions would give large relative changes in residual current traversing the whole stack. Relative bombardment intensities were therefore determined by measuring the ^{32}P activity of the otherwise unused foils after all other observable activities had decayed, and comparing these with the activity given by a standard bombardment. Comparisons of the ^{32}P activity were nearly always accurate to better than 25% and sometimes better than 10%. In all cases activities were observed with end-window Geiger counters, usually with a 7 mg/cm^2 window (G.M. 4).

§ 3. Energy Distribution of the Beams

Owing to the complex mechanism of acceleration of multiply-charged heavy ions (Walker, Fremlin, Link and Stephens 1954) the energy of the internal beam is not well defined as it is for deuterons.

This makes interpretation of the results of the experiment to be described much more difficult but there is at present no way of avoiding the difficulty. An extracted beam has been obtained, but since it has not yet been possible to ' shim ' the cyclotron appropriately for heavy ions, it is too small for radioactivation.

The distribution of energy in the ^{14}N beam at a radius of 63·5 cm under normal bombardment conditions was obtained as follows. The usual foil stack on the internal target was replaced by a thin platinum foil (2 mg/cm^2) and 12 mm behind this, on the usual current collector, was placed an Ilford C2 nuclear emulsion. This was so arranged as to receive, at a small angle to its surface, ^{14}N ions scattered elastically from the platinum foil together with any reaction products (mainly protons). The ^{14}N tracks in the developed plate were readily distinguishable by their appearance, and a range-histogram constructed for about 600 tracks at a scattering angle of about 40°. The range–energy relation is not accurately known but can be estimated well enough* for the present purpose and hence an energy-histogram can be obtained. For deflection at this angle from platinum, the Rutherford scattering law should be obeyed up to energies well beyond the potential barrier, viz. 80 MeV (lab. system); up to about 100 MeV therefore the scattering probability for the given angle must vary as $1/E^2$ where E is the energy of the nitrogen nucleus. The numbers obtained in the energy-histogram must then be multiplied by E^2 to give the distribution of energy in the original beam. The appropriate small allowance for loss of energy in the platinum has also been made, giving finally the range-distribution shown in fig. 1.

Fig. 1

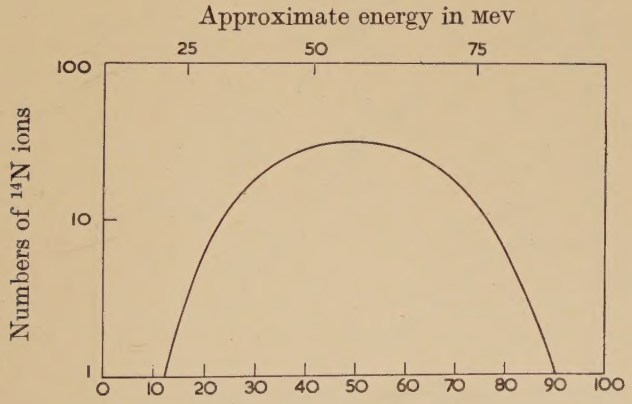

Range distribution of $^{14}N^{6+}$ ions in aluminium.

At this radius the highest energy to be expected is in the region of 125 MeV, but it can be seen that there is a maximum in the distribution at a little less than half this value. This is consistent with the measurements made here earlier with an internal crystal detector (Walker *et al.* 1954) although little of the latter work was done under the same operating conditions of the cyclotron. (In particular we have used somewhat higher gas pressures in the vacuum tank.) In considering the further results described below, it must of course be remembered that only 2/3 of the particle energy will be 'available' for reactions with aluminium.

* We are most grateful to Dr. D. Walker for the range–energy relation used.

§ 4. Results of Bombardments

The distribution of yield of each of the reaction products from ^{14}N bombardments which could be examined is shown in figs. 2 (*a*) and 2 (*b*). The products in fig. 2 (*a*) (' heavy ' products) comprise those of mass 24 to 38, those in fig. 2 (*b*) (' light ' products) of mass 11 to 18.

In all cases the yields are given in terms of number of detectable atoms of each isotope actually coming to rest at in each 10 μ of aluminium at the depth concerned. The yields are normalized to a fixed yield of ^{32}P found in the first 80 μ of the target below the 5 μ cover foil. Some of the results, namely those from ^{32}P, ^{28}Al and the rather sketchy results for ^{15}O (the production of which in this way is reported here for the first time) were obtained entirely from analysis of the decay curves of different foils,

Fig. 2 (*a*)

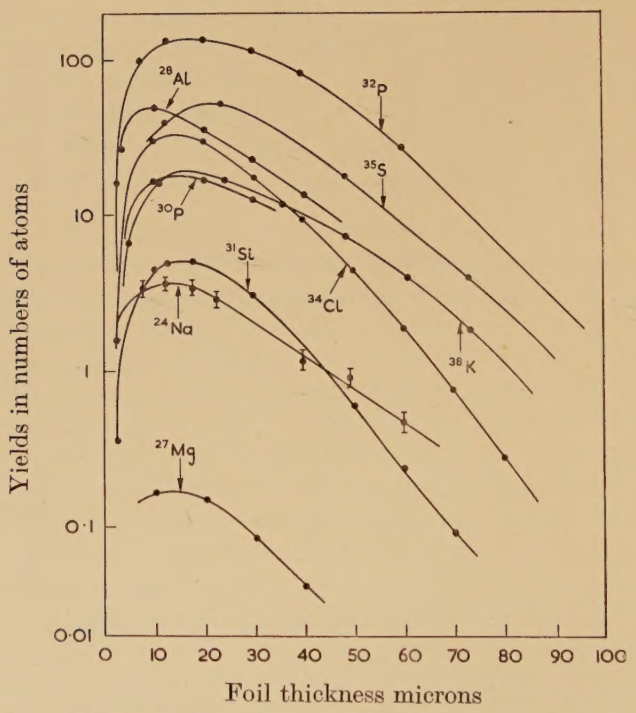

Distribution of ' heavy ' products of $^{14}N^{6+}$ bombardment of aluminium. Random errors were significant only in the case of ^{24}Na. The accuracy of normalization is usually better than 25%.

using an elementary charge-discriminator when necessary. The results for ^{35}S depend on differential counting using an end-window counter (window thickness 2 mg/cm^2) and a 4π-geometry windowless counter. The majority, however, were obtained by chemical separation of the isotopes concerned. In all cases they are averaged from two or more experiments, the ^{32}P and ^{34}Cl curves being obtained by averaging results from a dozen or more experiments.

Most of the chemical methods used have already been described (Chackett, Fremlin and Walker 1954, Chackett and Fremlin 1954). In one or two cases, however, some improvements to the earlier methods have been made. Thus, taking the elements in order of increasing Z, the following modifications were introduced :

(i) Carbon (^{11}C). The bombarded foils were dissolved in sodium hydroxide solution in a small reaction vessel through which passed a slow stream of air saturated at room temperature with ethanol vapour. The gas stream was roughly dried by bubbling through concentrated sulphuric acid and was then passed over copper oxide at 600°c. In this way the ^{11}C originally present in the foils was converted in the gas stream to $^{11}CO_2$ in the presence of a suitable quantity of CO_2 derived from the ethanol.

Fig. 2 (*b*)

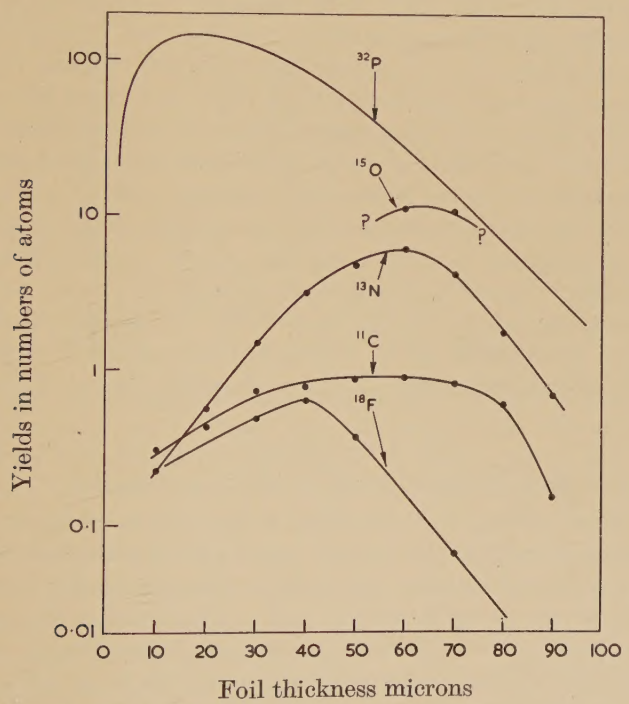

Distribution of ' light ' products of $^{14}N^{6+}$ bombardment of aluminium. N.b.

(i) The curve for ^{32}P is included for comparison.

(ii) Only two points for ^{15}O are included ; this isotope could not be detected with certainty in the range 0–50 μ and was not looked for beyond 70 μ. The errors of normalization in this isotope are large.

The gas was then bubbled through two centrifuge cones containing sodium hydroxide solution, which absorbed all the carbon dioxide. These cones were then detached from the apparatus and barium carbonate precipitated by addition of barium hydroxide. The barium carbonate was washed, mounted, and counted under an end window G.M. counters in the usual way.

It carried the ^{11}C activity practically quantitatively and completely free from all other activities.

(ii) Fluorine (^{18}F). The method used previously for this isotope was to dissolve the aluminium foils in sodium hydroxide solution containing suitable carriers, then to remove the aluminium as the hydroxide by adjustment of the pH, and finally to precipitate the required activity, with carrier, as calcium fluoride. This method is not very satisfactory as much of the activity is lost on the aluminium hydroxide. It was found preferable to add finely divided silica to the solution (with carriers), acidify with perchloric acid, and distill off the fluorine as silicon tetrafluoride. The latter was trapped in cold water, the silicon removed by precipitation as silica by boiling with ammonium carbonate and the fluorine finally isolated as calcium fluoride or as lead chlorofluoride.

(iii) Sodium (^{24}Na). The foils were dissolved in hydrochloric acid containing suitable carriers and sodium chloride was precipitated by addition of butanol saturated with hydrogen chloride. It was necessary to decontaminate the sodium chloride from other activities by repeated solution in a little hot water and precipitation by concentrated hydrochloric acid at 0°C. At least six recrystallizations were performed.

The activities induced by the bombardments were sufficient for a single operator to carry out chemical separations on six foils simultaneously for each element investigated having a half-life greater than half an hour. In the case of ^{27}Mg, ^{30}P and ^{38}K it was rarely possible to process more than two samples simultaneously ; in the case of ^{11}C the assistance of Mr. G. Clewes and Miss B. Hillman made it possible to make four separations from a single bombardment using the same apparatus for all of them.

§ 5. Discussion

5.1. *Relative Total Yields of Different Isotopes*

We are now in a position to extend and amend the yield figures for the nitrogen reactions given in our earlier paper (Chackett *et al.* 1954), to take account of total yield rather than yield in the upper foils of the target only. The figures are given in table 1 and are believed to be correct to 25% for our standard conditions. Some particular ratios, such as $^{30}P/^{32}P$ or $^{38}K/^{34}Cl$ are much better than this but there is no advantage at present in distinguishing these in view of the arbitrary nature of the conditions determining the original ^{14}N energy-spectrum.

The figures given are little changed apart from ^{32}P, ^{30}P and ^{35}S which are all higher than had been thought before, because of the relatively greater yield of these isotopes in the lower foils and in the case of ^{35}S, because of much more accurate counting. The preponderance of the neutron-excess isotopes is now even more striking. To explain this feature of the relative yields, we suggested that in many cases only part of the bombarding ion was captured by the target nucleus. The ^{14}N nucleus could then be regarded as a group of quasi-independent particles any or all of which could be involved in reactions. On this ' buckshot ' hypothesis, the distribution of

yields could be readily understood since a neutron would easily be captured, an alpha particle less easily and a single proton least easily owing to the considerable Coulomb barrier.

A feature of importance in this process is that particles would be captured from a bound state to another bound state of very similar energy. There would therefore, be little excitation of the compound nucleus produced, apart from the energy acquired from the kinetic energy of the original ^{14}N. Hence it was shown that for the probable range of energies involved, there would usually be not more than one secondary heavy particle ejected for initial compound nuclei up to perhaps ^{36}Cl.

Table 1. Relative Yields (in numbers of atoms) of Products of ^{14}N Bombardments of Aluminium

Isotope	Present work	Previous estimate (Chackett *et al.* 1954)
^{32}P	500	300
^{35}S	150	25
^{28}Al	140	140
^{34}Cl	100 (standard)	100
^{38}K	75	75
^{30}P	60	25
^{13}N	20	?
^{31}Si	14	15
^{24}Na	11	12
^{11}C	5	?
^{18}F	20	?
^{27}Mg	0·5	Small (<10)

Our new data suggest strongly that for the nuclei near ^{27}Al itself, not even one heavy particle has been emitted. Thus, we would expect ^{28}Al formed by the simple ' stripping ' of a neutron from ^{14}N, to be a very probable product which indeed it is. The yield of ^{27}Mg is barely one third of one per cent of ^{28}Al and though loss of a neutron would doubtless be more probable from an excited state of ^{28}Al than loss of a proton, the difference of excitation for evaporation of these particles required is small and it is not easy to believe that so little ^{27}Mg would be found if much of the ^{28}Al first formed were to break down. The higher yield of ^{24}Na (compared with ^{27}Mg) shows even more conclusively that most of this has not been derived from ^{28}Al as an intermediate stage, since an alpha particle requires more energy and faces a higher potential barrier than does a proton when leaving ^{28}Al. The production of ^{24}Na thus requires some other process. We postulate one in which the ^{14}N abstracts nucleons, i.e. two protons and one neutron, from the ^{27}Al. Such a process would not appear inherently very likely, but it may be helpful to regard it as an interchange of a neutron and an alpha particle. Stated in this way it becomes a simple extension of the ' buckshot ' principle.

We shall now go on to consider what can be learnt from the shapes of the distribution curves of figs. 2 (*a*) and 2 (*b*). Since the energy distribution of the beam is continuous, as shown in fig. 1, these shapes do not represent

the excitation functions of the various products. They depend on these in part but are mainly determined by the other factors considered below.

5.2. *Distribution of the Heavier Products, from* ^{24}Na *to* ^{38}K

A striking feature of the distribution of these products is the rapid rise in yield, by a factor of the order 10, on passing from the cover foil to a maximum occurring at a depth usually between 10 μ and 20 μ from the surface. (In figs. 2 (*a*) and 2 (*b*) we have plotted the relative yields at depths corresponding to the middle of the foils, although this involves slight inaccuracy when the yields are changing rapidly with depth.) This initial rapid rise is clearly connected with the recoil of active products following the impact of the ^{14}N ion. The depth in the target of the maximum is of course determined in part by the recoil, but other factors appear to come into play and it is not easy to find convincing correlations between the depths of the maxima and, say, the mass number of the products.

The next property of the curves to be discussed is their rate of fall-off in the deeper parts of the foil stack. In an earlier paper it was stated that the proportions of the different products varied by less than a factor of two at different depths. After the first 5 μ, which was not then examined, this is indeed true down to at least 40 μ. In the earlier work the ^{14}N beam was not intense enough to give useful activities much below this depth. It is now clear, however, that there is a real change in the relative yields in the deeper foils. The final slope of the curves is unfortunately rather sensitive to the initial spectrum of ^{14}N energies, which, as has been noted, varies somewhat from one bombardment to another. It is therefore unprofitable to attempt a quantitative discussion of minor differences observed. Some important general observations may however be made.

Firstly, the curves show similarity in that they all approach asymptotically to an exponential decrease. This is presumably connected with the fact that the range-spectrum of the incident ^{14}N beam also shows a roughly exponential fall-off at the greatest ranges ; however, recoil phenomena will again come into play here. Secondly, the rate of fall-off is not always the same. We may note in this connection that, had the products all been derived by particle evaporation from the compound nucleus ^{41}Ca, we should reasonably expect a bias in favour of the lighter products in the upper foils, since there more reactions can occur in which energy is available to cause evaporation of the many particles needed. But in fact the curves tend to show the opposite bias ; thus those for ^{24}Na, ^{27}Mg, ^{28}Al and ^{32}P fall off less steeply than that for ^{34}Cl. It is true that the fall-off for ^{38}K is even less steep than the others, but in this case it is clear that ^{38}K must be formed by the fusion of the ^{27}Al with nearly all, if not quite all, of the ^{14}N with subsequent particle evaporation. In either case it is therefore to be expected that an appreciable fraction of ^{38}K nuclei formed in the early foils will still have sufficient excitation to evaporate an alpha particle. This process will diminish the ^{38}K yield in this region and contribute to the ^{34}Cl yield. The third observation we can make is that the

curves do not approach the exponential fall-off at equal rates. The remarks above give an immediate explanation of why the ^{34}Cl curve should so quickly approach its asymptote (due to enhanced yields in say the first 40 μ) while the ^{38}K curve should do so slowly.

The enhanced ^{34}Cl yields at the expense of ^{38}K is in effect a competition phenomenon rather analogous to the well-known case of excitation functions of processes such as (α, n), (α, 2n) etc. As a test of the purely 'evaporation' model one would like to search for convincing cases of competition between processes leading to the lighter products. Such effects are however not at all obvious, although this might be because so many isotopes happen to be unobservable. Finally we notice that the ^{28}Al curve approaches its asymptote most rapidly of all. This fits very well with the supposition that ^{28}Al is formed simply by a neutron exchange, or stripping reaction, in which there is very little recoil in any direction.

5.3. *Distribution of the Light Products*

In our previous paper (Chackett and Fremlin 1954) we concluded that the ^{13}N ions must be produced by a 'stripping' process rather than by evaporation or fission. The evidence for this view was that the ^{13}N atoms are observed in greatest yield at a considerable depth (about 60 μ) in the foil stack, showing a very strong forward displacement from the site of formation. It is now clear from fig. 2 (*b*) that the mean forward range of the ^{13}N atoms is even greater than that of the ^{14}N ions from which they are derived. This can only mean that nearly all the product ^{13}N nuclei must be projected in a very narrow cone. Since on kinematical grounds one would not expect such a strongly peaked angular distribution for incident ^{14}N ions of low energy, it is probable that the cross section for the ^{13}N production rises fairly sharply with energy. In classical terms this is to say that the odd neutron in the ^{14}N can most easily be removed, without disrupting the residual light nucleus, in a high-velocity glancing collision. The other nucleus so formed will of course be ^{28}Al, and this will have very little recoil. In this connection it should be remembered that ^{28}Al is formed far more abundantly than is ^{13}N. It is therefore likely that the bulk of the ^{28}Al corresponds to interactions of the ^{14}N with the ^{27}Al, in which ^{13}N as first formed is sufficiently excited to undergo break-down to lighter nuclei and so escape detection. It is nevertheless still true since only a neutron is transferred from one nucleus to the other, that the ^{28}Al suffers only a slight recoil in the direction of the beam. In the cases where the ^{14}N and ^{27}Al nuclei undergo still closer interactions, involving a larger transfer of momentum, the predominant reactions will be those leading to other products.

The distribution curve for ^{11}C is noticeably broader than that for ^{13}N. This may be interpreted as indicating a larger interaction energy in its production, which would lead to a wider angular distribution and hence to a greater variability of penetration for any given energy of the bombarding nucleus. Nevertheless the interaction energy must still be fairly small

even though three nucleons are removed from the ^{14}N. The somewhat similar curve for ^{18}F also implies a reaction mechanism involving only a moderate interaction energy ; here the ^{14}N nucleus is evidently picking up nucleons. Some momentum will be carried by the remaining part of the ^{27}Al nucleus, but even if none were carried thus the velocity of the ^{18}F nucleus would be only 14/18 of that of the incident ^{14}N, so that an earlier maximum in the distribution is naturally expected. Also it seems likely that the ^{18}F ions have higher average state of ionization that the ^{14}N, so that even for a given initial velocity their ranges would be less. Little can be said as regards the ^{15}O. This isotope is formed in too small a yield in the upper foils to enable us to distinguish it from other short lived products. It is however the principal product of those with half-lives of the order 2–3 minutes at depths of 60–70 μ. There can be no doubt therefore that ^{15}O also fits well into this group of products as regards its depth distribution and hence mode of formation.

To conclude this section we should like to mention a few exploratory experiments on the distribution of products from ^{16}O bombardments of aluminium. While there is some difficulty in correlating the results in detail which is probably connected with the lack of reproducibility of operating conditions of the cyclotron, the same general features are observed. Thus ^{13}N and ^{18}F show strong forward displacements indicative of formation by a stripping or a pick-up process ; the main heavier products (^{30}P, ^{34}Cl, ^{38}K) show distributions which are qualitatively similar to those found in the ^{14}N bombardments.

§ 6. Conclusion

The results clearly show that there are two main groups of products from ^{14}N bombardments of ^{27}Al. These comprise a light group (^{11}C, ^{13}N, ^{15}O and ^{18}F) which are formed in small yield by ' stripping ' or ' pick-up ' processes, and a heavy group (^{24}Na, ^{27}Mg, ^{28}Al, ^{30}P, ^{31}Si, ^{32}P, ^{34}Cl, ^{38}K) mostly formed in much higher yield by the absorption by the ^{27}Al of part, or all, of the incident ^{14}N ions. Similar results are obtained with ^{16}O bombardments.

Although they are not discussed in previous sections, we should like to add the following comments.

(*a*) The isotopes of Ca and Sc which might be produced by ^{14}N and ^{16}O bombardments of Al are not detectable by our techniques.

(*b*) Many reactions will give rise to stable, as opposed to radioactive, products.

(*c*) The lower relative yield of the ' light group ', ^{11}C, ^{13}N, ^{15}O and ^{18}F may be due in part to the fact that, with quite moderate excitations they may split up into stable fragments.

(*d*) The absolute yield of the products is not known accurately ; the total observable reaction cross section is a few per cent of the geometrical cross section.

(*e*) The reactions (^{14}N, xn) and (^{16}O, xn) which are so well known with the heavier elements, might be invoked as an alternative mechanism for the production of say ^{38}K, regarded as the daughter of a short lived ^{38}Ca. But the value of x becomes impossible large for the production of even ^{34}Cl from ^{34}Ca let alone ^{30}P and ^{18}F, and of course this mechanism cannot contribute to the production of any neutron-excess product.

Acknowledgments

We are indebted to many members of the laboratory for discussions, and to Mrs. J. Jeffries and Mrs. J. Mathieson for much of the counting and photographic work. It is a particular pleasure to acknowledge the very careful work of Mme Jeannine Olkowsky at the Centre d'Etudes Nucleaires de Saclay who counted the ^{35}S in a 4π windowless counter.

References

Chackett, K. F., and Fremlin, J. H., 1954, *Phil. Mag.*, **45**, 735.
Chackett, K. F., Fremlin, J. H., and Walker, D., 1954, *Phil. Mag.*, **45**, 173.
Walker, D., Fremlin, J. H., Link, W. T., and Stephens, K. G., 1954, *Brit. J. Appl. Phys.*, **5**, 157.

II. *Inelastic Neutron Scattering in Manganese*

By Joan M. Freeman
Atomic Energy Research Establishment, Harwell*

[Received August 20, 1954]

Summary

Gamma-rays of energies 126, 853 and 980 kev have been observed following inelastic neutron scattering in ^{55}Mn, with neutron bombarding energies up to 1·3 Mev. The evidence indicates levels in ^{55}Mn at 126 ± 3 kev and 979 ± 8 kev, the second level decaying mainly ($\sim95\%$) by cascade through the lower level.

In order to study low excited states of ^{55}Mn the gamma rays following inelastic neutron scattering in ^{55}Mn have been examined, with both stilbene and sodium iodide crystal detectors, for neutron bombarding energies up to 1·3 Mev. Manganese chips (1050 g) were enclosed in a thin cardboard container of annular form placed to receive neutrons emitted from the T (pn) reaction at a mean angle of 7·4° to the proton beam direction. The crystal detector was situated at the centre of the ring, on the axis defined by the proton beam, so that it recorded γ-rays emitted from the manganese at a mean angle of about 83° to the neutron flux direction. The detector was shielded from direct neutrons by a polythene cone. Calibrated BF_3 counters were used to measure the neutron flux.

At each neutron bombarding energy the pulse-height distribution from the crysta was recorded on a thirty-channel kicksorter, first with the manganese ring in position and then with it removed. The two distributions were then subtracted to give the difference spectrum due to reactions in the manganese. Full details of the experimental method will be presented in another paper (Freeman, Lane and Rose 1955).

The reaction was first examined with a 1 in. cube stilbene crystal and, for neutron energies greater than 1 Mev, Compton spectra corresponding to γ-rays of energy about 850 kev were observed. Since iron is known to give γ-rays of about this energy, following inelastic scattering (see, for example, Rose and Freeman 1953, Kiehn and Goodman 1954) and might possibly have caused the observed γ-rays, the spectra due to an iron scatterer were measured at the same time. Examples of the difference spectra obtained for the two scatterers with 1·05 Mev neutrons are given in the inset of fig. 1, together with a calibration spectrum due to ^{137}Cs (662 kev). A small difference in energy for the two γ-rays was established. The Cs source and a ^{60}Co source (1·17 and 1·33 Mev) were used for absolute γ-ray energy calibration. The averages of a number of runs gave the

---

* Communicated by the Author.

results : 848±15 kev for the γ-rays from ^{55}Mn and 833±10 kev for the γ-rays from ^{56}Fe.

The relative γ-ray yields at different neutron energies were obtained from the Compton spectra after corrections had been applied for the elastically scattered neutrons (which produce the steep rise below the Compton peak in fig. 1, inset), and for the backgrounds due to harder γ-rays. The resulting excitation functions for Mn and Fe are shown in fig. 1. The curve for iron is similar to that obtained by Kiehn and Goodman (1954). The curve for manganese shows a threshold just below 1 Mev, indicating a level in ^{55}Mn at about 980±20 kev and showing that the 848 kev γ-rays arise from a cascade process through a lower level. The absolute cross section values given in the figure were obtained by calculating the crystal efficiency for the detection of 840 kev γ-rays from each scatterer, the calculation being based on absolute measurements

Fig. 1

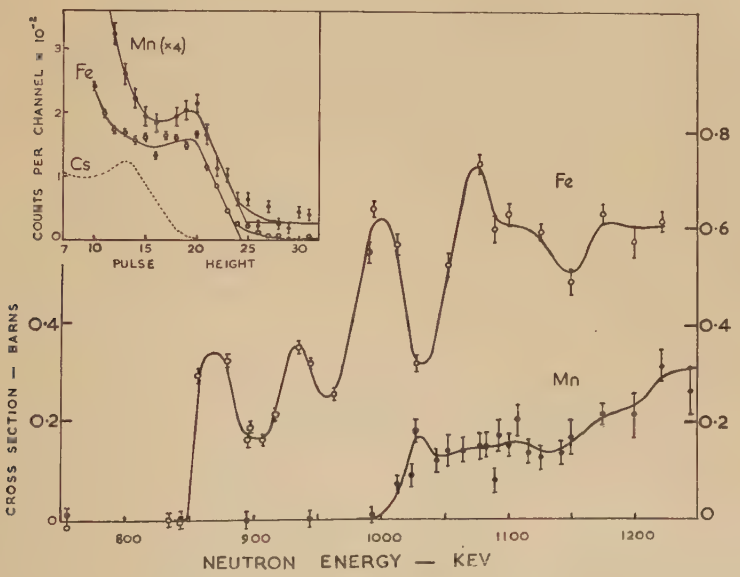

Relative yields of γ-rays of energies 848 and 833 kev from ^{55}Mn and ^{56}Fe respectively (neutron energy spread 20 kev).
Inset : The spectra obtained with a stilbene crystal for Mn, Fe and Cs.

made previously with a standard ^{7}Be (478 kev) source (see Freeman *et al.* 1955). An assumption of isotropy of the γ-rays (observed at ~90°) was made. The standard deviation of the absolute cross section scale is ±40%.

The investigation of manganese was continued with a sodium iodide crystal ($1\frac{1}{2}$ in. diameter by 1 in.). For neutron energies above the 1 Mev threshold, 850 kev γ-rays were again observed (see further discussion below) and 126 kev γ-rays were also detected. The latter group was still present when the neutron energy was reduced below the threshold for the

850 kev γ-rays, showing that in the cascade transition the 850 kev γ-rays must precede the 126 kev γ-rays. A typical 126 kev spectrum, obtained with 900 kev neutrons by subtracting the pulse-height distributions with and without the manganese ring in position, is given in fig. 2, together with calibration peaks due to americium and indium (γ-rays 59·8 and 191 kev respectively, from Hollander *et al.* (1953)).

The γ-ray measurements are summarized in the table, and indicate levels in ^{55}Mn at 126$\pm$3 kev and 979$\pm$8 kev. These results are in agreement with the observations of Hausman *et al.* (1952), who detected inelastic

Fig. 2

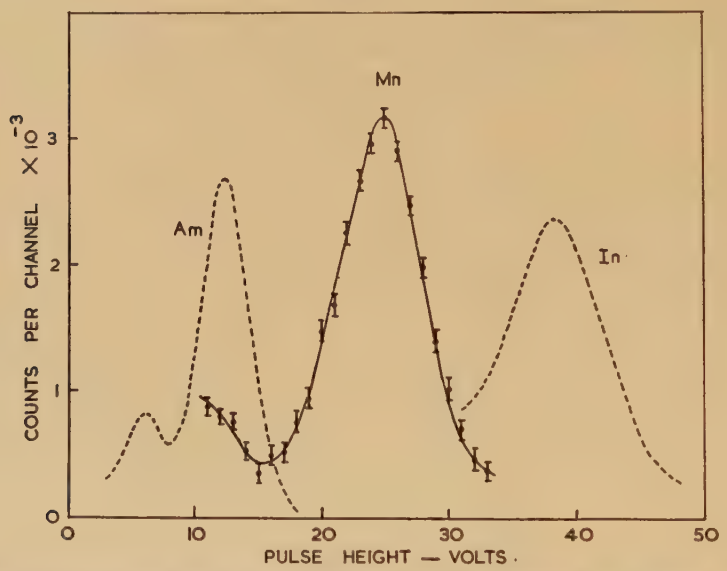

Sodium iodide pulse-height distributions due to γ-rays from ^{55}Mn (nn′) at a neutron energy of 900 kev, and from Am and In.

	Observed gamma rays			Nuclear levels
	Stilbene kev	NaI kev	Mean kev	kev
^{55}Mn	848$\pm$15	126$\pm$3 854$\pm$8 ~980	126$\pm$3 853$\pm$7	126$\pm$3 979$\pm$8
^{56}Fe	833$\pm$10	843$\pm$5	841$\pm$5	841$\pm$5

proton scattering to a 130 kev level and to a 1·0 Mev level, and of Temmer and Heydenburg (1954) who observed 128 kev γ-rays from manganese as a result of Coulomb excitation.

The γ-ray spectrum from manganese for γ-rays in the energy region 850 to 1000 kev, with neutron energies from 1·1 to 1·3 kev, was studied with the sodium iodide crystal in a search for the ground state transition from the second (979 kev) level. For this purpose pulse-height distributions were obtained with manganese, iron and graphite scatterers. The latter was chosen because carbon is known to give no γ-rays from inelastic scattering at the neutron energies used, so that the pulse height distribution with this scatterer represented the background due to γ-emitting processes in the sodium iodide crystal, produced by scattered neutrons. The counting rate at the 850 kev peak in the manganese distribution was about twice the rate at the same pulse height with carbon, and for iron the

Fig. 3

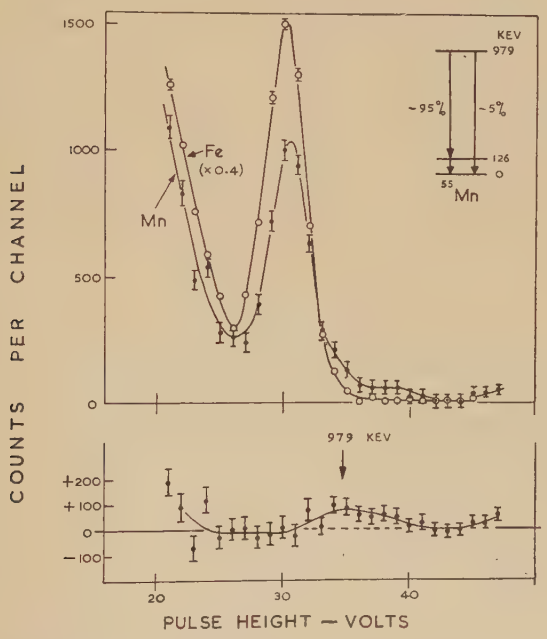

Average pulse-height distributions with a NaI crystal. Upper curves: Mn and Fe spectra showing peaks at 854 and 843 kev; lower curve: difference after fitting peaks.

ratio was about five. At pulse heights a little above that corresponding to 1 MeV in energy the rates in all three distributions were approximately the same. The carbon distribution was fitted to the manganese distribution by normalizing to the same average number of counts in the top channels (above 1 MeV) and was then subtracted from it to give the difference spectrum due to manganese γ-rays. The iron difference spectrum was obtained in the same way. The average results for three sets of runs are given by the upper curves in fig. 3. The peaks correspond, by reference to ^{137}Cs and ^{60}Co sources, to γ-ray energies of 854 ± 8 kev for

Mn and 843±5 kev for Fe. The manganese spectrum shows some sign of a small higher energy component. To analyse this the Fe spectrum was normalized by the appropriate pulse-height and intensity factors so that its peak fitted the main Mn peak, and the two distributions were then subtracted. The result is shown by the lower curve in fig. 3. It can be seen that a small peak occurs at the position expected for 979 kev γ-rays. The rate for coincident absorption of both 853 and 126 kev γ-rays in the crystal was calculated from the crystal efficiency for 126 kev γ-rays and was found to account for not more than 20% of the observed 979 kev peak. From this result and the relative peak intensities we conclude that the relative probability of emission of 853 and 979 kev γ-rays from the 979 kev level in Mn is about 20 : 1.

The work of Temmer and Heydenburg (1954) on Coulomb excitation of the first excited state (126 kev) of manganese demonstrates E_2 excitation and therefore the same parity for both the ground and 126 kev states. This result shows that the two competing γ-rays from the second (979 kev) level must have the same parity ; the observed preference for the cascade transition then indicates that the order of multipolarity of the 979 kev γ-ray is one unit higher than that of the 853 kev γ-ray.

I am grateful to Mr. B. Rose for valuable suggestions and criticisms during the course of this work.

References

Freeman, J. M., Lane, A. M., and Rose, B., 1955, *Phil. Mag.* (in the press).
Hausman, H. J., Allen, A. J., Arthur, J. S., Bender, R. S., and McDole, C. J., 1952, *Phys. Rev.*, **88**, 1296.
Hollander, J. M., Perlman, I., and Seaborg, G. T., 1953, *Rev. Mod. Phys.*, **25**, 469.
Kiehn, R. M., and Goodman, C., 1954, *Phys. Rev.*, **93**, 177.
Rose, B., and Freeman, J. M., 1953, *Proc. Phys. Soc.* A, **66**, 120.
Temmer, G. M., and Heydenburg, N. P., 1954, *Phys. Rev.*, **93**, 351 and *International Conference*, Glasgow.

III. *Inelastic Neutron Scattering in Lithium Seven*

By Joan M. Freeman, A. M. Lane and B. Rose
Atomic Energy Research Establishment, Harwell†

[Received August 25, 1954]

Abstract

The cross section for the reaction ^{7}Li(n n′)^{7}Li*, in which the residual nucleus is left in its first excited state (478 kev), has been measured as a function of neutron bombarding energy from the threshold up to 1·65 Mev. The reaction was studied by observation, with both stilbene and sodium iodide crystal detectors, of the γ-rays from the ^{7}Li*. Details of the experimental method are given. The shape of the excitation curve for the reaction immediately above threshold indicates a strong s-wave contribution due to a (1−) level in the ^{8}Li compound nucleus. Above this region the curve rises to a peak at a neutron energy of about 1·35 Mev, corresponding to a ^{8}Li level at 3·2 Mev ($\Gamma \simeq 1$ Mev), which can be interpreted in terms of theoretical models as either a (1+) or, possibly, a (1−) state.

§ 1. Introduction

A reaction of the type (n n′), in which the bombarded nucleus is left in an excited state after the emission of a neutron of energy lower than the bombarding energy, is generally studied by observation either of the inelastically scattered neutron or of the gamma-ray subsequently emitted as the residual nucleus reverts to the ground state (see, for example, Poole (1953), Kiehn and Goodman (1954), Eliot *et al.* (1954)).

Studies at a fixed neutron bombarding energy give data on the energy levels of the residual nucleus, and cross sections. Additional information can be obtained by varying the neutron energy and measuring the threshold and excitation function for a particular reaction.

The gamma-rays following inelastic scattering are usually observed with a sodium iodide crystal but can also be detected with an organic scintillator (Rose and Freeman (1953)). We have used both types of crystal for the observation of the gamma-rays and have found that the organic phosphor has particular advantages in the measurement of the excitation function and cross section in the neighbourhood of the threshold. A sodium iodide crystal is more useful for higher neutron bombarding energies.

A discussion of the use of the two types of detector will be given in the next section and the experimental details of the study of the reaction ^{7}Li (n n′) ^{7}Li* will then be described.

† Communicated by the Authors.

§ 2. The Choice of the Scintillator for γ-ray Detection

A crystal detector set up to record γ-radiation following inelastic neutron scattering will also receive neutrons scattered elastically and inelastically from the target material. It is therefore necessary to be able to distinguish between pulses in the detector due to the target γ-rays and pulses due to the products of neutron reactions in the crystal. In a sodium iodide crystal good resolution and efficiency are obtained for the γ-ray lines, but the neutrons induce inelastic scattering and capture reactions in the sodium and iodine nuclei, with consequent γ-ray emission. The latter constitutes an appreciable and varying background, so that near the threshold for the reaction under investigation, or whenever the cross section is small, the γ-ray peak due to this reaction may be less intense than the background groups. In this case quantitative estimates and even identifications are difficult. For example, when the reaction ^{7}Li (n n′) ^{7}Li* was studied with a NaI crystal, the 478 kev γ-rays from ^{7}Li* were found to be superimposed on a broad group at about 430 kev, due to inelastic scattering in sodium and iodine (see fig. 7, § 3.3). On this account quantitative yield measurements could not be made near the threshold.

In an organic crystal the γ-rays are detected from the Compton recoils and the main effect of scattered neutrons is the production of proton recoils, although some capture also occurs. The response of organic phosphors to protons is non-linear (Birks 1951), and in the energy region of interest in the study of the lowest excited states of nuclei, the proton recoil pulses due to neutrons are much smaller than the electron recoil pulses due to γ-rays of about the same energy. The γ-ray groups are then easily distinguishable from the scattered neutron groups. As far as the γ-ray background due to neutron capture is concerned, the Compton efficiency of the crystal is greater in the energy range of interest to us than for the unwanted harder γ-rays and this background is found to be small enough to require only a small correction.

The resolution obtainable with γ-ray spectra in an organic crystal, although not as good as that of a good NaI crystal, is better than is perhaps generally realized. Some typical spectra obtained with a one inch cube stilbene crystal and an E.M.I. Type 6260 photomultiplier are shown in fig. 1. The pulse-height distributions were recorded on a thirty-channel kicksorter. Curve A gives the spectrum due to the 1·277 Mev γ-rays from ^{22}Na ; the spectrum shows the characteristic peak, and a well defined end point is obtained by extrapolation of the linear part of the cut-off. Curve B is the distribution due to the 1·171 Mev and 1·331 Mev γ-rays from ^{60}Co. The peaks due to the two γ-rays, which are 13% apart in energy, are almost resolved. The end point corresponds, by reference to the ^{22}Na and other calibration sources, to 1·33 Mev, and if the ^{22}Na spectrum shape is used to subtract away the higher energy component, the residual spectrum (curve C) corresponds to the 1·17 Mev component. Curve D is the spectrum due to the

γ-radiation from the decay of ^{56}Mn, which gives γ-rays of 840 kev, 1·81 Mev and 2·06 Mev in the intensity ratio 10 : 3 : 2. The presence of two lines in the higher energy part of the spectrum is apparent from the change of slope, and the energies of the two components can be fixed by comparison with other calibration spectra.

Recoil proton spectra obtained from monoenergetic neutrons in the same stilbene crystal are shown in fig. 2. Examples for three neutron energies are given ; in each case the energy spread of the neutrons was ~20 kev. The broken curve shows, on the same pulse-height scale,

Fig. 1

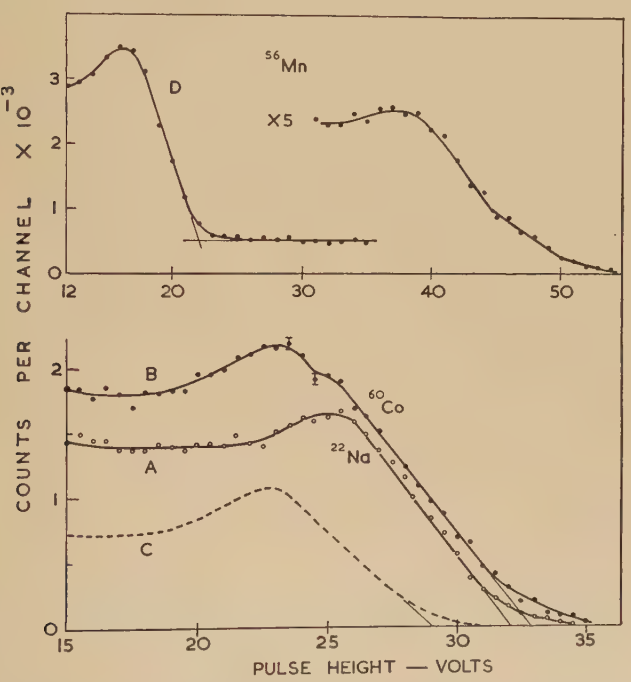

Stilbene spectra due to ^{22}Na (1·277 Mev) (curve A), ^{60}Co (1·33 and 1·17 Mev) (Curve B), ^{60}Co (1·17 Mev component) (curve C), ^{56}Mn (2·06, 1·81 and 0·84 Mev) (curve D).

the spectrum due to the 662 kev γ-rays from ^{137}Cs, and illustrates the difference in response of the crystal to neutrons and γ-rays, as mentioned above.

The stilbene crystal calibration for both γ-rays and neutrons is given in fig. 3, the extrapolated end points of the spectra being plotted against primary energy of the γ-rays and neutrons.

The organic crystal is thus very suitable for measuring the γ-radiation resulting from inelastic neutron scattering for neutron energies in the neighbourhood of the threshold for excitation of a given level. The

method can be extended up to neutron energies for which the spectrum produced by the elastically scattered neutrons begins to overtake the Compton peak of the γ-ray group. If the γ-ray transition takes place directly from the excited level under investigation to the ground state,

Fig. 2

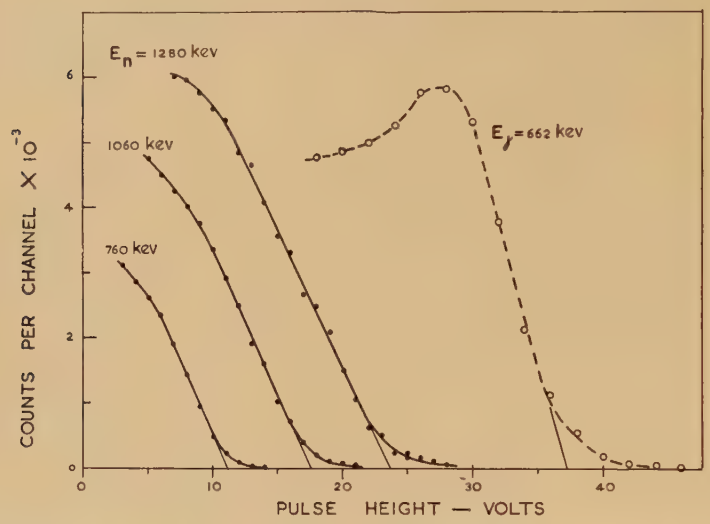

Stilbene crystal spectra for 760, 1060, and 1280 kev neutrons and for ^{137}Cs γ-rays (662 kev).

Fig. 3

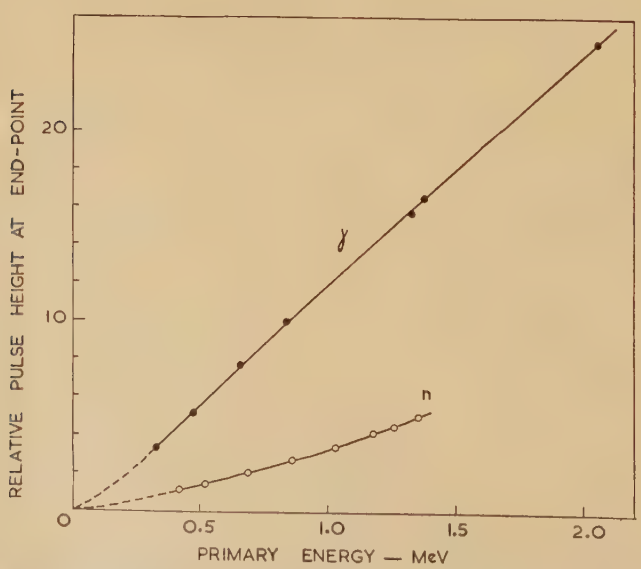

Stilbene crystal calibration for end points of γ-ray and neutron spectra.

it is possible for the reaction to be followed for neutron energies up to somewhat more than twice the threshold energy. If the γ-radiation occurs by cascade through a lower level, the observable range is correspondingly reduced. We have found, as will be described below, that there is adequate overlap between the neutron energy ranges for which the organic and NaI crystal detectors give good quantitative results.

§ 3. The Reaction ^{7}Li (n n′) ^{7}Li*

3.1. *Experimental Method*

The arrangement used for the study of the reaction ^{7}Li (n n′) ^{7}Li* is shown schematically in fig. 4. The source of neutrons was the T (p n) ^{3}He reaction produced by protons from the Harwell Van de Graaff machine bombarding a zirconium tritide target ($\sim 200\,\mu g/cm^2$ of Zr).

Fig. 4

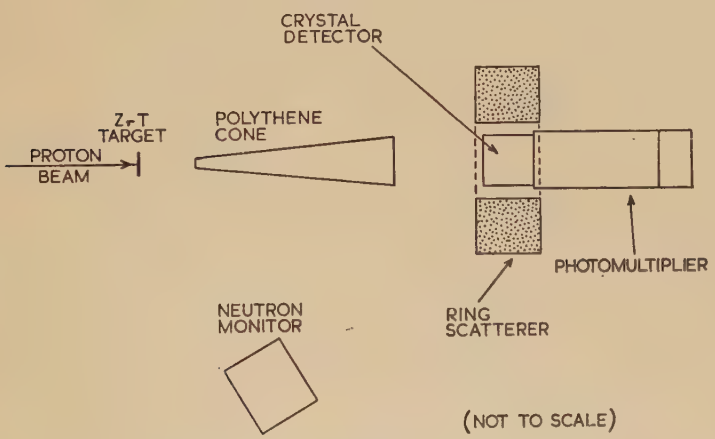

Experimental arrangement (schematic).

The lithium metal scatterer, which had been cast in a steel container and then removed, dipped in vaseline and wrapped with cellotape, was in the form of an annular ring of outside diameter 11·5 cm, inside diameter 5·6 cm and thickness 4·2 cm. It was placed with its axis in the direction of the proton beam and its centre 33 cm from the target spot so that it received neutrons emitted at a mean angle of 7·4° to the proton beam direction. The 1 in. cube stilbene crystal detector was mounted centrally inside the lithium ring, and a polythene cone 18 cm long set up between the source and the crystal served to shield the latter from neutrons emitted directly from the ZrT target. The energy of neutrons bombarding the lithium ring was calculated by reference to the threshold for the T (p n) reaction (1·02 Mev). The energy spread of the neutrons reaching the ring was 20 kev.

A boron trifluoride long counter embedded in paraffin wax was placed to count neutrons emitted at a mean angle of 60° to the proton beam direction and was used as a monitor throughout the runs ; it was afterwards compared with a second absolutely calibrated BF_3 chamber set up at a mean angle of 7·4° to the proton beam, so that the neutron flux in the lithium ring could be determined.

At each neutron bombarding energy the spectrum of pulses produced in the crystal detector was recorded first with the lithium scatterer in position and secondly with it removed. The difference between the two

Fig. 5

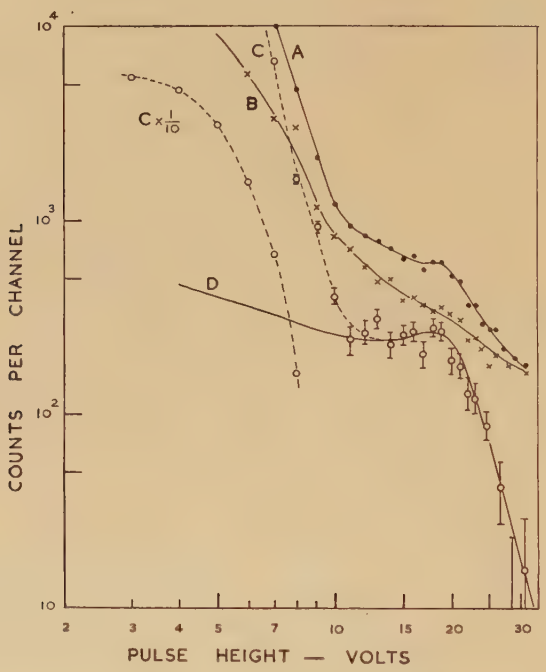

Stilbene crystal spectra with 720 kev neutrons bombarding lithium. Curve A: lithium in ; Curve B : lithium out ; Curve C (points marked o): difference ; Curve D : ^{7}Be spectrum.

spectra, normalized to the same number of neutron monitor counts, then represented the pulse distribution due to processes in the lithium ring. The results of a typical pair of runs for a neutron energy of 720 kev are given as log–log plots in fig. 5. Curves A and B are the pulse distributions obtained with and without the lithium ring respectively and the broken curve C, with points marked as circles, is the difference spectrum. The steeply falling lower energy part of curve C is due mainly to elastically scattered neutrons, and the group at higher energy, showing a Compton peak at a pulse height of about 18·5 volts, is due to 478 kev γ-radiation from the first excited state of ^{7}Li formed in the (n n′) reaction. For

comparison the spectrum obtained with a ^{7}Be source, which also produces γ-rays from the first excited state of ^{7}Li, is shown by the full curve D in fig. 5.

3.2. *The Excitation Function near Threshold*

Some of the difference spectra, obtained at the neutron bombarding energies indicated, are shown in a linear plot in fig. 6. The pulse distribution due to 478 kev γ-radiation, with an end point at 26·5 volts, is evident in the curves taken above the threshold (E_n=546 kev) for the inelastic process. All the curves, including that taken below the threshold, indicate the presence of a small amount of harder γ-radiation.

Fig. 6

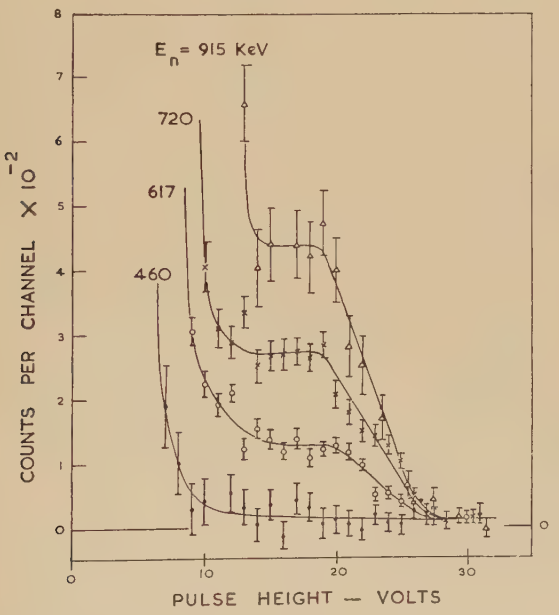

Spectra due to γ-rays from ^{7}Li (n n′) at the neutron energies marked.

This was found, from measurements of the end point, to have an energy of about 2·2 Mev, and was assumed to be due mainly to capture by protons in the stilbene crystal of neutrons scattered from the lithium ring; a small contribution could have been due to slow neutrons from the polythene scatterer being captured by ^{7}Li. The shape of the spectrum due to this harder γ-ray background was assumed to remain the same over the range of neutron energies used and to be represented by the average of all the difference spectra taken below the (n n′) threshold. The magnitude of the correction to be applied to each of the distributions obtained above threshold was then determined by fitting this average in each case at points above the 478 kev end point. The corrections were found to be fairly constant for all neutron bombarding energies.

Before estimations of the relative 478 kev γ-ray yields could be made, the effect had also to be calculated of the contribution to the spectrum due to the high energy tail of the elastically scattered neutron group. The latter was obtained for each neutron bombarding energy E_n as follows.

From the geometry of the system, the scattered neutrons which could be received by the crystal had a mean energy of 3/4 E_n (corresponding to 90° scattering) and a spread of $\pm 0{\cdot}07\ E_n$. The shape of the spectrum expected for this group was calculated from the appropriate distribution obtained with monokinetic neutrons (fig. 2). The curves derived in this way were found to fit the difference spectra taken below the (n n′) threshold. The use of log–log plots (as in fig. 5), which could be superimposed, was found useful for this curve fitting. The derived curves were then fitted to the experimental curves for neutron energies above the threshold to determine in each case the pulse height at which the scattered neutron contribution to the 478 kev γ-spectrum became negligible. The counts in each spectrum were integrated from this pulse height up to 23 volts. Use was then made of the known shape of the 478 kev distribution, obtained from a ^{7}Be source, to normalize these integrations to the same pulse height interval. From the values of the integrated gamma-ray counts obtained at different neutron energies and the corresponding neutron flux measurements, the relative excitation function for the reaction was thus obtained. The results are given by the points marked as circles in fig. 8, the standard deviations being indicated for each point. Most of the points represent the mean of two or three separate measurements. The greater errors at the higher neutron energies are due to the fact that the scattered neutron groups have reduced the usable ranges of the gamma-ray spectra.

A small correction to the excitation function had to be made for the loss of neutron flux in the lithium ring due to scattering. The magnitude of the total scattering cross section was obtained from published data (Bockelman *et al.* 1951). For neutrons of initial energy less than about 700 kev the scattered neutrons were effectively lost, but for higher initial energies some of the elastically scattered neutrons were still energetic enough to be able to contribute (at a reduced rate because of their loss of energy) to the inelastic scattering reaction. Appropriate corrections, which amounted to a few per cent, were calculated for this effect.

The higher energy points and absolute cross section values given in fig. 8 will be discussed in the next two sections.

3.3. *The Excitation Function at Higher Neutron Energies*

An attempt was made to record the inelastically scattered neutrons at higher energies, but the energy spread of these groups was too great, due to the geometry of the system, to allow satisfactory measurements. The stilbene crystal was then replaced by a $1\frac{1}{2}$ in. diameter $\times$ 1 in. thick NaI crystal for examining the ^{7}Li (n n′) excitation function above 1·1 Mev. An example of a difference spectrum obtained by subtracting runs

with and without the lithium scatterer in position is shown by curve A in fig. 7 ; the neutron energy was 1·22 MEV. The corresponding difference spectrum obtained with a graphite scatterer of the same dimensions is given by curve B. Since carbon cannot give γ-rays from inelastic scattering at this neutron bombarding energy, the spectrum B must be due to neutron-induced reactions in the NaI crystal. The shape of this spectrum was found to be insensitive to small changes of neutron energy, so that it could be assumed to represent the shape of the background component in the spectrum obtained with the lithium scatterer. The carbon curve B was therefore fitted to the lithium curve A at points well above the 478 kev peak and the difference was taken to give the spectrum due to the 478 kev γ-rays from the ^{7}Li (n n′) reaction. The curve C in fig. 7 shows this difference which agrees well in shape and position with cali-

Fig. 7

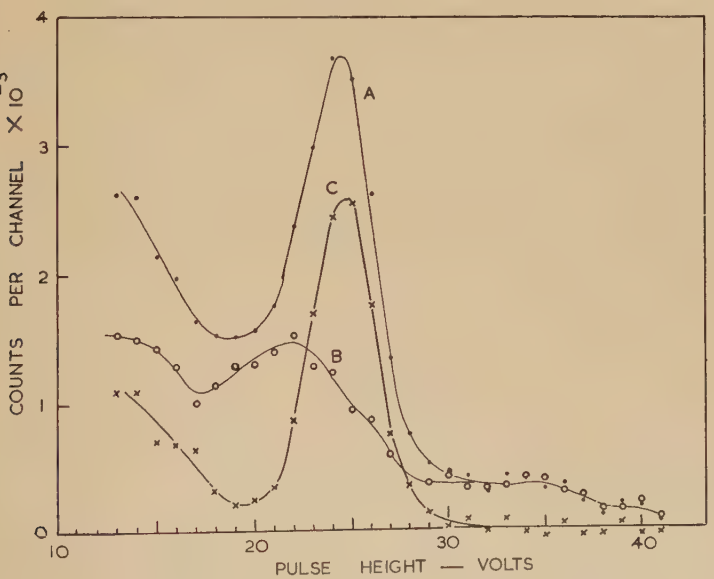

NaI spectra due to lithium (curve A) and carbon (curve B) for 1·22 MEV neutrons. Curve C is the difference spectrum.

bration spectra obtained with a ^{7}Be source. The relative γ-ray yields at different neutron energies were obtained by integrating over the peaks of curves of type C. The neutron flux estimates were again corrected for the effect of neutrons elastically scattered in the lithium ring. The yield results are given by the points marked as crosses in fig. 8. It was found possible to extend the NaI crystal points with reasonable accuracy down to a neutron energy of 800 kev, thus allowing enough overlap for fitting to the stilbene crystal results. This was done by drawing the best curve through the stilbene points, finding the ratios of NaI points to corresponding points on this curve and then taking the mean ratio for adjusting all the NaI results. The standard deviation of the mean ratio was 5%.

3.4. *The Absolute Cross Section*

Two partly independent determinations of the absolute cross section for the ^{7}Li (n n′) reaction were made, one for results obtained with the stilbene crystal at a neutron energy of 712 kev and the other for NaI crystal measurements at 1320 kev.

The efficiencies of both the stilbene and NaI crystals for the detection of 478 kev γ-rays were determined with the aid of a small ^{7}Be source of known strength. In each case the total counting rates in a fixed pulse height interval of the γ-ray spectrum were measured as the source was moved to different points in the space which the lithium ring occupied during the scattering experiment. The pulse height interval was chosen to be the same as that used in the integration of the counts due to γ-rays from the (n n′) reaction as described in §§ 3.2 and 3.3. The absorption due to the total lithium ring thickness was then measured and found to be about 10% in agreement with the theoretical value. It was thus possible to calculate the counting rate expected with each crystal for a 478 kev γ-ray source of known strength distributed uniformly throughout the lithium ring. The γ-rays from the first excited state of lithium were assumed to be isotropic (Ajzenberg and Lauritsen 1952).

The absolute neutron fluxes in the scatterer were obtained from the calibrated neutron monitors and the known geometry of the system, corrections being applied for the loss due to elastic scattering as discussed in § 3.2. The number of ^{7}Li atoms per cm^2 in the ring was estimated from its mass and volume after removal from the steel case in which it was cast. Allowance was made for the isotopic concentration of ^{6}Li (7·5%).

The value of the cross section obtained with the stilbene crystal and 712 kev neutrons was $0{\cdot}050\times10^{-24}$ cm^2. The standard deviation for each factor in the cross section calculation was as follows: integrated counts from the pulse height distribution, 4%; absolute crystal efficiency, 12%; effective neutron flux in the lithium ring, 13%; number of ^{7}Li atoms per cm^2, 10%. The total standard deviation was 21%.

The cross section found with the NaI crystal and 1320 kev neutrons was $0{\cdot}23\times10^{-24}$ cm^2 with the same standard error. From the excitation curve of fig. 8 the ratio of the yields at 1320 kev and 712 kev is 3·81 ($\pm$5%), so that the stilbene measurement of $0{\cdot}050\times10^{-24}$ cm^2 at 712 kev is equivalent to a cross section of $0{\cdot}19\times10^{-24}$ cm^2 at 1320 kev. We take therefore the average value of the cross section for the point at 1320 kev to be $0{\cdot}21\times10^{-24}$ cm^2 with a standard deviation of 19%. The ordinates given in fig. 8 are based on this value.

§ 4. Discussion

We now discuss the analysis of the excitation curve in fig. 8. The trend of the experimental points near the bombarding energy 1·35 Mev enables us to assume the presence of a resonance level in ^{8}Li centred at this energy and with a total width of roughly 1 Mev. The existence of

this level can also be inferred from the measurements of the total cross section of ^{7}Li (Bockelman *et al.* 1951).

The first problem in fitting an excitation curve is to determine the predominant angular momenta involved in the reaction. Assuming that the ground and first excited states of ^{7}Li have the same parity, we can immediately deduce that ingoing partial waves of one parity give rise to outgoing waves of the same parity. To try to discover which partial waves contribute most to the reaction, we first examine the energy dependence of the excitation curve near threshold. In fig. 8 (inset) curves A and B give the predicted dependences assuming s-waves in and out, and p-waves in and out, respectively (Wigner 1948). Higher partial waves give much steeper curves than B. It can be seen that curve A fits the observed points much better than curve B, not only at the

Fig. 8

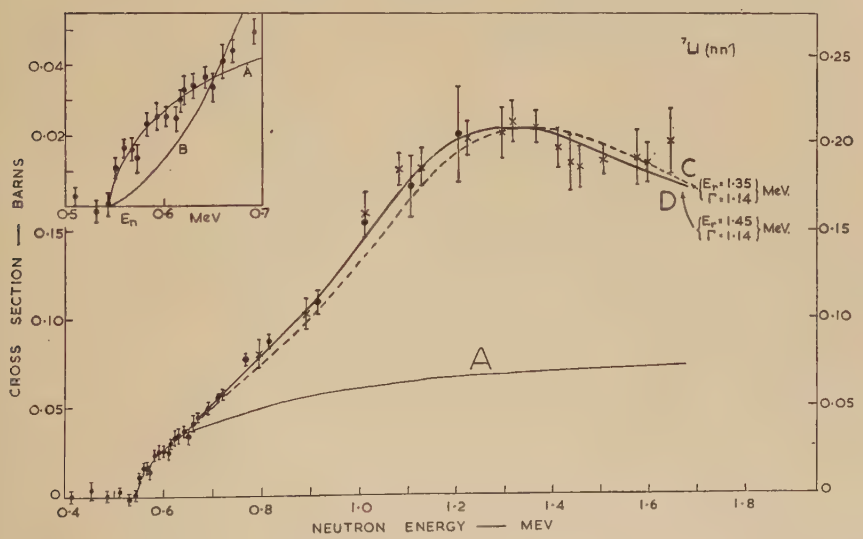

Excitation function for the ^{7}Li (n n') ^{7}Li* reaction. Circles and crosses represent the points obtained by stilbene and NaI measurements respectively. Inset shows the threshold region on a larger scale; curves A and B give the near-threshold energy-dependences for s-waves in and out, p-waves in and out, respectively. Curve C gives the best fit on the assumption (i) that the resonance is (1−). Curve D gives the best fit on the assumption (ii) that the resonance is (1+), superimposed on a strong s-wave background given by curve A. An interaction radius R of $4{\cdot}20\times10^{-13}$ cm is assumed throughout.

threshold, but up to 120 kev above it. This implies the presence of a strong s-wave contribution to the reaction. Such a contribution must arise from (1−) levels of the compound nucleus (assuming that the two states of ^{7}Li have spins (3/2−) and (1/2−) (Ajzenberg and Lauritsen

1952)). If we assume that only one level at some energy E_r and of reduced widths γ_{in}^2 and γ_{out}^2 is responsible, our threshold fit and the measured absolute value of the cross section give the relation

$$\frac{\gamma_{\text{in}}^2 \cdot \gamma_{\text{out}}^2}{(E_t - E_r)^2} \approx 0{\cdot}3$$

where a standard Breit–Wigner formula has been used and E_t is the threshold energy (478 kev in centre-of-mass). It is interesting to note that an indication of strong s-wave levels in ^{8}Li has also been found in the analysis of the thermal neutron elastic scattering cross sections of ^{7}Li (Ajzenberg and Lauritsen 1952).

It is tempting to assume that the level in our excitation curve at 1·35 Mev is indeed the (1−) level responsible for these strong s-wave effects. However, before making such an assumption, one must consider if any other spin assignments to this level are plausible. We can immediately rule out any odd-parity assignments other than (1−) on the grounds that this would imply formation or decay of the compound state by d- or higher waves, which would lead to reduced widths far in excess of the Wigner limit ($\hbar^2/MR^2$). An even parity state, excited by p-waves, is however possible, and the excitation curve could be interpreted as being due to a p-wave resonance at 1·35 Mev superimposed on an s-wave background (represented by curve A in fig. 8) due to a (1−) level at a higher neutron energy. This p-wave state could be either (1+) or (2+). Spin 0 is excluded because the observed cross section, after subtraction of the s-wave contribution, is greater than $\pi\lambda^2/8$, the maximum allowed for this spin. We are therefore left with the following possibilities for the resonance level :

(i) a (1−) state, with formation and decay mainly by s-waves, but with the possibility of some d-wave contributions,

(ii) a (1+) or (2+) state, with formation and decay by p-waves, the level being superimposed on the strong s-wave background given by curve A.

This ambiguity could presumably be resolved by angular distribution measurements. In the absence of such data, we can take advantage of the recent advances in our theoretical ideas on nuclear structure. It has been established (Inglis 1953, Lane 1953, 1955) that an intermediate coupling shell-model gives an extraordinarily accurate description of the structure of light nuclei. The success of this model for states of equivalent nucleons (Inglis 1953) and its extension to mixed configurations (Lane 1954) often enables us to identify an energy level merely from its position in the spectrum. It is an unfortunate coincidence that such a model predicts both a (1−) and a (1+) level in ^{8}Li in our range of investigation. Furthermore, we shall see below that detailed fittings of the experimental curve in the two cases give two sets of nuclear constants, each of which is consistent with the theoretical predictions. It seems however to be worth giving the details of the two cases to show how experimental material can be exploited in the light of recent advances in nuclear theory.

(i) *Interpretation of the Resonance as a* (1—) *State mainly of the Type* $(1p)^3 2s$ (*Lane* 1954)

An initial attempt to fit the whole excitation curve with only s-waves contributing resulted in poor agreement; either the theoretical Breit–Wigner curve fitted the points below 1·3 Mev and fell below those above this energy, or vice-versa. The best fit (curve C in fig. 8) was obtained by introducing d-waves according to the parameters

$$E_{res}=1{\cdot}35 \text{ Mev (lab.)}$$

$$\Gamma_{tot}(E_{res})=1{\cdot}14 \text{ Mev (lab.)}$$

$$\gamma_{in}^2(s)=\gamma_{out}^2(s)=\gamma_{in}^2(d)=\gamma_{out}^2(d)=12\%\ \hbar^2/MR^2.$$

(The Thomas correction (Thomas 1951) was not taken into account here.) The fit was fairly insensitive to variations in the ratios of the reduced widths by factors up to 2, except for the requirement that $\gamma_{in}^2(d)$ had to be at least as great as the mean of the two s-wave reduced widths. According to an analysis by one of us (Lane 1954), the ten or so levels in the 1p shell that are known to be formed by s-waves are all characterized by having reduced widths near the single particle value

$$\left(\sim 0{\cdot}8\frac{\hbar^2}{MR^2}\right).$$

This result implies that an incident s-nucleon couples so weakly to a target nucleus in the 1p shell that the latter is not appreciably excited above its ground state. However, in our case, the first excited state of ^{7}Li is so close to the ground state that even a quite weak coupling might be expected to excite it. This expectation is borne out by the near equality of the experimental values of the two s-wave reduced widths. The large d-wave reduced widths are rather surprising however, for they indicate a large amount of configuration mixing between the shell-model states $(1p)^3\,2s$ and $(1p)^3\,1d$. There is no obvious sign of such a mixing in the other known levels formed by s-waves. It should be noted that the presence of these d-wave effects has to be assumed in our case not only to fit the excitation curve, but also to bring the sum of the four reduced widths of the compound level up to a value near the single-particle value and so to satisfy the sum rule (Wigner 1949). The two s-wave reduced widths alone can only account for about 30% of this figure, whereas the sum over all four reduced widths can amount to 70% (the Thomas correction tends to increase this latter value).

(ii) *Interpretation of the Resonance as the* (1+) (T=1) *State from the Configuration* $(1p)^4$ (*Inglis* 1953)

Curve D in fig. 8 shows the result of fitting a Breit–Wigner curve to the experimental points on the assumption that the resonance is (1+) (p-waves in and out), superimposed on the strong s-wave background given by curve A. Almost identical fits could be obtained for all ratios of the two reduced widths $x=\gamma_{in}^2/\gamma_{out}^2$ from 1 : 10 to 10 : 1, provided that the resonance energy was suitably adjusted in the range 1·47 to 1·30 Mev.

A more severe restriction on the values of x is provided by the absolute p-wave cross section ($0{\cdot}14 \pm 0{\cdot}04$ barns at 1·3 MeV), which requires x to lie in the ranges 0·1 to 0·4 or 1·0 to 3·0. The fitting to the excitation curve demands a total width at 1·3 MeV of about 1·15 MeV, and this implies (for all x) that the sum of the two reduced widths is 0·7 ($\hbar^2/MR^2$) to within 20%.

Using the formulae given by Lane (1953) for reduced widths in terms of shell-model wave functions, we find that the predicted values of γ_{in}^2 and γ_{out}^2 are 0·5 and 0·5 for the ^{33}P[31] state in L–S coupling or 0·2 and 0·75 for the state of $J=1$, $T=1$ in j–j coupling, the unit being the single particle 1p reduced width ($\sim 0{\cdot}7$ ($\hbar^2/MR^2$)). Both of these sets of values are consistent with the rough ranges of experimental values given above.

We conclude from the above analysis of our data that the resonance level at 1·35 MeV could be either a (1−) or a (1+) state. Although both assignments are consistent with the data, the (1+) assignment is slightly preferred because (*a*) a rather better fit is obtained with the excitation curve (compare curves C and D), and (*b*) the fitting of the (1−) level implies an unexpectedly large amount of configuration mixing between $(1p)^3$ 2s and $(1p)^3$ 1d.

Acknowledgments

We should like to thank Dr. W. D. Allen for valuable discussions and interest in the work and for providing the calibrated BF_3 counters, Mr. W. B. Woollen for casting the lithium ring, Dr. R. C. Hanna for providing a calibrated ^{7}Be source, and Mr. A. E. Pyrah for his efficient running of the Van de Graaff machine.

References

Ajzenberg, F., and Lauritsen, T., 1952, *Rev. Mod. Phys.*, **24,** 321.
Birks, J. B., 1951, *Proc. Phys. Soc.*, **64,** 874.
Bockelman, C. K., Miller, D. W., Adair, R. K., and Barschall, H. H., 1951, *Phys. Rev.*, **84,** 69.
Eliot, E. A., Hicks, D., Beghian, L. E., and Halban, H., 1954, *Phys. Rev.*, **94,** 144.
Inglis, D. R., 1953, *Rev. Mod. Phys.*, **25,** 390.
Kiehn, R. M., and Goodman, C., 1954, *Phys. Rev.*, **93,** 177.
Lane, A. M., 1953, *Proc. Phys. Soc.* A, **66,** 977; 1954, *A.E.R.E.* (Harwell) Report T/R. 1289; 1955, *Proc. Phys. Soc.* (to be published).
Poole, M. J., 1953, *Phil. Mag.*, **44,** 1398.
Rose, B., and Freeman, J. M., 1953, *Proc. Phys. Soc.* A, **66,** 120.
Thomas, R. G., 1951, *Phys. Rev.*, **81,**, 148.
Wigner, E. P., 1948, *Phys. Rev.*, **73,** 1001; 1949, *Amer. Jour. Phys.*, **17,** 99.

IV. *Experiments on Supersonic Flow Past Bodies of Revolution with Annular Gaps of Rectangular Section*

By N. H. Johannesen
Fluid Motion Laboratory, University of Manchester*

[Received September 20, 1954]

Summary

The supersonic flow past flat-nosed circular cylinders with annular gaps of rectangular section was investigated by schlieren photography and pressure measurements. The length of the gap was varied in small steps, from low values, where the gap formed a single dead-air region, to high values, where the flow in the gap consisted of two dead-air regions with an intermediate region of attached flow. In particular, the length of the gap for which the flow changed from the type with one to the type with two dead-air regions was determined. The experiments throw some light on the details of the flow in the dead-air regions, and it was found that the velocities inside these regions may be of considerable magnitude. Qualitative information was obtained about the effects of the length of the gap on the drag caused by the gap.

§ 1. Introduction

Consider a long circular cylinder of diameter D placed with its axis in the direction of a uniform supersonic stream. At a station far enough away from the front of the body for the static pressure to have reached its free-stream value, an annular ring of rectangular section is cut away from the cylinder, reducing its diameter to d over a length a.

Fig. 1

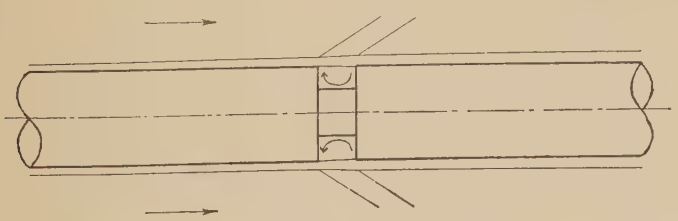

Flow with short gap.

If the gap thus formed is short, as in fig. 1, the boundary layer which separates at the upstream edge of the gap would be expected to form a narrow almost straight mixing region passing across the gap in a direction nearly parallel to the axis of the cylinder. The gap itself will form a

* Communicated by P. R. Owen.

so-called ' dead-air region ' in which the velocities are small compared with the free-stream velocity, and the pressure is nearly equal to the free-stream static pressure. Air will be supplied to the dead-air region at the downstream end of the gap, where the mixing region meets the sharp corner of the body, and will be drawn away from the dead-air region along the mixing zone.

If on the other hand the gap is long compared with the diameter of the cylinder, as in fig. 2, the boundary layer will no longer be separated right across the gap, but the flow pattern will be made up of three parts, namely two separated regions at the ends of the gap with an intermediate region of attached flow.

At the upstream end of the gap the flow will be similar to that at the base of a body of revolution with a supporting sting. At the corner there is an expansion fan which bends the mixing region towards the axis, and at

Fig. 2

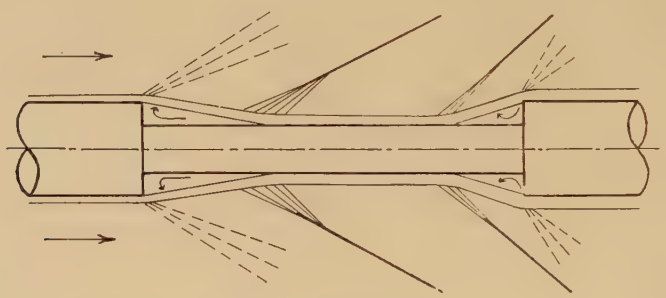

Flow with long gap.

the bottom of the gap the mixing region is bent parallel to the axis by a shock wave or compression fan. The approximately conical dead-air region receives air at its downstream corner, and air is drawn out along the mixing region.

This part of the flow which has been discussed by many authors (see for example Chapman 1950) will be followed by a region where the mixing zone is again attached to the body as a boundary layer.

This boundary layer will separate under the influence of the downstream end of the gap, and the flow here will be similar to that investigated by Mair (1952) who photographed the boundary-layer separation on probes in front of blunt-nosed bodies of revolution in supersonic flow. The dead-air region is again approximately conical, but the shock wave is now at the beginning of the mixing region, and the expansion at its end turns the flow in the direction of the axis of the body. The mechanism of the supply of air to and extraction of air from the dead-air region is similar to that at the upstream end of the gap.

The experiments described in this paper were made to investigate the changes in flow pattern when the length a of the gap was varied from a very small value where the flow pattern was of the first type described above, to a very large value where it was of the second type ; in particular, it was the aim to find out whether the transition from one type of flow

to the other was gradual or sudden. At first sight the photographs might seem to indicate that the change-over took place suddenly, but a more careful inspection combined with measurements of the pressure distribution along the gap showed that the sudden change was preceded by gradual changes as a approached its critical value. It was evident from the pressure measurements that the velocities in the so-called dead-air regions may have been of considerable magnitude.

The main parameters of the problem are the geometry of the gap, i.e. D, d, and a, the free-stream Mach number M_1, and some Reynolds number based on the free-stream velocity and kinematic viscosity and on some typical length. This may be either the length L of the cylinder upstream of the gap or, perhaps better, the displacement thickness of the boundary layer immediately upstream of the gap.

In the experiments, D, L, and the free-stream conditions were kept constant throughout, so that both the Reynolds numbers defined above were constant. Two values of d were used, and a was varied over a wide range.

The experiments throw some light on the flow inside the dead-air regions and they also show that the drag caused by such gaps on bodies of revolution may be considerable even for small values of the length of the gap.

§ 2. Notation

D	diameter of circular cylinder.
L	length of cylinder upstream of gap.
M_1	free-stream Mach number.
P	pressure coefficient.
U_1	free-stream velocity.
a	length of gap.
d	inside diameter of gap.
p	static pressure.
p_1	free-stream static pressure.
x	distance along gap measured from its upstream end.
ρ_1	free-stream density.

§ 3. Experiments

The experiments were made in an intermittent vacuum-operated supersonic tunnel with a 4 in. $\times$ 5 in. working section. The stagnation conditions were approximately atmospheric, the free-stream Mach number M_1 was 1·965, and the Reynolds number was $3{\cdot}4 \times 10^5$ per inch. The flow was observed with a conventional two-mirror schlieren system using a continuous mercury-vapour lamp for visual observations, while the photographs were taken either with a flash tube of effective duration about six microseconds or with a spark of duration just under one microsecond. The pressures were measured with absolute mercury manometers.

The two models are shown in fig. 3. They consisted of silver-steel rods of diameters $d = \frac{1}{4}$ in. or $\frac{1}{8}$ in. with a fixed and a moveable circular cylinder

both of outside diameter $D=\frac{1}{2}$ in. and length $L=1$ in. The first cylinder was always fixed with its upstream end flush with the end of the rod, whereas the second cylinder could be fixed in any position, so that the length a of the gap could be varied continuously from 0 to 2 inches. The steel rods were supported by cross-rods downstream of the working section.

The length of the first cylinder was twice its diameter. According to experiments by Holder and Chinneck (1954) on flat-nosed cylinders at a Mach number of 1·82, the free-stream static pressure was reached at a distance of about one and a half diameters downstream of the flat nose. It can therefore be assumed that the pressure just upstream of the gap was equal to the free-stream static pressure in all the experiments described here.

Fig. 3

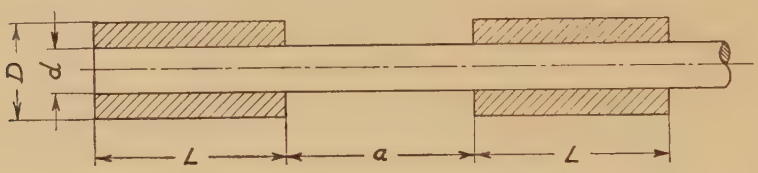

The models.

For the pressure measurements the $\frac{1}{4}$ in.-diameter rod was replaced by a $\frac{1}{4}$ in.-outside-diameter steel tube with twenty-one 0·015 in. holes drilled at equal intervals of 0·1 in. along the tube, the centre of the hole farthest upstream being in the plane of the base of the first cylinder. The holes were filled with soft solder and redrilled one at a time for the pressure measurements.

The flows past both models were photographed for a number of values of a from 0·1 in. to 2·0 in. It was found that to get as much information as possible, photographs with both flash-tube and spark were needed for each value of a. A flash photograph gives a clear picture of the mean flow whereas a spark photograph shows details of the turbulence in the flow.

Some typical photographs are reproduced in figs. 4–15 (Plates 1 and 2). They were all taken with the schlieren knife edge parallel to the direction of the free stream and arranged so that a positive density gradient upwards gives an increase in light on the photograph. Figures 4 and 9 (Plate 1) were taken with the flash-tube and the others with the spark discharge.

The pressures were measured on the model with $d=\frac{1}{4}$ in. for values of a from 0·1 in. to 2·0 in. with a increasing in steps of 0·1 in. Some typical pressure curves are shown in fig. 16 where each curve gives the pressure distribution across the gap for a particular value of a. The pressures are expressed as the non-dimensional pressure coefficient

$$P=\frac{p-p_1}{\frac{1}{2}\rho_1 U_1^2}$$

where p is the measured pressure, and p_1, ρ_1, and U_1 are the static pressure, the density, and the velocity in the free stream.

Fig. 16

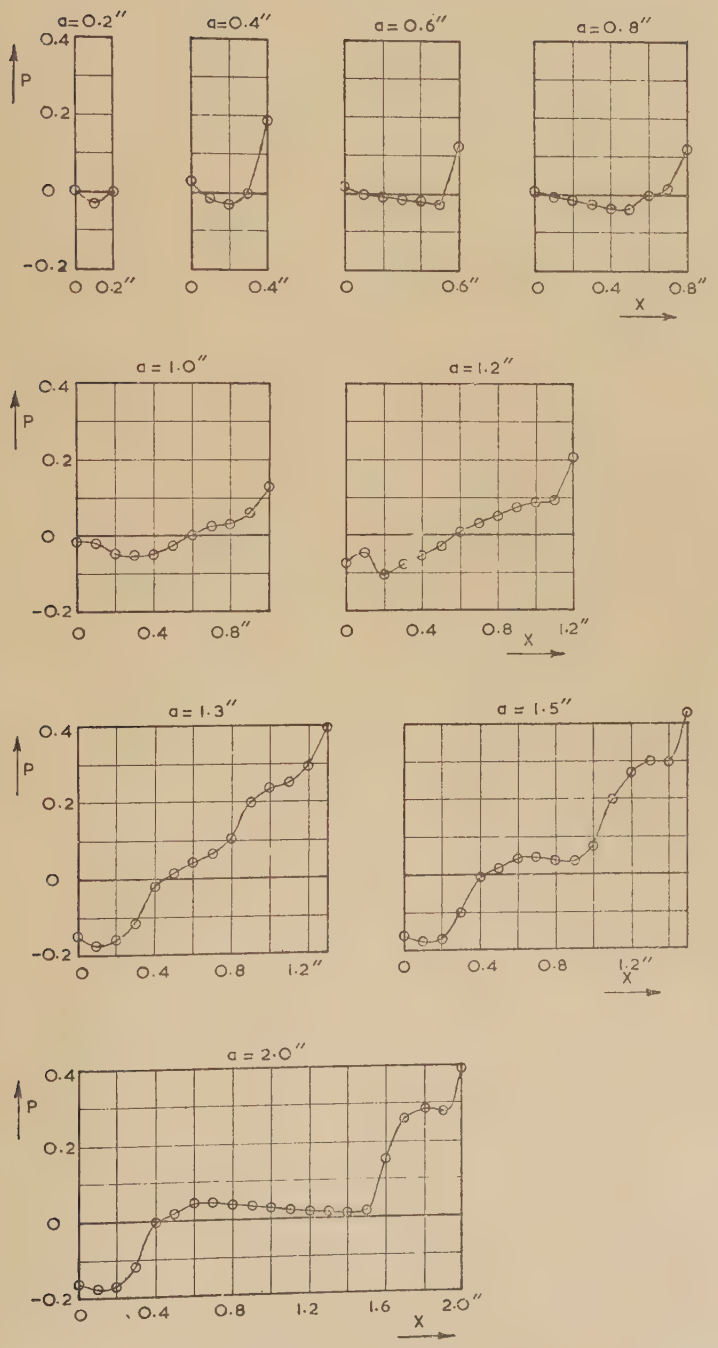

Pressure distributions.

§ 4. Discussion of the Experiments

From the visual and photographic observation of the flow pattern the value of a for which the flow changed character could be determined. For values of a below this critical value the flow was of the first type with one dead-air region extending across the whole of the gap. For values of a above the critical value there were two dead-air regions with an intermediate region of attached flow.

For the body with $d=\frac{1}{4}$ in. the critical value of a was found to be 1·250 in. This value of a was well defined. The flow was observed during a great number of tunnel runs for $a=1{\cdot}225$ in., 1·250 in., and 1·275 in. For $a=1{\cdot}225$ in. the flow was always of the type with one dead-air region, whilst for $a=1{\cdot}275$ in. there were always two dead-air regions. For $a=1{\cdot}250$ in. both types were possible, and either of them might persist throughout one tunnel run (about 30 sec), but in some runs a change-over was observed, and it was in all cases from flow with one to flow with two dead-air regions.

For the body with $d=\frac{1}{8}$ in. the critical value of a was found to be 1·650 in., but this value was less well defined than for the body with $d=\frac{1}{4}$ in. For a range of values of a around 1·650 in. the flow was unsteady, and photographs taken at random using the one-microsecond spark showed all intermediate stages between flows with one and two dead-air regions. Figures 11–14 (Plate 2) show photographs taken for $a=1{\cdot}650$ in.

It is believed that this difference in behaviour of the two bodies is not aerodynamically significant. The unsteadiness of the flow over the thinner body was probably caused by flutter of the model and might not have been present if it had been perfectly rigid.

It is easy to see that the critical value of a must increase as d is decreased. The conical dead-air regions in the gap on one body have very nearly the same cone angles as the corresponding regions on another body with a different value of d, and the smaller d is the larger a therefore has to be to accommodate both regions, provided D is kept constant.

Apart from the difference in the critical values of a, and the unsteadiness found on the body with $d=\frac{1}{8}$ in., the flow patterns around the two bodies were very similar, and the detailed discussion will therefore be based on the body with $d=\frac{1}{4}$ in. for which both photographs and pressure measurements are available.

Consider first the flow for large values of a. The photograph and pressure curve for $a=2{\cdot}0$ in. both confirm the qualitative description given in the introduction. In fact, the two patterns at the upstream and downstream ends can be treated as independent. The gradual decrease in pressure in the intermediate region with attached flow was to be expected, as the pressure on the body for very large values of a, or with no second cylinder at all, would settle down to a value very nearly equal to the free-stream static pressure, i.e., $P=0$.

The value of the pressure coefficient at the base of the first cylinder for large values of a (see for example the curve for $a=2{\cdot}0$ in.) was found to be $-0{\cdot}16$. This value of the base pressure coefficient was found by Chapman

(1950) to occur on a cone-cylinder at $M_1=2{\cdot}0$ for a Reynolds number, based on body length upstream of the base, of about 10^6. The Reynolds number based on body length in the experiments described here was $3{\cdot}4\times10^5$, which in Chapman's experiments gave a pressure coefficient of about $-0{\cdot}10$. However, from fig. 19 in Chapman's paper it can be seen that the base pressure coefficient falls very rapidly with increasing Reynolds number in this range, and it is not surprising that the Reynolds number based on the length of a bluff body should correspond to a considerably higher value for a cone-cylinder. The boundary layer on the flat-nosed cylinder starts growing on the nose, and its thickness is further increased by the laminar separation and reattachment. A comparison based on Reynolds numbers with the displacement thickness just upstream of the base as typical length (if this thickness could have been determined) would therefore probably have given much closer agreement between the present results and those obtained by Chapman.

A comparison of the cone angle of the separated region upstream of the second cylinder with the photographs by Mair (1952) of separation of laminar and turbulent boundary layers on probes in front of flat-nosed bodies, indicates that the boundary layer was turbulent in the present experiments. In fact, as discussed below, transition was found to occur at a distance of about 0·2 in.–0·3 in. downstream of the upstream end of the gap.

As a was decreased from $a=2{\cdot}0$ in. to the critical value of 1·25 in. the two separated regions approached each other, and the shock waves at the end of the first and the beginning of the second separated regions would coincide at $a=1{\cdot}25$ in. It will be seen from the pressure curve for $a=1{\cdot}3$ in. that the second cylinder began to affect the pressure at the base of the first cylinder before the critical value of a was reached.

To discuss the flow pattern in the cases with only one dead-air region it is convenient to start with small values of a and follow what happened when a was increased towards the critical value.

For $a=0{\cdot}1$ in. and 0·2 in. the pressure was found to be only slightly different from the free-stream static pressure. On the photographs (see fig. 4 (Plate 1)) there were weak compression waves at the beginning and the end of the mixing region, showing that this region was slightly convex outwards. This could not be concluded from the pressure curves.

For a between 0·3 in. and 0·8 in. the pressure at the upstream end of the gap was still only slightly different from p_1, but there was a steep rise in P at the downstream end. Furthermore, over most of the gap P decreased almost linearly (see for example the curves for $a=0{\cdot}6$ in. and 0·8 in.). The steep rise in the pressure near the end of the gap and the high value found at the hole farthest downstream can be explained by the impact of the mixing region where it meets the sharp corner at the end of the gap. Part of it is deflected outwards past the second cylinder giving rise to a compression wave which could be seen springing from the corner in some of the photographs not reproduced here. The other part of the mixing region is deflected towards the axis as a region of high velocity along the upstream face of the second cylinder thus causing the high pressure in the corner.

The pressure curves show that, if the pressure is assumed not to vary much in planes perpendicular to the axis (except very near the downstream end of the gap as discussed above), the mixing region must be convex outwards. This is confirmed by the fact that for a between 0·3 in. and 0·8 in. the photographs showed compression waves both at the beginning and at the end of the mixing region.

When a was increased above 0·8 in. the shape of the pressure curves changed, and for $a=1{\cdot}2$ in. P increased almost linearly over most of the length of the gap. This means that the mixing region was now concave outwards. This conclusion about its shape is in agreement with the photographs. On fig. 6 (Plate 1) where $a=1{\cdot}2$ in. the expansion at the first corner (which is also evident from the pressure curve) and the compression wavelets along the mixing region are visible. The concentrated compression at the downstream end of the gap can also be seen. It was followed by a (hardly visible) expansion bending the flow parallel to the axis.

The fact that the mixing region was curved outwards and P decreased with increasing x for small values of a, whereas the mixing region was curved inwards and P increased with x for larger values of a, may perhaps be explained by the transition from laminar to turbulent flow in the mixing region, which could be seen on some of the photographs to take place about 0·2 in.–0·3 in. downstream of the first cylinder.

An increase in pressure in the direction of the flow along the surface of the gap, i.e. from right to left, must be an inertial effect and correspond to a decrease in velocity. On the other hand, a decrease in pressure in the direction of the secondary flow may be an inertial effect and correspond to an increase in velocity, or it may be due to resistance caused by friction and turbulence. For small values of a the flow was probably not very turbulent and the resistance was only of moderate importance, whereas for larger values of a the pressure distribution was governed by the tendency of the turbulent losses to be balanced by a pressure gradient.

It will be seen from the above discussion that there was a gradual change in the flow pattern as a was increased towards its critical value.

Although the flow in the dead-air region is not known in detail, an attempt has been made in fig. 17 to sketch a possible flow pattern for the case of $a=1{\cdot}2$ in. It should be emphasized that this sketch is largely based on conjectures and is only intended to show qualitatively how some of the observed phenomena may be explained. It shows the mixing region curved inwards and drawing air from the dead-air region. At the end it is split up into two parts, one passing over the body, the other being added to the dead-air region.

The bump in the pressure curve for $a=1{\cdot}2$ in. with a local maximum in P at $x=0{\cdot}1$ in. is explained by a small secondary vortex in the corner. This would give a stagnation point with a relatively high pressure at $x=0{\cdot}1$ in.

Although no actual values of the velocities in the dead-air region can be deduced from the experiments, the great changes in pressure along the

Fig. 4

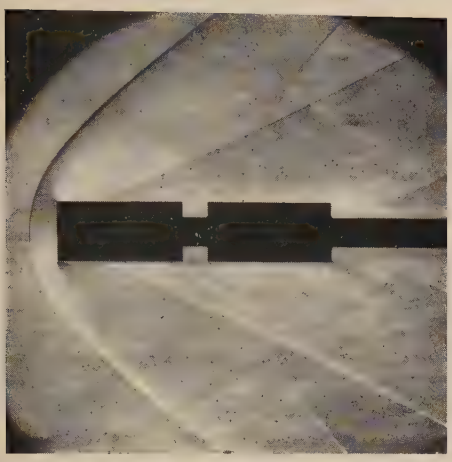

$d=\frac{1}{4}$ in., $a=0{\cdot}2$ in.

Fig. 5

$d=\frac{1}{4}$ in., $a=1{\cdot}0$ in.

Fig. 6

$d=\frac{1}{4}$ in., $a=1{\cdot}2$ in.

Fig. 7

$d=\frac{1}{4}$ in., $a=1{\cdot}3$ in.

Fig. 8

$d=\frac{1}{4}$ in., $a=1{\cdot}5$ in.

Fig. 9

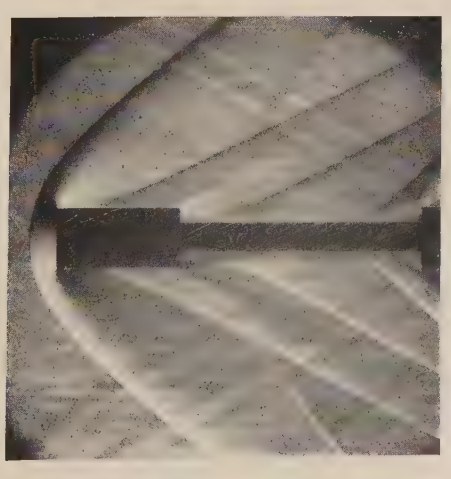

$d=\frac{1}{4}$ in., $a=2{\cdot}0$ in.

Fig. 10

$d=\frac{1}{8}$ in., $a=1{\cdot}5$ in.

Fig. 12

Fig. 11

$d=\frac{1}{8}$ in., $a=1{\cdot}65$ in.

Fig. 13

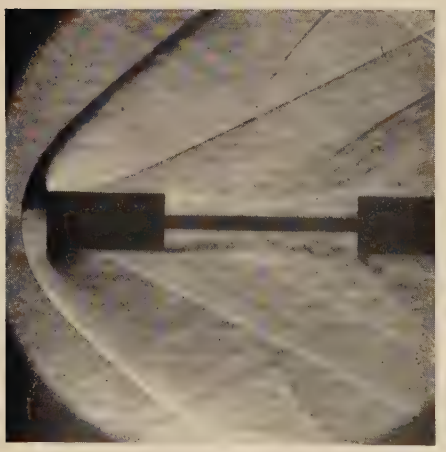

$d=\frac{1}{8}$ in., $a=1{\cdot}65$ in.

Fig. 14

$d=\frac{1}{8}$ in., $a=1{\cdot}65$ in.

Fig. 15

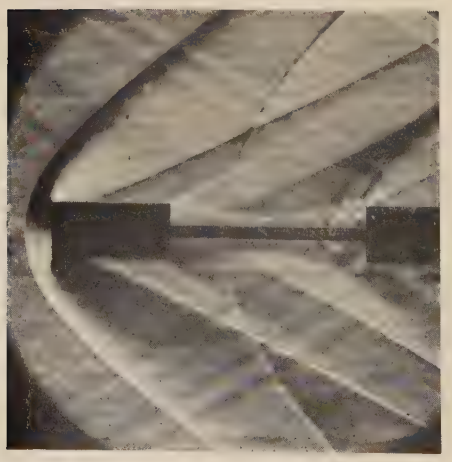

$d=\frac{1}{8}$ in., $a=1{\cdot}65$ in.

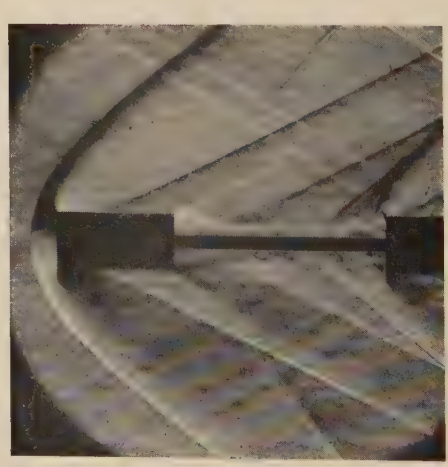

$d=\frac{1}{8}$ in., $a=1{\cdot}8$ in.

gap show that they may be of considerable magnitude. The difficulty in giving absolute values of the velocities arises from the fact that the effects of viscous and turbulent shear stresses are unknown. Some of the photographs indicate that the flow was highly turbulent, and the Reynolds stresses may well play a very important part in the production of the flow pattern. It would therefore be very desirable to make measurements in the dead-air region with hot wires, but this was not possible with the experimental set-up described here.

In order to determine the actual values of the drag caused by the gaps it would be necessary to measure the pressure distributions on the upstream and downstream faces of the gaps. It may, however, be concluded from the experiments, that on the body with $d=\frac{1}{4}$ in. the drag was small for a smaller than 0·3 in. It then increased but stayed nearly constant for a between 0·4 in. and 1·0 in. It then again increased as a was increased to the critical value of 1·25 in. Above the critical value the drag was nearly constant independent of the length of the gap.

Fig. 17

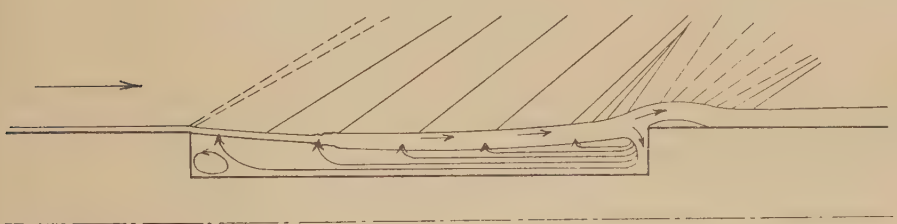

Sketch of flow for $a=1{\cdot}2$ in.

In conclusion it is interesting to compare the results described here with some experiments by Kavanau (1954) on the flow at the base of sting-supported bodies of revolution at a Mach number of 2·84 and low Reynolds numbers. Kavanau used a supporting sting which was continued after a certain length in a much thicker cone-cylinder. The critical sting length was defined as the minimum sting length possible for obtaining a base pressure within 0·5% of that obtained with an infinitely long sting. This length is therefore slightly greater than the critical value of a as defined in the present paper.

Kavanau found that the critical length increased rapidly with decreasing Reynolds number based on body length. He also plotted the base pressure against sting length. A similar curve would be obtained by plotting P for $x=0$ as a function of a as determined in these experiments.

References

Chapman, D. R., 1950, *N.A.C.A., Tech., Note*, No. 2137.
Holder, D. W., and Chinneck, A., 1954, *Aeron. Quart.*, **4**, 317.
Kavanau, L. L., 1954, *Journ. Aero. Sc.*, **21**, 257, 274.
Mair, W. A., 1952, *Phil. Mag.*, **43**, 695.

V. *Experimental Determination of the Aerodynamic Damping on a Vibrating Circular Cylinder*

By J. T. Stuart and L. Woodgate
Aerodynamics Division, National Physical Laboratory*

[Received June 29, 1954]

Summary

For an infinitely-long circular cylinder oscillating rectilinearly along a diameter, the damping force is determined from experimental measurements of the damping force on a circular cylinder oscillating about one end. At very small amplitudes of vibration, up to about one-tenth of the diameter, good agreement is obtained with Stokes' theoretical result for the viscous damping force at infinitesimal amplitudes of vibration. But at larger amplitudes, the damping force is found to increase linearly with amplitude ; an empirical theory is given which is in qualitative agreement with this result.

§ 1. Introduction

The viscous damping force on an infinitely-long cylinder vibrating rectilinearly normal to its length with infinitesimal amplitude has been calculated by Stokes (1851), who showed that the force is proportional to the product of angular frequency ω, velocity U and mass of fluid M' displaced by the cylinder. A boundary-layer treatment of the problem by Stuart (1952) gives a value of the coefficient of proportionality k' which is half that of Stokes' formula. Martin (1925) has obtained values of the damping on vibrating strings of circular cross section, and his results agree well with Stokes' result. His experiments were carried out with small amplitudes of vibration, and he states that no influence of amplitude on the damping could be detected. On the other hand, measurements on bridge models by Scruton (1952) show a very marked increase of damping with amplitude. Accordingly the experiments described in this report were devised to test the validity of the theoretical formulae and to determine the influence of amplitude.

For simplicity, the damping was measured on a long circular cylinder oscillating as a pendulum about one end. For amplitudes at the lower end of the pendulum of up to about one-tenth of the diameter, no effect of amplitude on the aerodynamic damping could be detected, and the results are in good agreement with Stokes' formula. Martin's (1925) amplitude of vibration was of the same order of magnitude. In the present tests, it was found that at very much larger amplitudes than this, the pressure damping far exceeds the viscous damping.

* Communicated by W. P. Jones.

Additionally, the result for the viscous damping at small amplitudes confirms the view that the boundary-layer method used by Stuart (1952) is not valid for the calculation of viscous damping, because the pressure distribution is modified by viscosity by an amount of the same order of magnitude as the damping force.

§ 2. Description of Apparatus and Method of Measurement

2.1. *Measurements at Low Amplitudes*

The apparatus consisted of a circular cylinder (with a length to diameter ratio of 24) suspended at one end by a cross-spring hinge from a metal plate, the whole being mounted in a cylindrical pressure tank to enable experiments to be made at several pressures. In addition, the pendulum could be suspended in free air, in order to examine the aerodynamic effects of the pressure tank walls.

The movement of the pendulum was indicated electrically on a double-beam cathode-ray oscillograph, and the trace together with a suitable time base was recorded on moving film. Five records were taken, one in free air at atmospheric pressure, and four in the tank at various pressures. From each record the corresponding logarithmic decrement was found, and this was constant within the limits of experimental accuracy for amplitudes less than 0·004 radians. The frequency f also was measured from the film records, while the moment of inertia I was determined from stiffness and frequency measurements. The aerodynamic decrement δ_v was obtained by subtraction from δ of the extrapolated (apparatus) damping δ_0 at zero pressure. Results are given in table 1.

Table 1

Location of cylinder	Moment of inertia I lb ft^2	Frequency f c.p.s.	Pressure p inches of mercury	Log. dec. δ	Aerodynamic log. dec. δ_v
Free air	10·60	0·690	30·30	0·00736	0·00223
In tank	10·60	0·700	58·70	0·00842	0·00329
	10·60	0·702	30·59	0·00722	0·00209
	10·60	0·703	14·66	0·00646	0·00133
	10·60	0·703	0·54	0·00520	—

2.2. *Measurements at Large Amplitudes*

A spot of light was projected onto a screen on the floor via a mirror on the pendulum near to the pivot. An average logarithmic decrement δ_a for the amplitude range was then obtained from the time t taken for the oscillation to decay between two given amplitudes θ_0 and θ_1, and from the frequency f; the aerodynamic decrement δ_v was given by subtraction of the known apparatus decrement δ_0, which was assumed

to be independent of amplitude. The experiment was repeated for several different average amplitudes.

Fig. 1

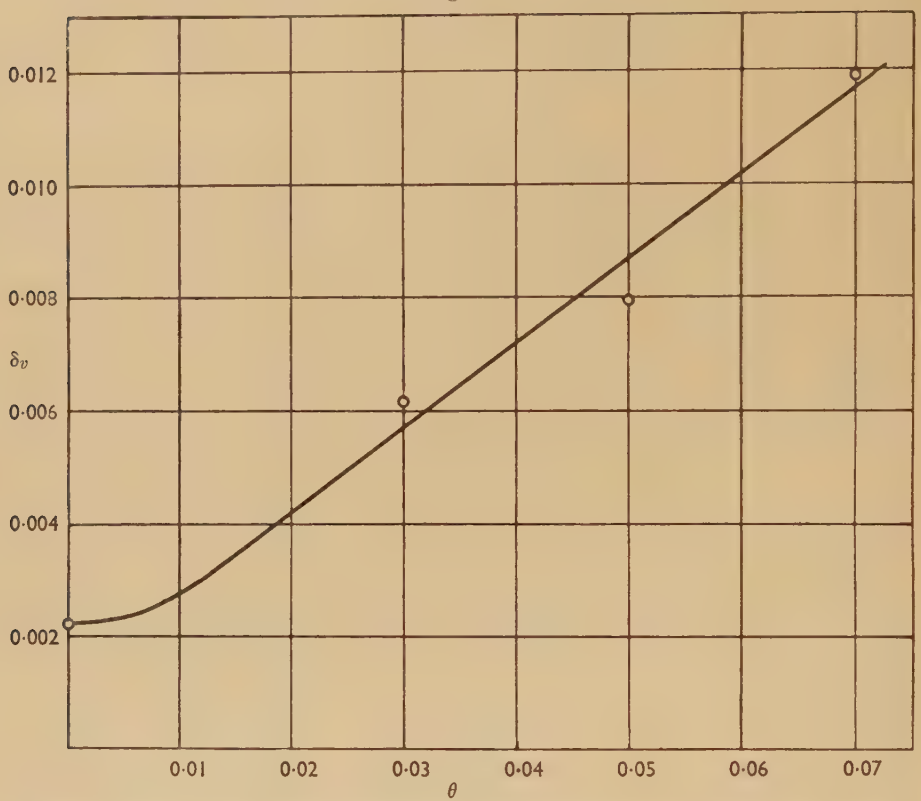

Aerodynamic logarithmic decrement against angular amplitude for large amplitudes.

Results are given in table 2, while fig. 1 shows the quantity δ_v plotted against the average amplitude θ. The curve is drawn to pass through the logarithmic decrement δ_v at small amplitudes. An empirical theory for large amplitudes is given in an Appendix.

Table 2

Amplitude range		Mean amplitude $\theta=(\theta_0+\theta_1)/2$	δ_a	δ_v	f
θ_0	θ_1				
rads.	rads.	rads.			c.p.s.
0·079	0·060	0·070	0·0171	0·0119	0·692
0·059	0·040	0·050	0·0130	0·0079	0·692
0·040	0·020	0·030	0·0113	0·0061	0·692

§ 3. Comparison with Theory for Small Amplitudes

It is first necessary to relate the logarithmic decrement of the pendulum with Stokes' damping function for an infinitely long cylinder vibrating normal to its length.

Fig. 2

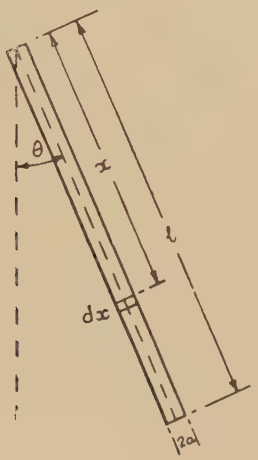

Notation.

The notation for the circular cylinder is shown in fig. 2. Consider an element of length dx, and assume that the aerodynamic force on the element is given by $k'\omega UM'$ (see § 1) for an infinite cylinder vibrating normal to its length. Then the damping force is $\pi\rho a^2 x\dot{\theta}\omega(k'+k'')\,dx$, where k' is the aerodynamic damping coefficient, k'' is the apparatus damping coefficient, and $\dot{\theta}$ is the angular velocity. The total moment about the pivot of the damping force is found by integration to be

$$(-\tfrac{1}{3})\rho\pi a^2 l^3\omega(k'+k'')\dot{\theta}.$$

Thus the equation for the pendulum's motion is

$$I\ddot{\theta}+\tfrac{1}{3}\rho\pi a^2 l^3\omega(k'+k'')\dot{\theta}+\sigma\sin\theta=0, \quad . \quad . \quad . \quad . \quad . \quad (1)$$

where I is the moment of inertia, including the aerodynamic inertia, σ is the stiffness, and $\ddot{\theta}$ is the angular acceleration. Putting $I=\frac{1}{3}\rho_1\pi a^2 l^3$, where ρ_1 is an equivalent density, and $\sigma=I\omega^2$, we have

$$\ddot{\theta}+\frac{\rho}{\rho_1}\omega(k'+k'')\dot{\theta}+\omega^2\theta=0, \quad . \quad . \quad . \quad . \quad . \quad . \quad (2)$$

for small amplitudes. Thus the total logarithmic decrement δ is given by $\delta=(\rho/\rho_1)\pi(k'+k'')$, while the aerodynamic logarithmic decrement is

$$\delta_v=\frac{\rho}{\rho_1}\pi k'. \quad . \quad . \quad . \quad . \quad . \quad . \quad . \quad . \quad (3)$$

From experiment $\delta_v=0{\cdot}00223$ and $\rho_1=22{\cdot}8$ lb ft^{-3}, while $\rho=0{\cdot}0765$ lb ft^{-3}. Thus $k'=0{\cdot}211$.

When the parameter $a\sqrt{(\omega/\nu)}$ is sufficiently large, Stokes (1851, eqn. (7.27)) gives the damping function k' as

$$k' = \frac{2}{a}\sqrt{\frac{2\nu}{\omega}} + \frac{2\nu}{a^2\omega} + \ldots \quad . \quad . \quad . \quad . \quad . \quad . \quad . \quad (4)$$

In the present case $a\sqrt{(\omega/\nu)}$ is 13·8, which certainly lies within Stokes' asymptotic range. Substitution of various quantities into (4) gives $k'=0{\cdot}215$, which is very close to the experimental value of 0·211. But if the second term in (4) is neglected and the assumption $k'=(C/a)\sqrt{(\nu/\omega)}$ is made, where C is a constant, C may be calculated from the experimental k' to be 2·94, which is in good agreement with the value $2\sqrt{2}$ of Stokes (1851) and the value 2·87 obtained experimentally by Martin (1925).

Since the viscosity, $\mu=\nu\rho$ does not vary much with density, it is seen from (3) and (4) that δ_v is theoretically proportional to $\rho^{1/2}$, where ρ is the air density, or to $p^{1/2}$, where p is the pressure. The values of the logarithmic decrement in the tank (table 1) for different pressures are only in qualitative agreement with this. The ratio of δ_v at a pressure of 58·70 in. of mercury to that at 30·59 is 1·57, and the ratio of δ_v at a pressure of 30·59 in. of mercury to that at 14·66 is also 1·57, while each should approximately be $\sqrt{2}$. This discrepancy may be due to the influence of the tank wall.

§ 4. Concluding Remarks

The range of amplitude for which the damping is effectively viscous and independent of amplitude is found to be about 0·004 radians, which at the lower end of the pendulum corresponds to one-tenth of the diameter. Above this amplitude, pressure damping increases in importance, as shown by the rough experiment done to determine the damping at large amplitudes (fig. 1). An empirical, quasi-steady theory for large amplitudes is presented in an Appendix. In spite of the extravagant nature of the assumptions made, the theory predicts a linear increase of damping with amplitude of the same order as that found by experiment.

Before reaching the above conclusions about the results for the small amplitude tests, the following factors were considered :

(*a*) The effect of pressure variations on the results obtained inside the tank is not quite in accordance with the square root law.

(*b*) The wall of the tank may have an influence on the damping even at low amplitudes ; this view is supported by the comparison of the logarithmic decrement at atmospheric pressure inside the tank (0·00209) with that in free air (0·00223). This may account for the divergence noted under (*a*). But, of course, the tank wall has no effect on the extrapolated value of the apparatus damping.

(*c*) The transfer of results from the case of a cylinder vibrating about one end to the case of a cylinder vibrating normal to its length neglects the longitudinal acceleration in the former case. But if θ_0 is the maximum angular amplitude of the pendulum the maximum tangential acceleration

of the fluid is of order $l\omega^2\theta_0$, while the maximum longitudinal acceleration is of order $l\omega^2\theta_0^2$; the ratio of longitudinal to tangential acceleration is thus θ_0. This is required to be small compared with unity, and in fact was about 0·004 radians in the small amplitude tests.

(*d*) In view of the large length to diameter ratio of the pendulum, end effects seem unimportant.

The authors are indebted to Mr. C. Scruton for his continued interest and helpful suggestions during the course of this work.

The work described above was carried out in the Aerodynamics Division of the National Physical Laboratory, and this paper is published on the recommendation of the Aeronautical Research Council and by permission of the Director of the Laboratory.

References

Goldstein, S., 1938, *Modern Developments in Fluid Dynamics* (Oxford: Clarendon Press), **1,** 15.
Martin, H., 1925, *Ann. Phys. Lpz.*, (4) **77,** 627.
Scruton, C., 1952, *Proc. Instn. Civil Engrs., Lond.*, Part I, p. 189.
Stokes, G. G., 1851, *Math. Phys. Papers*, **3,** 1.
Stuart, J. T., 1952 (unpublished work).

APPENDIX

Empirical Treatment of Damping at Large Amplitudes

The logarithmic decrement of an oscillation is normally defined as the ratio of amplitudes of successive cycles. It can also be expressed as an energy decrement. Suppose an oscillation of energy E at a given amplitude suffers a loss of energy ΔE due to damping during the next cycle; then the logarithmic decrement δ is $\Delta E/2E$, provided δ is small compared with unity.

For the case of an oscillation of large amplitude, it is now assumed that the damping force or drag on the cylinder is given by the quasi-steady expression CV^2 per unit length, where C is a constant and V is the local velocity at a point of the pendulum. In the notation of § 3, the work done by the drag per cycle is

$$\Delta E = 4\int_{x=0}^{l}\int_{t=0}^{\pi/2\omega} Cx^2\dot{\theta}^2 x\, d\theta\, dx. \qquad \text{(A 1)}$$

Since δ is small, we can neglect the amplitude decrement during one cycle and write $\theta=\theta_0 \sin \omega t$, where θ_0 is the angular amplitude at the particular stage of oscillation. It then follows from (A 1) that $\Delta E=(\frac{2}{3})Cl^4\omega^2\theta_0^3$, and since $E=(\frac{1}{2})I\omega^2\theta_0^2$, it follows that

$$\delta_v = \frac{2}{3}\frac{Cl^4}{I}\theta_0. \qquad \text{(A 2)}$$

Since the damping force is assumed to have the quasi-steady form CV^2, C is given by steady motion results (Goldstein 1938). In the large

amplitude tests summarized in fig. 1, θ_0 varies between about 0·07 and 0·03 radians. Thus the Reynolds number based on diameter has a maximum value of between 1270 and 540 at the lower end of the pendulum. Reference to Goldstein (1938) then shows that the drag coefficient C_D may be taken as unity, so that $C=a\rho$, where a is the cylinder radius and ρ the air density.

On substituting in (A 2) the values $a=1/12$ ft, $l=4$ ft, $I=10{\cdot}60$ lb ft^2 and $\rho=0{\cdot}0765$ lb ft^{-3}, we obtain for the aerodynamic logarithmic decrement

$$\delta_v=0{\cdot}102\theta_0, \quad . \quad . \quad . \quad . \quad . \quad . \quad . \quad . \quad . \quad \text{(A 3)}$$

compared with the value

$$\delta_v=0{\cdot}153\theta_0 \quad . \quad . \quad . \quad . \quad . \quad . \quad . \quad . \quad . \quad \text{(A 4)}$$

indicated by fig. 1.

This empirical theory thus shows (eqn. (A 2)) that the logarithmic decrement, δ_v, is proportional to the angular amplitude, θ_0, as indicated by experiment to be the case approximately. In addition, the numerical value obtained for δ_v is in fair agreement with experiment.

The assumptions made are :—

(i) That the logarithmic decrement is small compared with unity, an approximation which is justified by the magnitude (0·01) of the experimental values of δ_v. For far higher amplitudes, the expression $\delta_v=\Delta E/2E$ requires modification.

(ii) That the damping force is given by a quasi-steady expression, which entails neglect of acceleration.

(iii) That a single constant, C, which in the present case is based on a maximum velocity, is sufficient to specify the drag in the form CV^2 at all velocities.

VI. *The Effect of a Magnetic Field on the Heat Conductivity of a Superconductor*

By C. A. Renton
Clarendon Laboratory, Oxford *

[Received September 6, 1954]

Abstract

A comparison is made between the heat conductivity data below 1°K in which the specimens were exposed to the magnetizing field and those observations in which the specimens were shielded. The thermal resistance of a tin single crystal in which superconductivity was destroyed by a transverse magnetic field has been examined in detail. The results are discussed and an explanation for the heat conductivity minimum in the intermediate state is suggested.

§ 1. Introduction

The heat conductivity of pure superconductive metals has in recent years been the subject of a great deal of investigation and a fairly clear pattern of its behaviour has been evolved. K_n, the heat conductivity in the normal state, measured below the critical temperature T_c by destroying superconductivity with a magnetic field, is found to pass through T_c without a break. K_s, the heat conductivity in the superconductive state on the other hand is found to depart from K_n at T_c. W_n and W_s which will be referred to are the corresponding heat resistivities.

When a transverse magnetic field is applied to a superconducting cylinder, penetration commences when the applied field H is equal to $1/2H_c$, and is complete when $H=H_c$; H_c is the critical field. Between $H=1/2H_c$ and H_c the specimen is said to be in the intermediate state. The exact structure of this intermediate state has been the subject of many theories and investigations which in a rather over-simplified form suitable for use here reduces to a pattern of alternate layers of normal and superconductive material. Then, if the fraction of the length which is in the normal state is proportional to the strength of the penetrating field, it is easily seen that the thermal resistance W should change linearly from W_s at $H=1/2H_c$ to W_n at $H=H_c$. This behaviour was indeed found in the first experiments (Mendelssohn and Pontius 1937, de Haas and Rademakers 1940) but a quite unexpected effect was found by Mendelssohn and Olsen (1950 a, b) in specimens of columbium and lead with a trace of

* Communicated by Dr. K. Mendelssohn, F.R.S.

bismuth. In these, when entering the intermediate state, W first increased to a maximum before falling to W_n. This has more recently been observed for pure metals (Webber and Spohr 1951, Detwiler and Fairbank 1952).

The experimental investigations which have been made by us have been chiefly concerned with the temperature variation of K_s for some pure superconductors below 1°K. This has been fully reported elsewhere (Mendelssohn and Renton 1954) and it was observed that distinct differences in the experimental results are found, depending on whether or not the specimen is shielded from the applied magnetic field used for the cooling process. The results of the preliminary work not employing magnetic shielding were reported earlier (Olsen and Renton 1952, Mendelssohn and Renton 1953). The explanation of this discrepancy lies in the fact that there may be some ' frozen in ' field in the specimen after demagnetization and the resulting measurements will then refer to the heat conductivity in the intermediate state.

The thermal resistivity maximum in the intermediate state was found in a lead single crystal (Olsen and Renton 1952) at three temperatures. The specimen here was not shielded and the results are inconclusive, hence a further experiment has been performed using a shielded tin single crystal.

In this paper a comparison is made between these preliminary results and the results obtained when the specimen is magnetically shielded. We also give the results of a field transition cycle and in the discussion we propose a possible explanation of the occurrence of this maximum of the thermal resistance in the intermediate state.

§ 2. Results

Figure 1 shows a transition cycle between the superconducting and normal state for the tin single crystal specimen the heat conductivity of which had been measured earlier. The specimen which is shielded from the demagnetizing field starts with its heat conductivity in agreement with the results given in Mendelssohn and Renton (1954), exhibits a maximum in W in the intermediate state, and on returning to zero field shows evidence of a ' frozen-in ' field which reduces its conductivity by a factor two in agreement with the preliminary result of Mendelssohn and Renton (1953). On reversing the field the repeated cycle no longer shows the maximum in the intermediate state.

The general pattern of the comparative results for K_s for the various specimens with and without shielding is as follows.

Lead Single Crystal. The heat conductivity is the same in both cases.

Tin Single Crystal. The heat conductivity is higher with shielding than without.

Tin Polycrystal. The heat conductivity is higher with shielding than without.

Fig. 1

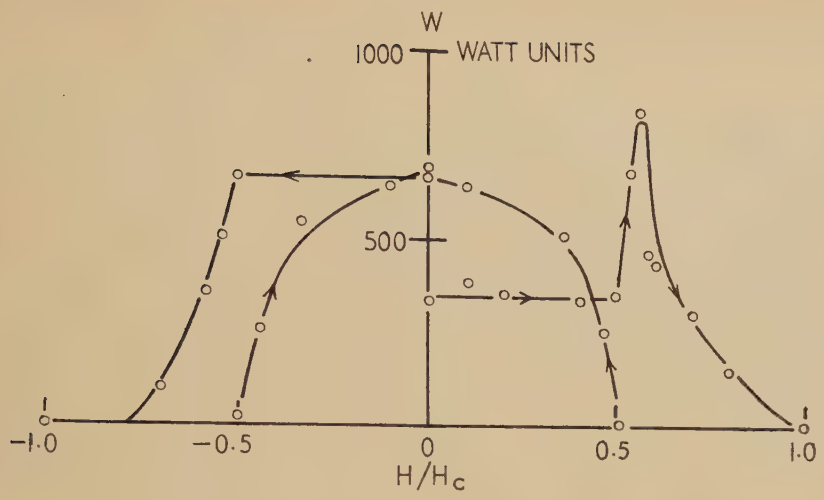

The change in the thermal resistance W is shown as superconductivity is destroyed by a transverse field. The specimen used was the tin single crystal whose conductivity had previously been measured below 1°K. This cycle was performed at a temperature of 0·34°K where K_s is purely lattice conduction.

Fig. 2

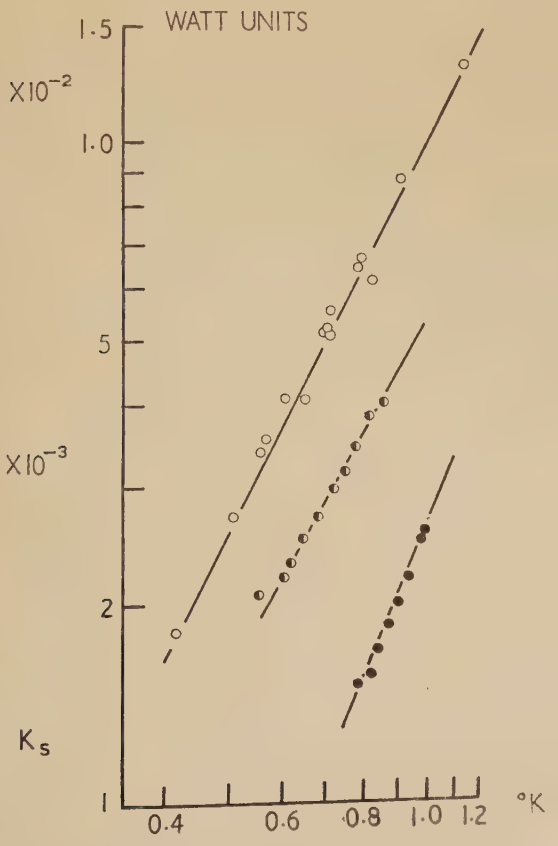

Variation of the heat conductivity with temperature of the tantalum specimen are shown in a double logarithmic plot. ○ results with specimen magnetically shielded. ●◐ results of two separate runs with the unshielded specimen.

Indium Single Crystal. The heat conductivity of this specimen is higher than that of a polycrystalline specimen of the same source, both of which were magnetically shielded. Both these specimens in turn had a higher conductivity than another single crystal made from metal of the same source which was not magnetically shielded.

Thallium Polycrystal. Of all the specimens investigated, here alone the heat conductivity for the shielded specimen was lower. It should be noted, however, that the specimen used in the preliminary work had been destroyed by oxidization. The second specimen which was shielded was made from metal of the same source.

Tantalum Polycrystal. The heat conductivity is higher with shielding than without. The results for this specimen are shown on a double logarithmic plot in fig. 2. The results for the shielded specimen are derived from three separate experiments whilst the two unshielded results, showing different amounts of ' frozen-in ' field, are each the result of one particular cooling.

Columbium Polycrystal. The heat conductivity is higher with shielding than without.

§ 3. Discussion

The results for the specimens which have not been magnetically shielded fall readily into place if it is considered that the specimens contain a frozen-in field. The measurements then refer to a particular stage of the intermediate state such as values lying between $H/H_c=0{\cdot}5$ and 1 in fig. 1. Since in all cases except lead and thallium the conductivity under these conditions is reduced, it appears that these specimens would all exhibit a maximum in the thermal resistance in the transition from the superconducting to the normal state. In the case of lead alone it appears that there is no frozen-in field, whilst, as has already been discussed, the two specimens of thallium are not really comparable.

No explanations of the maximum in the intermediate state can be made by any additive process. The explanations which have been put forward have been comparatively discussed by Detwiler and Fairbank (1952) who come to the conclusion that the most probable explanation lies in the assumption of some additional scattering mechanism of either lattice waves or electrons at the superconducting–normal boundaries of the laminae. Two further accounts have since appeared due to Cornish and Olsen (1953) and to Hulm (1953) both of which are open to slight objections. Cornish and Olsen propose a model of a lattice and electronic system side by side having effectively a different temperature distribution and with an interaction proportional to the temperature difference between them. Such a detailed separation into two distinct systems may be over-simplified (for instance see Mendelssohn (1953), discussion) and can really only be used where the conduction due to one system is of a different order of magnitude to the other.

If the additional thermal resistance is due to either scattering of electrons or lattice waves at the superconducting–normal boundaries, then the amount by which the heat conductivity is decreased will give a minimum estimate for whichever conduction mechanism is considered. Now, electronic conduction predominates at the highest temperatures and lattice conduction at the lowest temperatures and since it is found that the effect increases at lower temperatures, and in most cases does not occur at temperatures near T_c at all, this would seem to point to the effect being due to the lattice component. Moreover, the effect can be observed at the lowest temperatures where conduction is known to be almost exclusively lattice conduction (Mendelssohn and Renton 1954, *loc. cit.*). In this temperature range it would be impossible to account for the increase in resistance as due to the scattering of electrons at these boundaries. This collected evidence would favour the explanation in terms of a lattice resistance at the superconducting–normal boundary and seems therefore to rule out such attempts as have been made (Webber and Spohr 1952, Hulm 1953) to explain the maximum as a decrease in electronic conduction.

The way in which such an increased lattice resistance will occur can be seen from the Casimir (1938) theory of the boundary scattering of lattice waves. Here the wavelength of the lattice waves is limited by the physical boundaries of the specimen. If, as will be discussed below, the superconducting–normal boundaries act in the same manner as physical boundaries, the effect can easily be understood. In the intermediate state an increase in the overall length of the normal regions tends to decrease the thermal resistance of the specimen whilst an increase in the number of superconducting–normal boundaries tends to increase the resistance by reducing the mean free path of the lattice waves. The progression into the intermediate state involves the relative rates of change in these opposing mechanisms. At first the number of boundaries increases to increase the thermal resistance more rapidly than the change in length of the normal regions decreases the resistance. The resistance rises to a maximum and then falls when the overall length of the normal regions changes more rapidly. After this maximum the decrease in the resistance probably changes more rapidly still if the normal regions expand into one another, eliminating some of the superconducting laminae rather than forming new normal laminae within existing superconducting laminae.

To allow for this explanation of the maximum, it is necessary to substantiate our postulate that a superconducting–normal boundary acts in the same way as a physical boundary. At first sight this would seem unlikely since the difference between the two states is purely electronic. As recent experiments (Mendelssohn and Renton 1954) have however shown, there exists an important indirect effect due to the much reduced scattering of lattice waves by electrons in the superconductive state. On the other hand, in the normal state scatter by electrons was found to be the predominant process in limiting lattice conduction. Thus, in the normal regions of the intermediate state where the density of normal

electrons is high, lattice waves will be subject to a great deal of scattering. In the superconducting regions where the density of normal electrons is low and gets lower with decrease of temperature, the lattice waves will hardly be scattered. For the lattice waves the normal regions will therefore act as a dense medium while the superconducting regions will be transparent. The degree of this transparency increases as the temperature falls and in this way the boundary between the two media can limit the mean free path of the lattice waves. It may be that the magnitude of the effect increases at lower temperatures not only because the proportion of lattice conduction increases but also possibly because the transparency of the superconducting region relative to the normal region increases. This would then make the boundaries a more effective limit to the lattice waves.

The relevance of the comparison of the results with and without a frozen-in field is of interest in considering the superconducting heat switch. It is seen that in most cases a frozen-in field reduces the heat conductivity of the specimen and that most specimens show evidence of such a frozen-in field. In the use of a heat switch the superconductor is first rendered normal with a magnetic field and then superconducting by removing this field and so the conditions for producing such a frozen-in field occur. Thus, conveniently, the efficiency of this switch is greater than expected since it is required that K_s should be as low as possible. It has been found in practice (Darby, Hatton, Rollin, Seymour and Silsbee 1951) using a lead wire that K_s was indeed a factor 60 smaller than the value extrapolated from results at 2°K. This could be due to both a frozen-in field and also due to the fact that whilst the value at 2°K is predominantly electronic conduction which is known to fall off rapidly, below 1°K the conductivity will be limited by lattice conduction. Thus below 1°K the conductivity will be limited by the size of the crystallites of the specimen and any frozen-in superconducting–normal boundaries which further reduce the size of the internal structure.

References

Casimir, H. B. G., 1938, *Physica*, **5**, 495.

Cornish, F. H. J., and Olsen, J. L., 1953, *Helvetica Physica Acta*, **26**, 369.

Darby, J., Hatton, J., Rollin, B. V., Seymour, E. F. W., and Silsbee, H. B., 1951, *Proc. Phys. Soc.* A, **64**, 861.

De Haas, W. J., and Rademakers, A., 1940, *Physica*, **7**, 992.

Detwiler, D. P., and Fairbank, H. A., 1952, *Phys. Rev.*, **88**, 1049.

Hulm, J. K., 1953, *Phys. Rev.*, **90**, 1116.

Mendelssohn, K., 1953, *Physica*, **19**, 775.

Mendelssohn, K., and Olsen, J. L., 1950 a, *Proc. Phys. Soc.* A, **63**, 2 ; 1950 b, *Phys. Rev.*, **80**, 859.

Mendelssohn, K., and Pontius, R. B., 1937, *Phil. Mag.*, **24**, 777.

Mendelssohn, K., and Renton, C. A., 1953, *Phil. Mag.*, **44**, 890 ; 1954, to be published.

Olsen, J. L., and Renton, C. A., 1952, *Phil. Mag.*, **43**, 946.

Webber, R. T., and Spohr, D. A., 1951, *Phys. Rev.*, **86**, 384.

VII. *Experiments on Supersonic Flow Over Flat-Nosed Circular Cylinders at Yaw—II: Pressure Measurements on a Cylinder at 10° Yaw*

By I. M. Hall
Fluid Motion Laboratory, University of Manchester*

[Received September 13, 1954]

Summary

In a previous paper (Hall 1954) the supersonic flow over flat-nosed circular cylinders at yaw was investigated by schlieren photography. This investigation was continued for the case of a cylinder at 10° yaw by measurements of the surface pressure distribution, which are described in the present paper.

Close to the nose the cross force, obtained by integrating the pressure distribution, was found to be large. This was due to the asymmetry of the boundary layer separation. Further downstream the variation of the cross force with distance from the nose was in good qualitative agreement with the variation with time of the drag force on a two-dimensional circular cylinder started impulsively from rest.

§ 1. Introduction

In an earlier paper (Hall 1954) the flow pattern about a flat-nosed circular cylinder at yaw to a supersonic stream was deduced from schlieren photographs. An analogy was drawn between the development of the cross flow with distance from the nose and the development of the two-dimensional flow pattern around a circular cylinder started impulsively from rest.

Additional information has since been obtained from pressure measurements on the surface of a cylinder at 10° yaw. The results are described below.

§ 2. Experiments

The experiments were made in the same wind tunnel and under the same conditions as in the first paper.

The model was a straight steel tube 5/16 in. outside diameter with a thin disc soldered on the upstream end. Pressure holes were drilled at points on a generator of the cylindrical surface and on a diameter of the nose. The centres were all in one plane. The holes were of 0·015 in. diameter except for one hole near the edge of the nose which was of 0·005 in. diameter. They were filled with solder and each hole was redrilled as required.

* Communicated by P. R. Owen.

The model was supported in the wind tunnel with its axis inclined at 10° to the free-stream direction. By rotating the model about its axis the pressure holes were set at different values of ψ, the angle between the plane containing the centres of the pressure holes and the plane of symmetry of the flow.* The pressure, p, was measured at each hole for several values of ψ.

The pressure distributions on the nose and on the cylindrical surface are presented separately using two different non-dimensional pressure coefficients. This facilitates comparison with work by other authors. The pressure distribution on the nose is given in terms of p/H_2 where H_2 is the stagnation pressure behind a normal shock wave in the free-stream of Mach number 1·965, calculated from the measured stagnation pressure upstream of the throat, H.

Fig. 1

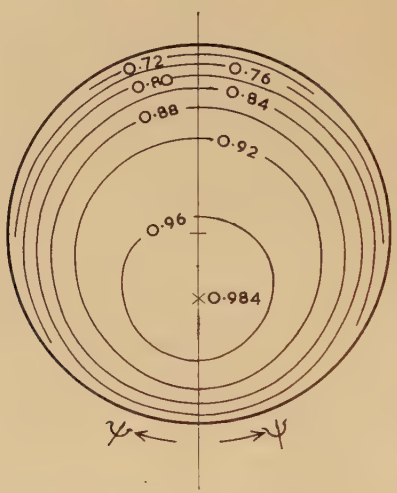

Pressure contours on the nose. Values given are of p/H_2.

For the distribution on the cylindrical surface the non-dimensional coefficient $C_p=(p-p_s)/\frac{1}{2}\rho U^2$ is used. p_s, ρ, and U are the static pressure, the density, and the velocity in the free stream. At a free-stream Mach number of 1·965 the pressure coefficients are related by

$$C_p=2{\cdot}020\frac{p}{H_2}-0{\cdot}370.$$

§ 3. The Pressure Distribution on the Nose

The pressure distribution on the nose of the cylinder at 10° yaw is given in fig. 1. The position of the stagnation point can be determined approximately from the pressure distribution along the diameter in the

* $\psi=0^\circ$ is on the pressure side of the body. This is not consistent with the previous paper but the change was made to conform with the usual practice.

plane of symmetry (fig. 2). It occurs at about $0{\cdot}17d$ from the axis, where d is the diameter of the cylinder. At the stagnation point

$$\frac{p}{H_2} \simeq 0{\cdot}984.*$$

Since H_2 is the minimum stagnation pressure just behind a shock wave in a stream of Mach number 1·965, it is evident that there must have been a loss of total pressure somewhere upstream of the body, in addition to the known loss through the shock wave. A similar loss was observed by Murphy (1953) during the calibration of supersonic wind tunnels with a pitot tube. It is hoped to make further investigations to try to explain the mechanism of this loss.

Fig. 2

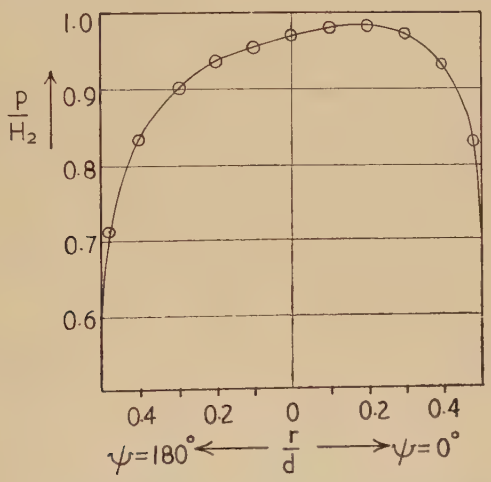

The pressure distribution on the diameter of the nose in the plane of symmetry of the flow.

The coefficient of normal force on the nose may be defined as

$$C_F = \frac{\text{Force} - \frac{1}{4}\pi d^2 p_s}{\frac{1}{2}\rho U^2 \cdot \frac{1}{4}\pi d^2}$$

$$= \frac{8}{\pi} \cdot \frac{H_2}{H} \cdot \frac{H}{p_s} \cdot \frac{1}{\gamma M^2} \int_0^{1/2} \int_0^{2\pi} \frac{p}{H_2} y \, dy \, d\psi - \frac{2}{\gamma M^2}$$

where y is the distance in diameters from the centre of the nose. The integral was evaluated with the assumption that p/H_2 was equal to the sonic value of 0·528 at the edge of the nose (Holder and Chinneck 1954). This value may be in error but the precise value is not important for the evaluation of the integral. It was found that

$$C_F \simeq 1{\cdot}38.$$

* The last figure should not be taken as significant but the value of p/H_2 may be assumed with certainty to lie between 0·98 and 0·99.

The value of C_F when the body is at zero yaw was determined by extrapolating the results of Holder and Chinneck, in the Mach number range 1·4 to 1·8, to a Mach number of 1·965. In this case

$$C_F \simeq 1{\cdot}43.$$

§ 4. The Pressure Distribution on the Cylindrical Surface

A point on the cylindrical surface of the body is specified by the coordinates x, ψ, where x is the distance from the centre of the nose measured along the axis of the body. The distribution of pressure with ψ was measured at several values of x. The results are given in figs. 3 to 7.

The pressure distribution close to the nose is governed by the boundary layer separation at the shoulder and the reattachment further downstream. Inside the separation ' bubble ' there is a ' dead-air ' region in which the pressure is approximately constant. This is shown in figs. 3 and 4, which show pressure curves at stations close to the nose. At $x'=x/d=0{\cdot}06$ the pressure is almost constant for all ψ indicating that the boundary layer is separated all round the body. Further downstream the constant pressure region does not extend over all ψ, showing that reattachment has taken place for some values of ψ.

On the pressure side of the body the pressure increases after the reattachment of the boundary layer. The pressure curves for $x'=$ constant and for ψ between 0° and 90° tend towards a curve which is in good agreement with the pressure curve calculated with the assumption of a potential cross flow. The theoretical curve is shown as a dashed line in fig. 4 and represents the following pressure distribution :

$$C_p=(1-4\sin^2\psi)\sin^2 10°.$$

Between $x'=1{\cdot}18$ (fig. 4) and $x'=2{\cdot}46$ (fig. 5) there is a large increase in pressure near $\psi=180°$. This was observed in the schlieren photographs as a shock wave (Hall 1954). On this side of the body the region adjacent to the body is essentially a ' dead-air ' region for x' less than 1·18, whereas, for x' greater than 2·46 it is essentially a vortex wake. In the latter region, the wake consists of two symmetrical vortices which induce a flow towards the body. This results in a high pressure near $\psi=180°$. For x' greater than 2·78 the pressure near $\psi=180°$ falls slowly with increasing x'. This is attributed to a decrease in the maximum flow velocity between the vortices as they become further apart. Eventually, the pressure peak disappears completely ($x'=9{\cdot}50$, fig. 7) where the wake no longer consists of two steady, symmetrical vortices.

The wake is not formed in exactly the same manner as would be expected from the two-dimensional analogy. In the latter case the initial separation occurs at the rear stagnation point. The separation point moves forward and the vortices are formed. In the case of the yawed cylinder the separated boundary layer from the nose does not reattach near $\psi=180°$ and merges into the beginning of the wake. This is illustrated in fig. 8.

Figs. 3 and 4

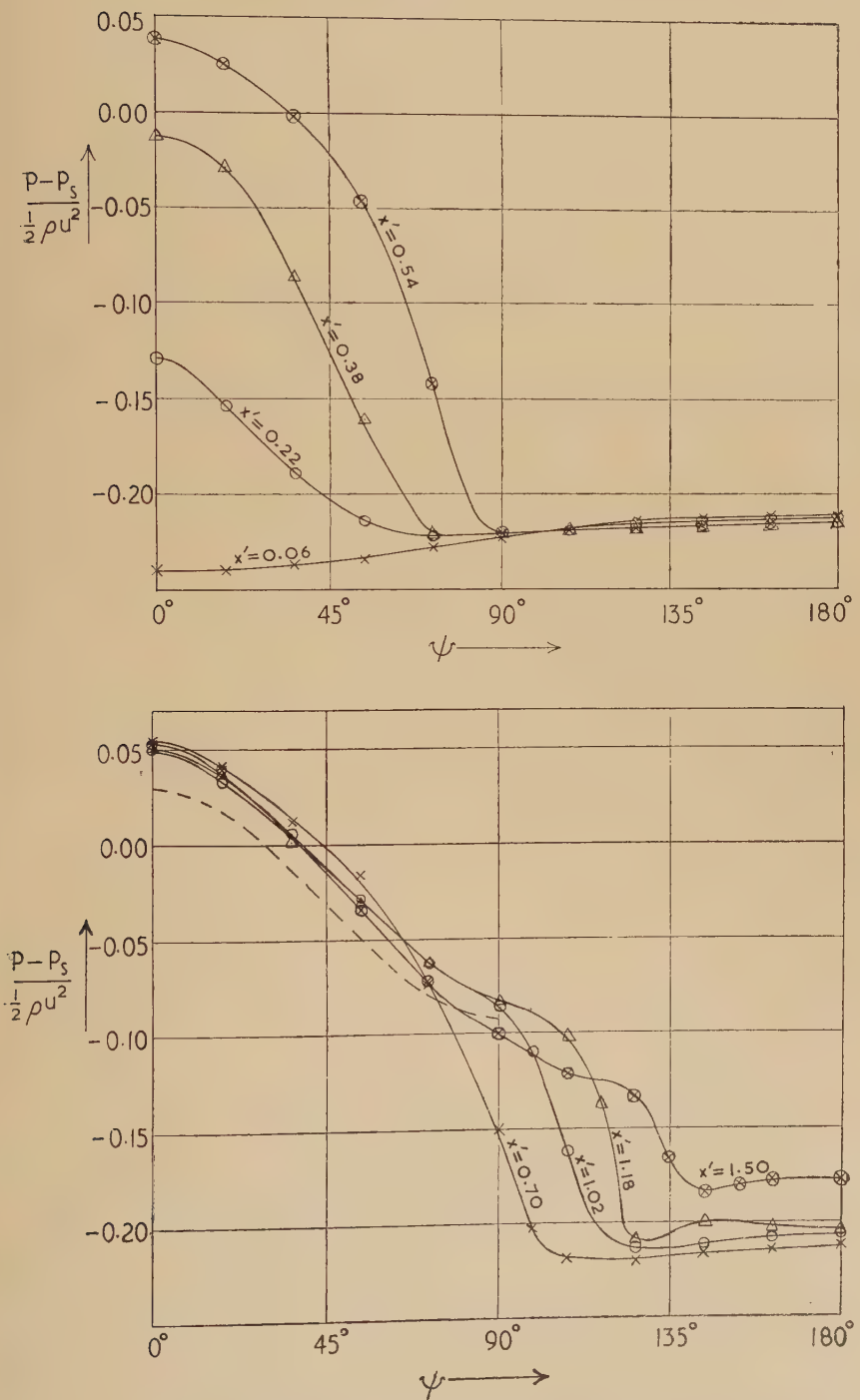

Pressure distributions at stations on the curved surface.

Figs. 5–7

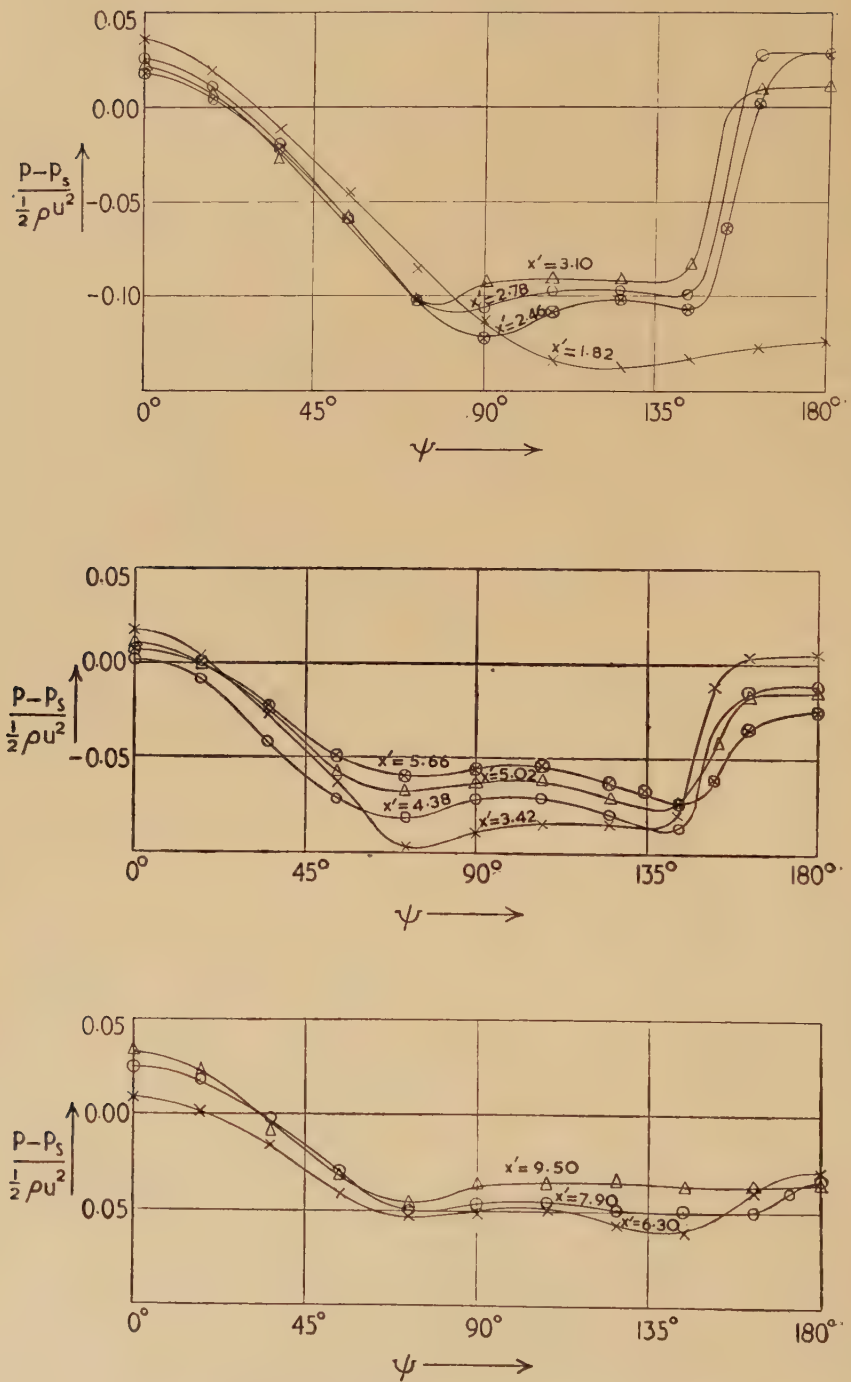

Pressure distributions at stations on the curved surface.

The pressure distribution in the analogous two-dimensional flow about a cylinder started impulsively from rest has been obtained by Schwabe (1935): the results are given by Goldstein (1938). His pressure curves closely resemble those in figs. 5 and 6. In addition to showing the pressure rise near $\psi=180°$ they also exhibit similar undulations between $\psi=90°$ and $\psi=144°$.

A force coefficient, C_{CD} due to the cross flow drag, is defined by

$$C_{CD}=\frac{\int_0^{\pi}(p-p_s)\cos\psi d\psi}{\frac{1}{2}\rho U^2\sin^2 10°}.$$

Fig. 8

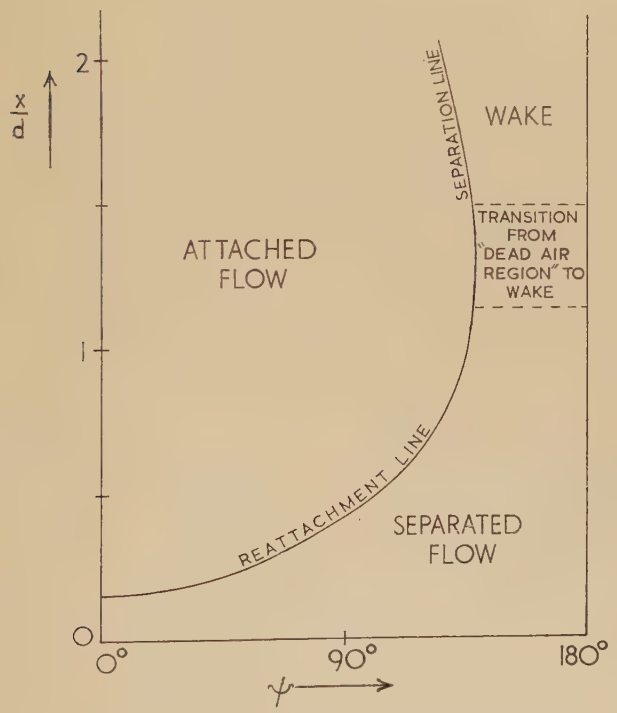

Flow phenomena adjacent to the curved surface.

This coefficient is analogous to the corresponding drag coefficient for the two-dimensional flow past a circular cylinder.

The variation of C_{CD} with x' is shown in fig. 9. The peak near the nose is caused by the asymmetry of the separation bubble. Where the boundary layer is attached (on the pressure side) there is a high pressure, whereas there is a much lower pressure where the layer remains separated. The formation of the vortex wake causes a large increase in pressure on the suction side, and C_{CD} falls to a minimum near $x'=4$. Further downstream the force coefficient increases to approximately 1·48 and then

falls again. A similar peak value (2·07) was found by Schwabe in the two-dimensional case.

Unfortunately, it was not possible to make measurements far enough downstream for the cross flow to have become steady. It is likely that C_{CD} would fall to approximately 0·35 since the boundary layer would probably be turbulent at this station. The last point on the curve is consistent with this decrease.

Fig. 9

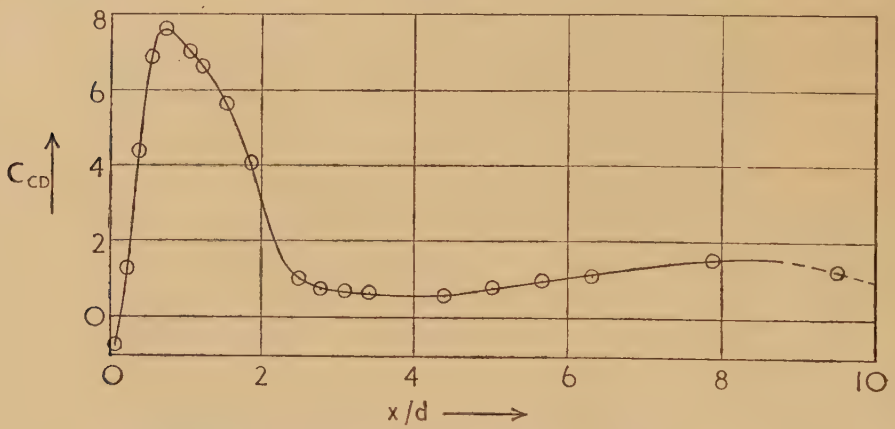

The variation of cross force with distance from the nose.

Acknowledgments

The author wishes to thank Dr. N. H. Johannesen for his advice and criticism during the preparation of this paper. The author has also had helpful discussions with Professor M. J. Lighthill, Mr. P. R. Owen, and Mr. I. S. Donaldson.

During the course of this work the author was in receipt of a maintenance grant from the Department of Scientific and Industrial Research of the Ministry of Supply.

References

Goldstein, S. (Editor), 1938, *Modern Developments in Fluid Dynamics*, 419.
Hall, I. M., 1954, *Phil. Mag.*, **45**, 333.
Holder, D. W., and Chinneck, A., 1954, *Aero. Quart.*, **4**, 317.
Schwabe, O., 1935, *Ing. Arch.*, **6**, 34 (translated as *N.A.C.A.* TM 1039).

VIII. *Neutron Deficient Isotopes of* Pb *and* Tl—*I : Isomers of* Pb *and* Tl

By I. Bergström and A. H. Wapstra*
Nobel Institute of Physics, Stockholm, Sweden†

[Received September 20, 1954]

From the point of view of isomerism all the isotopes of Pb and Tl are interesting. The odd isotopes of Pb should have isomeric transitions of the type $i_{13/2} \rightarrow f_{5/2}$ ($N<126$). ^{206}Pb, ^{204}Pb and ^{202}Pb have all been shown to have high spin isomeric states (Alburger and Pryce 1954, Maeder *et al.* 1954, Hollander *et al.* 1953) and the same may be true for even–even Pb isotopes of lower masses. Tl has 81 protons and its odd isotopes might have isomeric transitions of the same type earlier found in Au (Gillon *et al.* 1954) ($Z=79$). Recently a 0·54 s activity has been reported in Tl (Henrikson *et al.* 1953), which may belong to this class. In the odd–odd isotopes of Tl both the odd neutron and the odd proton can be in high spin states making a resulting high spin state possible. Recently such a case was found in ^{198m}Tl (Bergström *et al.* 1953).

For this reason an extensive β-spectrometer investigation was started at the Nobel Institute of Physics, Stockholm and at the Gustaf Werner Institute for Nuclear Chemistry, Uppsala. Though not yet completed it is worth while to point out some of the most striking features of this investigation, reported more in detail in the two following letters. It should be emphasized that the recent calculations of the L-conversion coefficients by Rose *et al.* highly facilitated the interpretations of the results.

Pb. *Even–odd isotopes.*—There is only one $i_{13/2} \rightarrow f_{5/2}$ transition known with certainty in lead (Hollander *et al.* 1953). (^{207m}Pb $E_\gamma=1{\cdot}063$ and 0·565 Mev, $\tau=0{\cdot}9$ s.) No activity due to ^{205m}Pb is reported. A 5·6 s activity has been assigned to ^{202m}Pb ($E_\gamma=0{\cdot}89$ Mev) and a 50 s activity to ^{201m}Pb (Hopkins 1952). ($E_\gamma=0{\cdot}25$, 0·42 and 0·67 Mev.) After the discovery (Maeder *et al.* 1954) of 3·5 h ^{202m}Pb the mass assignment of the 5·6 s activity seems doubtful and it could therefore be due to ^{302m}Pb. For this reason lead was irradiated with 60 Mev protons in the Uppsala synchro–cyclotron. The Bi activity produced was absorbed in a Dowex 1 column. The lead activity washed through was directly counted with a scintillation spectrometer. In addition to the well-known 1 h ^{204m}Pb activity there was a strong indication of an activity of $\approx$10 s ($E_\gamma \approx 0{\cdot}9$ Mev). Its mother substance decayed with a half-life of $\approx$10 h and is probably ^{203}Bi. ^{204}Bi has a similar half-life (12 h) but it is not probable that this is the mother substance of the 10 s activity, since ^{204}Pb already has an isomeric state (1·1 h). The 10 s activity should therefore belong to ^{203m}Pb. It may be identical with the 5·6 s activity earlier assigned to ^{202m}Pb. Indications were also found for a $0{\cdot}5 \pm 0{\cdot}1$ Mev γ-ray in the 10 s activity.

* On leave from the Instituut voor Kernphysisch Onderzoek, Amsterdam.
† Communicated by Professor Siegbahn and Professor Svedberg.

If this γ-ray could be confirmed it should be a strong indication that the ground state of ^{203}Pb has a spin 1/2 or 3/2 instead of $f_{5/2}$ (Prescott 1954).

The Uppsala experiments (cf. III) showed that ^{199}Pb has a 12 min isomeric state from which a 423 kev M4 γ-ray is emitted. No second γ-transition has yet been found. There were also some indications that the 234 kev γ-ray in ^{197}Pb ($\tau \approx 1$ h) may be due to an isomeric transition.

Though the information still is incomplete the discussion above shows that also in the lead isotopes the energy of the $i_{13/2} \rightarrow f_{5/2}$ transition increases (decreasing half-lives) towards the magic number $N=126$ (see also Mihelich and de Shalit 1954).

Pb. *Even–even isotopes.*—^{206}Pb, ^{204}Pb and ^{202}Pb have been suggested to have 7^-, 7^-, and 9^- states respectively (Alburger and Pryce 1954, Maeder *et al.** 1954). The reinvestigation of ^{202m}Pb mainly confirmed the results of Maeder *et al.* It has earlier been suggested that ^{198}Pb should have a 25 min high spin isomeric state (Passel *et al.* 1954). This assumption was based on the fact that a Tl activity of $\approx$2 h assigned to ^{198}Tl was milked from a lead activity of $\approx$25 m (Neuman and Perlman 1950). Since a 1·8 h ^{198m}Tl activity later was shown to be due to a high spin isomeric state the same should be true for the 25 min Pb activity. However, in our experiments there was no evidence for any isomeric ^{198}Pb and ^{200}Pb activities. If they exist at all they must be short lived. It is therefore concluded that the 2 h Tl and the 25 min Pb earlier assigned to ^{198}Pb are identical with the 2·8 h ^{197}Tl and 42 min ^{197}Pb (cf. III) not known when the conclusion above was made.

Recently (Krohn and Raboy 1954) a third γ-ray has been reported in the decay of ^{204m}Pb with an energy 15 ± 5 kev less than that of the isomeric transition and the decay scheme given in fig. 1 has been suggested. Recent measurements by us confirm the existence of a γ-ray with an energy $13{\cdot}2\pm0{\cdot}5$ kev lower than the isomeric 913 kev γ-ray (cf. II); if it is in cascade with the isomeric ray as suggested by the experiments of Krohn and Raboy, the intensity of its K-line indicates it to be an E2 transition. This suggests the spin assignment given in fig. 1. Thus the first two excited states are $2+$ and $4+$ in agreement with the empirical systematics of even–even nuclei. It has earlier been found (Maeder *et al.* 1954) that the most reasonable nuclear shell model assignment for an isomeric level in ^{204}Pb should be 9^- and its excitation energy comparable with the 9^- level in ^{202}Pb; and a 1 Mev lower 7^- level could only be explained by an extremely large configurational interaction in this case. In addition there should be a 5^- level in the neighbourhood of the 9^- level. This 5^- level is not found in ^{204}Pb and only slightly below the 9^- level in ^{202}Pb. Considering also the position of the 5^- level in ^{206}Pb (see fig. 1) this suggests that for lower mass numbers the 5^- level might be still lower. In this case the half-life of the isomeric level would be determined by a rather fast E4 ($9^- \rightarrow 5^-$) transition, which may explain the fact that we were not able to observe isomers in ^{200}Pb and ^{198}Pb.

* This work gives references to previous investigations of ^{204m}Pb.

Tl. *Odd–odd isotopes.*—^{198}Tl has been shown (Bergström *et al.* 1953, Passel *et al.* 1954) to decay with three γ-rays in cascade having energies 261 (M4), 282 (M1+E2) and 48·7 (E2) kev. In the decay of the 3·5 h ^{202m}Pb activity three γ-rays of energies 460 (E3), 389 (M1) and 401 (E2) kev converted in Tl were found. In both ^{198m}Tl and ^{202m}Tl the sequence of the non-isomeric γ-rays has not been established. If the ground states of ^{198}Tl and ^{202}Tl are 2^-, the excited levels are 2^-, 3^- or 4^-, 5^-, 9^+ and 2^-, 3^- or 4^-, 5^-, 8^+ respectively. In addition in the decay of ^{198}Pb and ^{200}Pb strong E2 γ-rays are found of 173 and 148 kev respectively, probably originating in 0^- states decaying to the groundstate.

Fig. 1

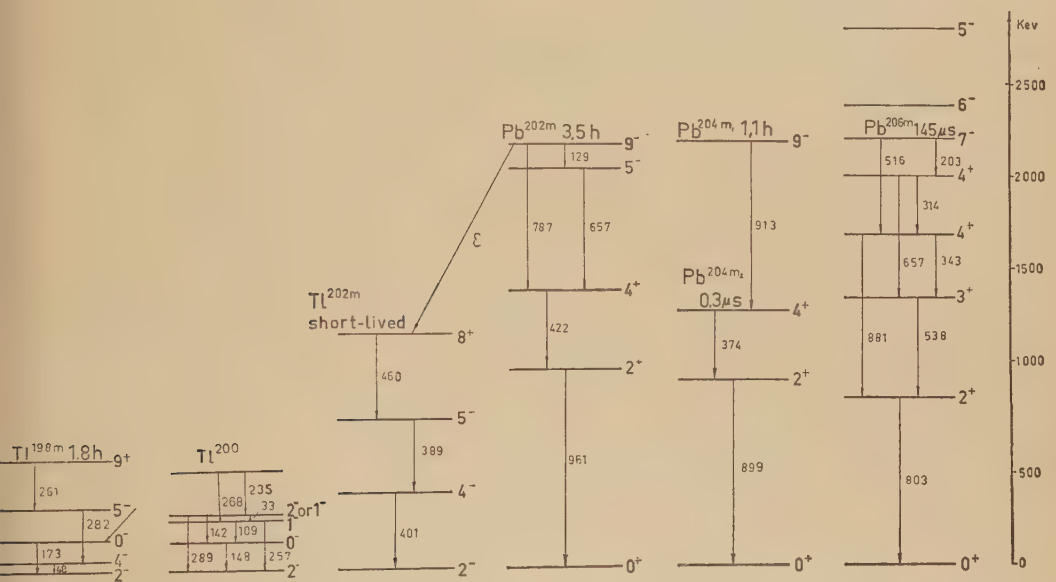

Levels of some Pb and Tl isotopes.

Tl. *Even-odd isotopes.*—In the isotopes ^{203}Tl, ^{201}Tl, ^{199}Tl and ^{197}Tl the first excited states (presumably $d_{3/2}$ states) are situated 279, 330, 367 and 388 kev respectively above the $s_{1/2}$ ground states. The second excited states (presumably $d_{5/2}$ states) are 679, 692, 722 and probably 774 kev respectively above the groundstates. It is probable that the isomeric $h_{11/2}$ levels are situated above the $d_{5/2}$ states and therefore do not decay by M4 transitions to the $d_{3/2}$ states but by E3 transitions to the $d_{5/2}$ states, as is also the case in Au (Gillon *et al.* 1954). The half-lives would then be short which may explain why only ^{197m}Tl has been observed. (Henrikson *et al.* 1953).

It should be noticed that in the decay of ^{201m}Pb three γ-rays are observed. According to the shell model only one or two should be emitted. It cannot be excluded that one or two of the γ-rays reported in ^{201m}Pb are emitted from ^{201m}Tl.

References

Alburger, D. E., and Pryce, H. M. L., 1954, *Phys. Rev.*, **95**, 1482.

Bergström, I., Hill, R. D., and De Pasquali, G., 1953, *Phys. Rev.*, **92**, 918.

Gillon, L. P., Gopalakrishnan, K., de Shalit, A., and Mihelich, J. W., 1954, *Phys. Rev.*, **93**, 124.

Henrikson, A., Breckson, S. W., and Foster, J., 1953, *Proc. Roy. Soc. Canada*, **47**, 127A.

Hollander, J. M., Perlman, I., and Seaborg, G. T., 1953, *Rev. Mod. Phys.*, **25**, 469.

Hopkins, J. N., 1952, *Phys. Rev.*, **88**, 680.

Krohn, V. E., and Raboy, S., 1954, *Phys. Rev.*, **95**, 1354.

Maeder, D., and Wapstra, A. H., 1954, *Phys. Rev.*, **93**, 1433.

Maeder, D., Wapstra, A. H., Nijgh, G. J., and Ornstein, L. Th. M., 1954, *Physica*, **20**, 521.

Mihelich, J. W., and de Shalit, A., 1954, *Phys. Rev.*, **93**, 135.

Neumann, H. M., and Perlman, I., 1950, *Phys. Rev.*, **78**, 191.

Passel, T., Michel, M., and Bergström, I., 1954, *Phys. Rev.*, **95**, 999.

Prescott, J. R., 1954, *Proc. Phys. Soc.* A, **67**, 254.

IX. *Neutron Deficient Isotopes of* Pb *and* Tl—*II: Mass Numbers* 204, 202, 201, *and* 200

By K. E. Bergkvist, I. Bergström, C. J. Herrlander, S. Hultberg, H. Slätis, E. Sokolowski, A. H. Wapstra* and T. Wiedling†
Nobel Institute of Physics, Stockholm, Sweden‡

[Received September 20, 1954]

The investigation of the decay of $^{200-202}$Pb was started mainly in order to obtain more detailed information about ^{202m}Pb (Maeder and Wapstra 1954, Maeder, Wapstra, Nijgh and Ornstein 1954) and, since it has been suggested that ^{198}Pb should also have a high spin isomeric state (Passel, Michel and Bergström 1954), to check whether a similar case of an even–even isomer existed in ^{200}Pb.

Tl was bombarded with deuterons (E_{max}=25 Mev) in the Stockholm cyclotron and with protons (E_{max}=190 Mev) in the Uppsala synchro-cyclotron. The almost carrier free lead activities were evaporated in vacuum on to thin Al foils (0·15 mg/cm^2), which were used as sources in a two-directional focusing β-spectrometer (r=50 cm, resolution ~0·3%). Conversion electrons were investigated in the energy region 10–1600 kev. The preliminary results of the measurements are given below. (A detailed report of the work still in progress will be given in *Arkiv för Fysik*.) The energy values given in table 1 have an accuracy of 0·2% or better. The K/L ratios may in some cases be uncertain. In spite of the high resolution used, the large number of conversion lines makes the overlapping of lines rather probable.

^{204m}Pb.—Krohn and Raboy (Krohn and Raboy 1954) recently found by delayed coincidence measurements (NaI counters) that, in addition to the isomeric 913 kev γ-ray in ^{204m}Pb there existed another γ-ray with a 15 kev lower energy. Figure 1 shows the K-conversion lines of the 913·0 and 899·3 kev γ-rays. If the 913, 374 and 899·3 kev γ-rays are emitted in cascade, as suggested by the experiments of Krohn and Raboy, the intensity ratio $K_{899\cdot3}/K_{913}$=0·12 (expected value=0·12) suggests that the 899·3 kev is due to a pure E2 transition assuming that the 913 kev γ-ray is due to an E5 transition.

^{202m}Pb *and* ^{202m}Tl.—Due to the high resolution of the β-spectrometer, some uncertainties in the decay scheme suggested by Maeder and Wapstra (1954) could be eliminated. Some weak conversion lines assigned to possible γ-rays from levels in ^{202}Pb were now shown to be converted in Tl, suggesting a 10% branching from the isomeric state in ^{202}Pb to a

* On leave from the Instituut voor Kernphysisch Onderzoek, Amsterdam.
† Department of Physics, University of Stockholm.
‡ Communicated by Professor Siegbahn and Professor Svedberg.

Table 1

Nuclide	E_γ	K-conversion intensity	Converted in	Multipolarity	Based on
^{201m}Pb 68 min	913·0	100	Pb	E5	Earlier assignment
	899·3	12·0±1	Pb	E2	K899·3/K913=0·12
^{202m}Pb 3·5 h	129·4	2	Pb	E4	$\tau_{1/2}$; K/L<0·003 L_{II}/L_{III}=1·7
	421·9	35	Pb	E2	K/L=2·5; α_K=0·035
	657·6	3·5	Pb	E1	K/L=7·5; α_K=0·005
	786·9	100	Pb	E5	$\tau_{1/2}$; K/L=1·35; α_K=0·089
	961·2	12	Pb	E2	K/L=5·9; α_K=0·006
	389·2	27	Tl	M1+E2	α_K=0·16
	401·3	5	Tl	E2	α_K=0·030
	459·9	14	Tl	E3	K/L=1·51±0·15
^{201}Pb 9·4±0·2 h	129·1	—	Tl		
	284·4?	0·7		Only K-line observed	
	310·0	0·5	Tl	E2 ?	K/L=0·7 ?
	330·3	100·0	Tl	M1+E2 ?	K/L=4·7
	361·2	25	Tl	M1	K/L=5·6
	394·3	0·6	Tl	E2 ?	K/L=2·5
	405·6	2·7	Tl	E2 ?	K/L=2·8
	585	1·9	Tl		K/L=5·5
	692	0·6	Tl	E2 ?	K/L=6·5
	708 ?	0·3		Only K-line observed	
	766	1·0	Tl		K/L=5·5
	825 ?	0·4		Only K-line observed	
	907	1·3	Tl		K/L=5·5
	946	1·6	Tl		K/L=6·5
	1099	0·2	Tl		K/L=5·5
^{201}Tl 3·0 d	30·6		Hg	M1	L_I/L_{II}=10
	32·1		Hg	M1	L_I/L_{II}=10
	135·0	60	Hg	M1	L_I/L_{II}=10; K/L=7·0
	167·2	100	Hg	M1	L_I/L_{II}=10; K/L=6·2

Table 1 (*contd.*)

Nuclide	E_γ	K-conversion intensity	Converted in	Multipolarity	Based on
^{200}Pb					
21·5±0·4 h	32·8		Only w	eak M and	N lines observed
	109·5	3	Tl	M1	No L_{III}
	142·2	43	Tl	M1	K/L=4·5 ; no L_{III}
	148·0	100	Tl	E2	K/L=0·4 ; $\frac{L_I+L_{II}}{L_{III}}=1·9$
	158·9	4		L-line h	idden
	235·3	22	Tl	M1	K/L=5·5 ; no L_{III}
	257·3	7	Tl	M1	K/L=4·5 ; no L_{III}
	268·0	14	Tl	M1	K/L=4·5 ; no L_{III}
	289·5	1	W	eak, no L-l	ine observed
	450		Onl	y M and N	lines observed
^{200}Tl					
27 h	116·3	5	Hg		
	252·1	4	Hg		
	289·1?	2		Only K-lin	e observed
	367·6	100	Hg	E2	K/L=2·0
	578·8	7	Hg	E2 ?	K/L=4
	628·4?	1		Only K-lin	e observed
	660·2?	1		Only K-lin	e observed
	788·4	1	Hg		K/L=5
	828	8	Hg		K/L=4
	1205	9	Hg		K/L=4·3
	1224	1	Hg		
	1363	1	Hg		
	1515	1	Hg		

high spin isomeric state in ^{202}Tl (odd–odd) from which three γ-rays of energies 460, 389, and 401 kev (E3, M1, and E2) may be emitted in cascade.

^{201}Pb *and* ^{201}Tl.—As can be seen in table 1, the decay of ^{201}Pb is very complex. In addition to the γ-rays listed, there are several weak conversion lines with a half-life $\sim$ 9 hours, which are not assignable. By e^- e^--coincidence measurements in a double lens spectrometer* (Gerholm, to be published) the strong 330 and 361 kev γ-rays were shown to coincide. Because of their intensities (cf. table 1) the latter γ-ray should be emitted first. The 692 kev γ-ray may be due to a cross over transition and the 361 and 330 kev γ-rays emitted from the first two excited states in ^{201}Tl, which probably are $d_{3\,2}$ and $d_{5\,2}$ states. There were no conversion lines indicating a long-lived isomeric state in ^{201}Pb.

It has previously been shown that the 167 and 135 kev γ-rays from the excited levels in ^{201}Hg are M1 transitions (Bergström, Hill and de Pasquali

* We are indebted to fil. lic. T. R. Gerholm for putting his spectrometer at our disposal and for help with the measurements.

1953). The L_I/L_{II} ratios of the 30·6 and 32·1 kev γ-rays are both $\sim$10, showing that also these two γ-rays are due to M1 transitions. e^- γ-coincidences in a β-spectrometer showed that the 30·6 and 32·1 kev γ-rays both coincide with the 135 kev γ-ray, but not with the 167 kev γ-ray. No coincidences were found between the 135 and 167 kev γ-rays. Assuming an $s_{1/2}$ ground state in ^{201}Tl the following level assignment for ^{201}Hg agrees with the experiments: $p_{3/2}$ (0 kev), 5/2–(1·5 kev), 3/2–(32·1 kev), and 1/2–(167·2 kev). No transitions were detected between the 167·2 and 1·5 kev levels, which may be explained by the low emission and conversion probability of E2-rays. Since all the observed γ-rays

Fig. 1

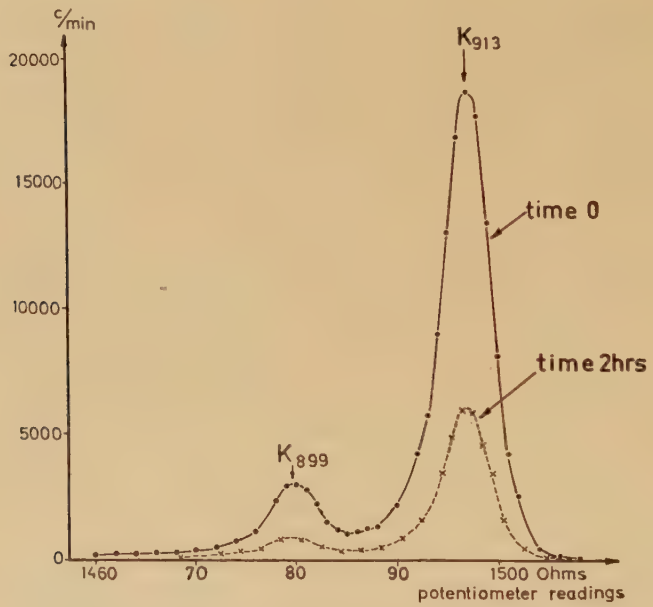

K-lines of E=899·3 kev and E=913 kev in ^{204m}Pb.

are M1 transitions the level scheme requires that the intensity ratio of the 30·6 and 32·1 kev γ-rays is $(30{\cdot}6/32{\cdot}1)^3=0{\cdot}86$ and that of the 167 and 135 kev γ-rays $(167/135)^3=1{\cdot}9$. This is in agreement with the experimental values 1·0 and 3·2 supporting the suggested level scheme.

^{200}Pb *and* ^{200}Tl.—e^-—e^- coincidences in a double lens spectrometer (Gerholm, to be published) showed that the following γ-rays coincide with the strong 148 kev γ-ray in ^{200}Pb: 109, 142, 235, and 268 kev. The 159, 257, and 289 kev γ-rays do not coincide with the 148 kev γ-ray. All γ-rays but two (159 and 450 kev) fit into a level scheme in agreement with the measurements. The excited levels have the energies: 148, 257, 289·5, and 525 kev. The parity and spin assignments are still uncertain. There was no evidence for an isomeric state in ^{200}Pb, having a half-life larger than about one hour.

The measurements on ^{200}Tl are yet incomplete. However, the γ-rays found confirm earlier measurements (Bergström, Hill and de Pasquali 1953). There are several other conversion lines having a 27 h half-life.

References

Bergström, I., Hill, R. D., and de Pasquali, G., 1953, *Phys. Rev.*, **92,** 918.
Gerholm, T. R. (to be published).
Krohn, V. E., and Raboy, S., 1954, *Phys. Rev.*, **95,** 1354.
Maeder, D., and Wapstra, A. H., 1954, *Phys. Rev.*, **93,** 1433.
Maeder, D., Wapstra, A. H., Nijgh, G. J., and Ornstein, L. Th. M., 1954, *Physica*, **20,** 521.
Passel, T., Michel, M., and Bergström, I., 1954, *Phys. Rev.*, **95,** 999.

X. *Neutron Deficient Isotopes of* Pb *and* Tl–*III*: *Mass Numbers below* 200

By G. Andersson and E. Arbman
The Gustaf Werner Institute for Nuclear Chemistry,
University of Uppsala, Uppsala, Sweden
and
I. Bergström and A. H. Wapstra*
Nobel Institute of Physics, Stockholm, Sweden†

[Received September 20, 1954]

The present investigation of Pb and Tl isotopes with $A<200$ is closely connected to similar work on higher mass numbers going on at the Nobel Institute in Stockholm (cf. I and II). Mainly because of the short half-lives in this region, however, the measurements have been performed at the Gustaf Werner Institute for Nuclear Chemistry.

The activities, produced by Tl (p, xn) reactions in the Uppsala synchro-cyclotron, have been studied in a two-directional focusing β-spectrometer ($r=18{\cdot}5$ cm, resolution $\sim 0{\cdot}3\%$) (Arbman and Svartholm). Most spectra were obtained by means of an automatic device, using a ratemeter and a Speedomax recorder. For mass assignments and in some cases when preparing β-spectrometer samples, an electromagnetic isotope separator of the 90° type (Andersson *et al.*) has been used.

So far the conversion electron spectrum has been investigated only in the region 50–700 kev. All the activities except ^{199m}Pb were shown to decay by electron capture. A full account of the investigations, still in progress, will later be published in *Arkiv för Fysik*. The following is a summary of the preliminary results (cf. table 1).

^{199m}Pb *and* Pb.—A 12 minute activity has been assigned to $A=199$ partly because of excitation relations. Moreover, the decay curve of a mass-separated sample of $A=199$ showed a strong $\approx$10 minute activity. In the same way a 90 minute activity was assigned to the same mass number. Since this activity was not found in the electron spectrum of a pure Tl sample and the conversion definitely occurs in Tl, the 90 minute activity must be due to the ground state. It is therefore concluded that ^{199}Pb has an isomeric state, not known earlier, agreeing with the fact that the electron lines of the 12 minute activity are converted in Pb.

If the 354 and 367 kev γ-rays are emitted in cascade from levels in ^{199}Tl as indicated by a possible 722 kev γ-ray, the 367 kev γ-ray should be emitted from a lower level for intensity reasons.

^{197}Pb.—There are indications that the 169 and 234 kev γ-rays are converted in Pb, suggesting an isomeric state which may have about the same half-life as the ground state. (The half-lives of the γ-rays in the table have not all been measured with the given accuracy.)

---

* On leave from the Instituut voor Kernphysisch Onderzoek, Amsterdam.
† Communicated by Professor Siegbahn and Professor Svedberg.

Table 1

Nuclide	E_γ	K-conversion intensity	Converted in	Multi-polarity	Based on
^{199m}Pb 12·2±0·3 m	423		Pb	M4 ?	K/L=1·9, no γ-ray detected
^{199}Pb 90±10 m	354	43	Tl	M1	K/L≈5, no L_{III}
	367	100	Tl	M1	K/L≈5, no L_{III}
	722?	3			
^{198}Pb 2·3±0·2 h	173	>60	Tl	E2	K/L≥0·5 $(L_I+L_{II})/L_{III}$=1·9
	276?	5	Tl		
	291	100	Tl	M1 ?	No L_{III}
	330?				
	365	100	Tl		
	383	17	Tl		
	398?	10	Tl		
	420?	8	Tl ?		
^{197}Pb 42±3 m	169?	>13	?		
	223	100	Tl	E2	K/L≥0·4 $(L_I+L_{II})/L_{III}$=2·3
	234?	67	?	E2 ? M4 ?	K/L≈0·3 $(L_I+L_{II})/L_{III}$=2·0
	323?	13			
	386	85	Tl	M1	K/L≈5, no L_{III}
	388	59	Tl	M1	K/L≈5, no L_{III}
^{197}Tl 2·8±0·4 h	134	>3	Hg	E2	K/L≥0·1 $(L_I+L_{II})/L_{III}$=1·4
	152	>100	Hg	M1	K/L≥2·5, no L_{III}
	174	>5	Hg	M1	K/L≈5, no L_{III}
	269?	5	Hg		
	434	7	Hg ?	M1	K/L≈6
	583?	6			
	588?	1			
	611	4	Hg ?		
	637?	3			
^{196}Tl ? ≈4 h	426		Hg		

^{199}Tl *and* ^{198}Tl.—The γ-rays found in the decay of these nuclides confirm earlier measurements (Bergström *et al.* 1953). As to ^{198m}Tl the γ-rays reported by Bergström *et al.* (1953) and Passel *et al.* (1954) were not observed. One possible explanation is that the isomeric state of ^{198}Pb has not the half-life $\approx$25 minutes as suggested by Passel *et al.* (1954), but is so short-lived that it decays considerably before the chemical separation of Pb from the Tl target.

^{197}Tl.—The 134 kev γ-ray found in the decay of ^{197}Tl is undoubtedly identical with the γ-ray of the same energy emitted in the decay of ^{197m}Hg.

^{196}Tl.—The assignment of the 426 kev γ-ray to ^{196}Tl is supported by the following facts. Excitation relations indicated $A < 198$. In the electron spectrum of $A = 197$ (mass separated), however, the conversion lines of the 426 kev γ-ray did not show up, in spite of their strong intensities. Furthermore a 426 kev γ-ray has been observed in the β-decay of ^{196}Au (Staehelin 1952).

References

Andersson, G., *et al.*, unpublished.
Arbman, E., and Svartholm, N., to be published in *Arkiv för Fysik.*
Bergström, I., Hill, R. D., and de Pasquali, G., 1953, *Phys. Rev.*, **92**, 918.
Passel, T., Michel, M., and Bergström, I., 1954, *Phys. Rev.*, **95**, 999.
Staehelin, P., 1952, *Phys. Rev.*, **87**, 374.

XI. *Dislocation Energies and Choice of Slip Plane in Face-Centred Cubic Metals*

By A. J. E. Foreman and W. M. Lomer
Atomic Energy Research Establishment, Harwell, Berks.*

[Received October 2, 1954]

In interpreting the modes of deformation of a metal crystal in terms of the theory of dislocations it is usually assumed that the direction and plane of slip are determined by the criterion of minimum dislocation energy. Since the energy of a dislocation varies as the square of the Burgers vector, it follows that the slip direction is the closest packed direction in the crystal, in agreement with observation, but a more detailed analysis appears to be necessary before the occurrence of slip on only certain prominent crystallographic planes may be adequately explained.

Calculations have recently been made of some dislocation energies in the face-centred cubic lattice, using the anisotropic elasticity theory of Eshelby, Read and Shockley (1953), for various edge, mixed and screw dislocations in several different slip planes containing the $\langle 110 \rangle$ Burgers vector. Eshelby (1949) has shown that the energy per unit length of a straight dislocation line (Burgers vector **b**) takes the form

$$E = \frac{Kb^2}{4\pi} \ln \frac{R}{r_0}, \qquad \ldots\ldots\ldots \quad (1)$$

where K is a function of the elastic constants, edge-screw composition and dislocation slip plane ; R is the radius of the dislocation strain field (i.e. the mean spacing in a dislocation array, typically about 10^4 b), and r_0 is an effective radius of the central core of the dislocation. For elastic isotropy the energy factor K becomes independent of the slip plane orientation and is given by

$$K = G\left(\cos^2\theta + \frac{\sin^2\theta}{1-\nu}\right), \qquad \ldots\ldots \quad (2)$$

where θ is the angle which the Burgers vector makes with the dislocation line, G is the shear modulus and ν is Poisson's ratio.

In the numerical calculation of K we use the following values for the single crystal elastic constants (units of 10^{12} dynes/cm^2).

	C_{11}	C_{12}	C_{44}	A	Reference
Al	1·08	0·622	0·284	1·2	Schmid and Boas (1950)
Au	1·87	1·57	0·436	2·9	Schmid and Boas (1950)
Cu	1·710	1·239	0·756	3·2	Lazarus (1949)

The 'anisotropy factor' $A = 2C_{44}/(C_{11}-C_{12})$ is unity for an isotropic crystal.

* Communicated by the Author.

The calculated values of the energy factor K for aluminium and copper are shown in the figure for the {100}, {110} and {111} dislocation slip planes, with curves of best fit drawn through the calculated points. The curves for gold fall near those for copper and have been omitted from the figure for the sake of clarity. The notable features of these results are

(*a*) the variation of K with θ still approximates to the isotropic form

$$K = K\,(\text{screw})\cos^2\theta + K\,(\text{edge})\sin^2\theta \quad . \quad . \quad . \quad . \quad (3)$$

for each slip plane,

(*b*) except for a pure screw dislocation the spread of values for different slip planes increases with increasing anisotropy,

(*c*) the ratio K (screw)/K (edge) has the order of magnitude of $1-\bar{\nu}$, where $\bar{\nu}$ is the mean (polycrystalline) value of Poisson's ratio,

(*d*) for none of the metals considered has the observed {111} slip plane corresponded to the lowest K values.

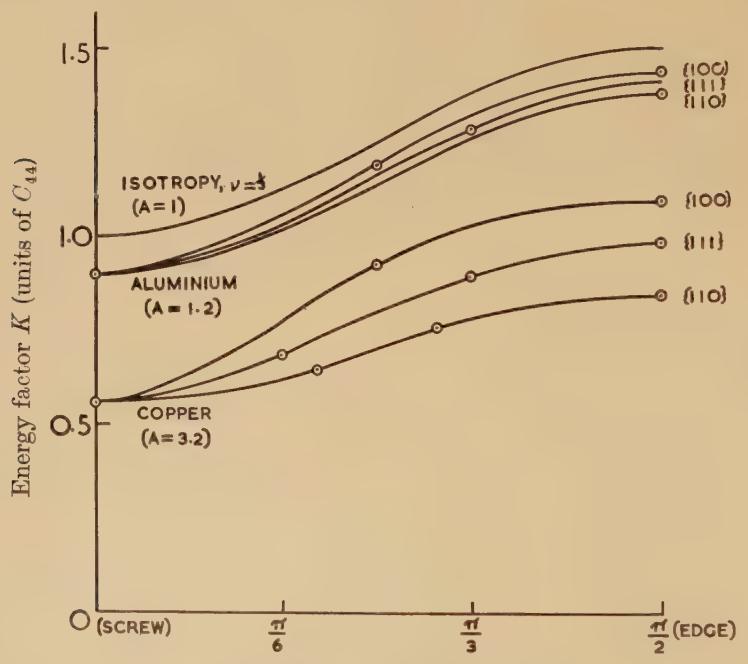

Variation of K with the angle θ between the dislocation line and ⟨110⟩ Burgers vector, for three dislocation slip planes.

The value of r_0 in eqn. (1), also, will depend on the choice of dislocation slip plane, especially since dissociation into a pair of partial dislocations connected by a stacking fault may occur in the {111} plane, with a consequent lowering of energy. Seeger and Schöck (1953) have investigated this extended dislocation, using the Peierls dislocation model with anisotropic elasticity theory and taking as the stacking fault energy the coherent

twin boundary energy of the crystal. For copper the stacking fault width is shown to be about 8 b for a screw and 12 b for an edge dislocation, and the corresponding energy gains as compared with the energy of a narrow Peierls–Nabarro dislocation may be shown to be about 8% and 10% respectively, if we take the dislocation strain field radius as of the order of 10^4 b. In the case of aluminium the stacking fault is only 1 or 2 atoms wide, which hardly constitutes a true dissociation, and the resulting energy gains are only a few per cent.

These results indicate that even when the gain in energy due to dissociation is taken into account the energy of an edge dislocation in a {111} plane still exceeds that for a {110} plane. The screw dislocation is, however, energetically favoured in the close packed {111} plane by a factor of about 8% for copper and a few per cent for aluminium. Thus the mean energy of a dislocation ring in a {110} plane is approximately equal to that for a ring in a {111} plane, and it therefore seems unlikely from energy considerations that the dislocation content of a crystal as grown should be composed of predominantly {111} dislocation rings.

It is suggested that dislocations may initially exist on numerous planes in a face-centred cubic crystal, but that the pure screw segments of any general dislocation loop will become extended into a close packed {111} plane and their subsequent glide motion may then be limited to the plane of dissociation. It is not at present clear what is the smallest degree of dissociation which is sufficient to effectively capture the screw dislocations into the {111} plane. If the remaining mixed and edge-type segments are sufficiently mobile to glide under the applied stress they could give some slip on planes other than {111}, but it is unlikely that this would be in observable amounts unless some dislocation multiplication mechanisms were to operate. A Frank–Read source is not expected to work on any plane other than {111}, however, since it would require the expanding loop of dislocation to repeatedly pass through the screw orientation without being captured into a {111} plane.

Another factor which may contribute to the choice of slip plane is the lattice mobility of the dislocations. Nabarro (1952) has suggested that when a dislocation becomes extended the decrease in elastic energy is accompanied by an increase in mobility, so that dislocations would be expected to glide more easily on the {111} planes of a face-centred cubic metal. Aluminium is an interesting metal in this respect, since the nearly isotropic elastic properties and small dissociation give the dislocation energy only a small dependence on the slip plane orientation. The dislocations in the {111} plane will, however, be slightly wider so that dislocation mobility, which is a sensitive function of width, is expected to be greatest in this plane. This could explain the predominance of {111} slip at room temperatures; the occurrence of slip on other planes at higher temperatures is in agreement with the conclusion that the dependence of dislocation energy and mobility on slip plane orientation is smaller for aluminium than for most other face-centred cubic metals.

References

Eshelby, J. D., 1949, *Phil. Mag.*, **40**, 903.
Eshelby, J. D., Read, W. T., and Shockley, W., 1953, *Acta Metallurgica*, **1**, 251.
Lazarus, D., 1949, *Phys. Rev.*, **76**, 545.
Nabarro, F. R. N., 1952, *Advances in Physics*, **1**, 385.
Schmid, E., and Boas, W., 1950, *Plasticity of Crystals* (London : Hughes), p. 19.
Seeger, A., and Schöck, G., 1953, *Acta Metallurgica*, **1**, 519.

XII. *Soft X-Ray Spectra of Magnesium–Aluminium, Magnesium–Silicon and Aluminium–Silicon Alloys*

By K. Das Gupta* and E. Wood
University of Liverpool†

[Received October 1, 1954]

Abstract

The soft x-ray L spectra of the elements Mg, Al and Si have been determined in all three of the sets of binary alloys, and have been compared with the spectra of the pure elements. Several differences appear: (*a*) a widening of the emission edges with alloying, (*b*) in one case a probable diminution of band width and (*c*) structural changes in the shapes of the bands. We can attempt to understand these effects on the assumption that the alloys consist of two or more phases. No case of identity of the bands of the two constituents, such as might be expected from a perfectly ordered single-phase alloy, has been found.

§ 1. Introduction

The $L_{2,3}$ emission spectra of magnesium, aluminium and silicon in binary alloys of magnesium–aluminium, magnesium–silicon and aluminium–silicon of different percentage compositions have been studied with a ruled grating grazing incidence spectrograph. An investigation of the K spectra of these metals in some alloys has been made by Das Gupta (1946) and in magnesium–aluminium alloys by Farineau (1938). The $L_{2,3}$ spectra of magnesium, aluminium and silicon in a pure state have been investigated by Skinner (1940), and the structures in the bands have been interpreted in terms of the structure of the electron bands in the solid state. The high energy kinks in the spectra are evidence of the overlapping of Brillouin zones in these metals. Our purpose is to find out how the structures of the bands are changed on alloying.

§ 2. Experimental Technique

The spectrograph was the same as that employed by Skinner (1940). The concave glass grating of one metre radius of curvature having 30 000 lines per inch was set at 6° grazing incidence and the region

* Now at the Physics Department, University College of Science, Calcutta
† Communicated by H. W. B. Skinner, F.R.S.

40–400 A could be investigated in one fixed setting of the spectrograph. The slit system consists of three slits S_1, S_2 and S_3 set in proper alignment so that about 15 mm of the ruled grating are utilized to produce the spectrum. The slit S_1 immediately in front of the anti-cathode which acts as the source was 0·03 mm in width. The middle slit S_2 is about 1·5 mm and the slit S_3 nearest to the grating is about 0·7 mm.

In the designing of the x-ray tube, the technique of Skinner (1940) has been essentially followed. The modification that has been made consists mainly in introducing a liquid air trap very close to the copper target. A glass bulb of one litre volume was used for the x-ray tube.

It is considered preferable to use a glass tube rather than a metal tube from the point of view of cleaning and degassing, and also for observation during the exposure. The anticathode was a square sectioned copper tube, of 8 mm side and $\frac{1}{2}$ mm wall, mounted vertically on a glass cone. In this way any of the 4 faces could be used as a target for the exposure. If radiation is not to be wasted, the position of the anticathode face must be adjusted so as to present an oblique face to the slit S_1 which lies within the acceptance angle of the spectrograph. This involves the accurate adjustment of the axis of the anticathode relative to the spectrograph slit. In order to do this, a flange on the glass bulb is sealed by means of wax to the flange on which the slit is mounted, so that, by warming the wax, the bulb may be slid relative to the slit. The glass bulb is joined to the pumping system by a copper bellows in order to provide latitude for this adjustment. The electron gun was a vertical coil of nickel wire with oxide coating. This was placed a few mm from the anticathode face, and was surrounded by a cap in order to concentrate the beam on to an area of about 2×10 mm on the anticathode. An electron current of 50–100 mA at 3 kv could be obtained. This method, using a dull emission filament, rather than the tungsten filament used by Skinner, is convenient, but has the disadvantage that it is very difficult to avoid all traces of a Ba line at 165 A which may in certain cases be a nuisance.

It is most important to ensure that the surface of the metal used as target is free from contamination (oxide, etc.). For pure metals, therefore, we adopted the method of Skinner (1940) and evaporated thin layers of the material in a high vacuum on to the copper anticathode. For this purpose, an evaporating unit was placed behind the anticathode, on the opposite side to the electron gun. The problem for alloys is more difficult, and three methods were used.

(1) The two metals A and B to form the alloy are placed in small lumps separately in two conical tungsten filaments, in front of the target of the x-ray tube. When the vacuum of the order of 10^{-6} mm is attained, the filaments are raised to two different temperatures by regulating the current passing through them to adjust the rates of evaporation of the metals A and B so that an alloy of suitable composition is deposited on the target by the simultaneous evaporation of

the metals A and B. The evaporation rate of the metals must be slow and steady in order to give a homogeneous deposit. When a sufficiently thick layer has been obtained, the deposition must be ended by turning the target with the evaporation still running in order to ensure that the surface layer has the right composition. The target with the thin deposit of the alloy was then heated for about one hour at about 400°C in an attempt to make the structure homogeneous and ordered. It is difficult to judge how effective this procedure was. This method has the disadvantages that the composition of the alloy cannot be pre-determined with any accuracy, and also that the percentage can only be very roughly determined from the exposure time and density of the spectra obtained.

(2) The alloy is prepared beforehand in an induction furnace and the percentage composition is accurately determined by chemical analysis. The prepared alloy is placed in small lumps in a conical tungsten filament. When the proper vacuum is attained, the tungsten filament is raised very quickly to a very high temperature so that the entire lump is immediately evaporated and a deposit on the water-cooled copper target is formed having the same composition as that of the starting material. Several photographs were taken of one particular composition and the reproducible results justify the assumption that the composition was approximately maintained.

(3) A rectangular strip of alloy 2 cm × 5 mm of thickness varying from 0·3–0·5 mm of known composition was fixed to the water-cooled rectangular face of the copper target. A good contact of the alloy strip with the flat copper face of the target was obtained by grinding the alloy strip, as well as the anticathode, flat. The strip of alloy clamped to the target was cleaned in vacuum at regular intervals during the exposure by means of a steel wool brush. This method of obtaining a surface free from impurity turned out to be surprisingly effective, and of course the constitution of the alloy is much better guaranteed than with methods (1) and (2). But the method has the disadvantage that, since there is only a poor heat contact between the specimen and the copper anode, high excitation currents cannot be used.

Some of the alloys used in methods (2) and (3) were kindly supplied by the British Aluminium Company, with a report of the chemical analysis.

For methods (1) and (2) the x-ray tube was usually run at 3000 volts, 50–75 mA, and for method (3) 3000 volts, 20–30 mA. Exposures ranged from about $\frac{1}{2}$ hour for the pure metals up to several hours for weak alloys.

Several standard photographs of L_3 edges of pure magnesium and aluminium were taken in 1st and 2nd orders. The sharpness of the emission edges (of the order of 0·20 ev at room temperatures) was used as a check on the proper focusing of the spectrograph. Photographs were taken with different periods of exposure and from the photometer curves the most suitable exposure period to give a good photograph of a band was estimated.

Ilford Q_1 emulsions coated on to thin glass about $\frac{1}{3}$ mm thick were used throughout. No method of calibrating the blackening of the plate with intensity was used, and this must be borne in mind in studying the results to be given, because the denser exposures show definite signs of saturation.

The dispersion curve was obtained from the known wavelengths of a characteristic point on the K-band of graphite, which, by painting colloidal graphite on to a face of the anticathode, could be obtained in 8 different orders. These were found to agree well in form and wavelength with those obtained previously by Skinner (1940). Three spectra could be taken side by side by the use of a shutter in front of the plate, and it was usually arranged that the spectrum of the pure metal was taken side by side with the spectrum of the element in an alloy being investigated. In fact, if we are using method (1) of alloy preparation, the juxta-position of a spectrum of the pure metal is necessary so that one can judge roughly the composition of the alloy by the relative intensity of the two bands.

§ 3. Experimental Results

3.1. Mg–Al *Alloys*

In fig. 1, the $L_{2,3}$ spectra of Mg and Al are shown for various compositions of alloy. The corresponding spectra for the pure metals are also given for comparison.

(*a*) *Sharpness of Emission Edges*

In all the curves there is a sharp drop at the short wavelength limit of the band. This feature is known as ' the emission edge '. It is seen clearly separated into two components, the L_2 and L_3 edges, corresponding to the two x-ray levels excited. In all cases, there is no appreciable shift in the energy of the edge due to alloying. The L_3 edge breadth may be defined as the energy gap between the beginning of the drop in intensity of the L_3 edge and the beginning of the corresponding drop in the L_2 edge. Table 1 shows the results. The alloy compositions which are asterisked were determined chemically and were used as strips fixed to the target (method 3). The remainder were obtained by simultaneous evaporation (method 1), and therefore the compositions are only roughly known.

Table 1. Observed L_3 Edge Breadths for Mg and Al in Mg–Al Alloys

%Al	Al edge breadth (ev)	Mg edge breadth (ev)
0	—	0·2
5	—	0·4
9	—	0·4
50	0·7	0·3
60	0·5	0·4
70*	0·8	0·5
93*	0·6	—
95*	0·7	—
100	0·2	—

The values for the pure metals agree with those obtained at room temperature by Skinner (1940).

It will be seen that there is a marked rise in the edge breadths both for Al and Mg with even an alloy containing 5% of the other metal.

Fig. 1

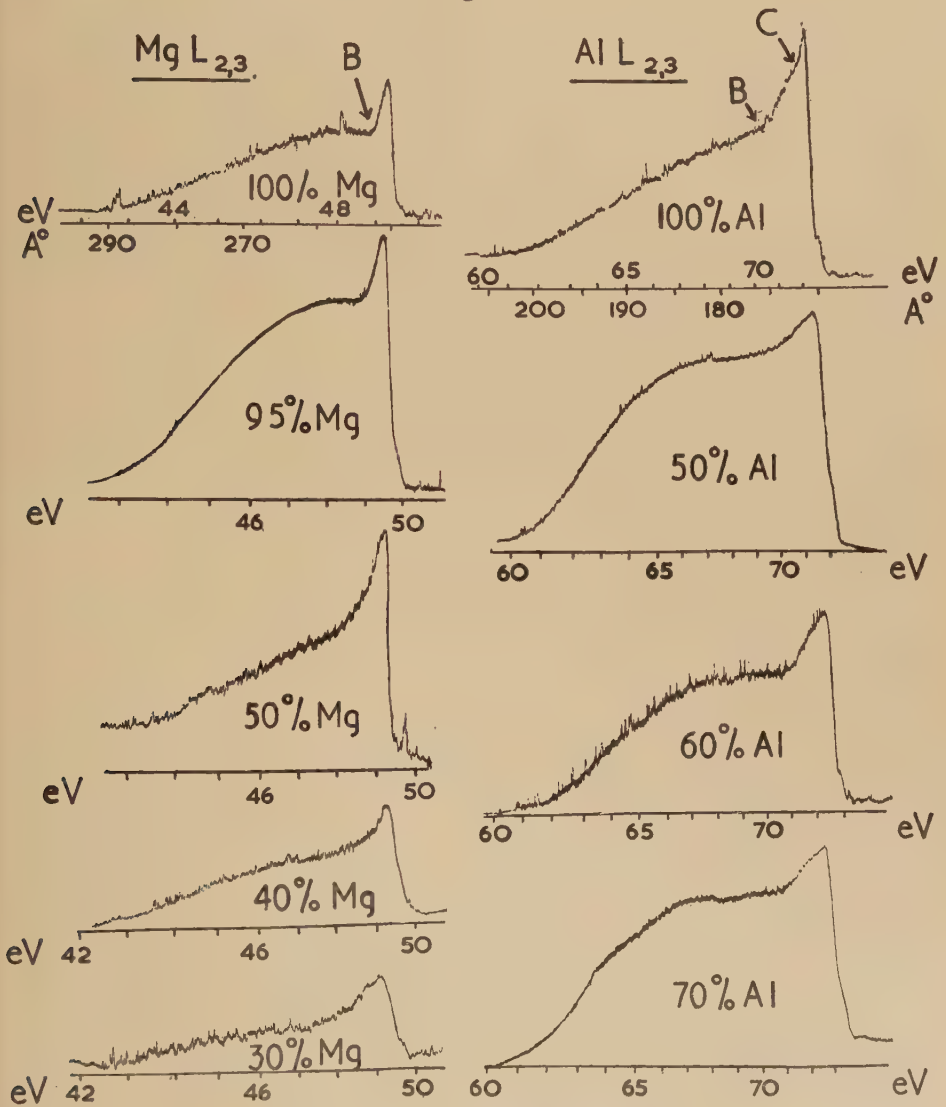

$L_{2,3}$ spectra from Mg–Al alloys.

A higher percentage does not appear, within the limits of error, to have much further effect.

The increase is a very clear effect. In a pure metal, Skinner (1940) has shown that the edge-widths correspond fairly accurately with the statistically calculated breadth of the Fermi edge at different temperatures.

But in the alloys, the edges are considerably wider than could be explained as a temperature effect; in fact the alloys would have to be molten to give so large a breadth. One may perhaps try to think of this effect as due to slight differences in the energy of individual transitions for emission by atoms differently placed in the lattice. In a pure metal, of course, each atom is surrounded by an identical array of atoms, but in an alloy, different arrangements of neighbours are obviously possible.

It is to be observed that we did not get any case of complete disappearance of the edge, such as was reported by Yoshida (1935) for the Al K band from a dilute solution of Al in Cu and by Skinner and Johnston (1937) for the Al L band and Be K band for weak solutions in Cu, and also, in the latter case, in Al. But it must be noted that we have not in the present experiments on Mg–Al alloys been able to use an alloy of less than 30%, whereas the effect reported by the other authors only appears in the Al–Cu alloys at less than 10%, and in the case of the Be alloys at roughly 1 to 2%. It is possible that the disappearance of the edge only occurs in the case of genuine solid solution. This cannot be proved from Skinner and Johnston's results on account of the considerable inaccuracy of their estimate of composition, but there certainly seem to be signs of the development of edges as the percentage rises to a figure much beyond the solubility limits. For comparison, these are given in table 2.

Table 2. Approximate Solubility Limits (% by weight) at Room Temperature for Various Alloys

Al in Mg	Al in Cu	Mg in Al	Be in Cu	Be in Al
2	9	2	0·2	?

(*b*) *Band Shapes*

The shapes of the bands for pure Mg and Al also correspond well with those of Skinner (1940). In Al, there are two clear kinks at B and C, but in Mg only one.

Figure 1 shows that the kink C in Al is obliterated on alloying. It is, however, possible that this is simply related to the widening of the edge. A similar obliteration was shown by Skinner to occur on simply heating pure Al to 670°K, in which case the edge breadth was 0·4 ev.

There is no clear movement of the point B on alloying in the case of Al, but there is certainly a definite progressive movement towards lower energies in the case of Mg. We might interpret this as an increase in the zone overlap due to the increased number of conduction electrons in the band on account of the fact that Al has 3 valence electrons as against 2 for Mg. Such a simple argument would lead to a movement of B for Al to higher energies on alloying. Actually B stays nearly fixed, and so the argument is probably oversimplified.

(*c*) *Band Widths*

With regard to the band widths, although many of the traces of fig. 1 are not suitable for accurate estimation, it will be seen that the L-bands

for both Al and Mg are not greatly altered in width by alloying. The Mg band is about 7 ev in width and the Al band about 11 ev, as compared with Skinner's results for the pure metals, namely $7{\cdot}2\pm0{\cdot}2$ and $13{\cdot}2\pm0{\cdot}4$. Our band width for pure Al therefore does not exactly agree with Skinner's value, but the low energy end of the photometer trace is not satisfactory for an accurate estimate, and subsequent work by Jacob and Wood has confirmed that Skinner's width is correct. There seems therefore to be a small decrease in the Al band-width on alloying with Mg. This is what would be expected if we assume that the band corresponds to an alloy with an average of rather less than 3 electrons per atom. The Mg bands are not sufficiently good to judge whether there is a corresponding increase in the band width of Mg. It is clear that there is no equality of band widths of Al and Mg in any alloy. Farineau (1938) reported such an equality in the case of the K-bands of Mg and Al in the compounds Mg_2Al_3 and Mg_3Al_2, which gave band widths of about 10·5 volts in each case as against his results of about 8 and 13 volts for the pure metals. The band shapes also changed into an identical form for the two constituents, possibly slightly different for the alloys Al_3Mg_2 and Al_2Mg_3. This result is certainly what one would expect in the case of an alloy which is a perfectly ordered inter-metallic compound. Farineau remarks that it is difficult to obtain such an alloy in a homogeneous phase. So, although we have covered the range between these two alloys (37·5% to 57·5 Mg by weight), and although we used heating to 400°C on the target for ordering, there is no positive test that our alloys were homogeneous. In view of the importance of the matter, further work is required, with an alloy of proved homogeneous phase.

At present it is clear that, at any rate for alloys which are not perfectly ordered intermetallic compounds, the electron band in the neighbourhood of one constituent is not of the same shape as in the neighbourhood of the other. From the work of Skinner and Johnston (1937), this conclusion also follows for dilute alloys of Be in Al and Cu. Since the band widths of pure Be, Al and Cu are not very different, no conclusion can be made about the equality of band widths in these cases. It appears from the present work for a whole range of Mg–Al alloys that neither the band widths nor shapes are the same, and, as we shall see subsequently, the same applies to other alloys.

3.2. Al–Si *Alloys*

Our results are shown in fig. 2, which consists of tracings of photometric curves. The dotted parts of the curves are uncertain. The alloys were of known composition and were clamped to the anti-cathodes as strips, the surface being cleaned by the wire brush. Other exposures were obtained using the method (2) of evaporation, but gave similar results. The broadening of the Al L_3 edge is somewhat less pronounced than in the case of the Mg–Al alloys but as the edge breadth in the case of the 5% alloy is about 0·5 ev, the effect seems present. It will be noted

that the kink C is still clear in spite of the edge widening. As in the case of the Mg alloys, the kink B remains, but a new marked kink at A has appeared, which might be interpreted as additional zone-overlapping through alloying with tetra-valent silicon.

Fig. 2

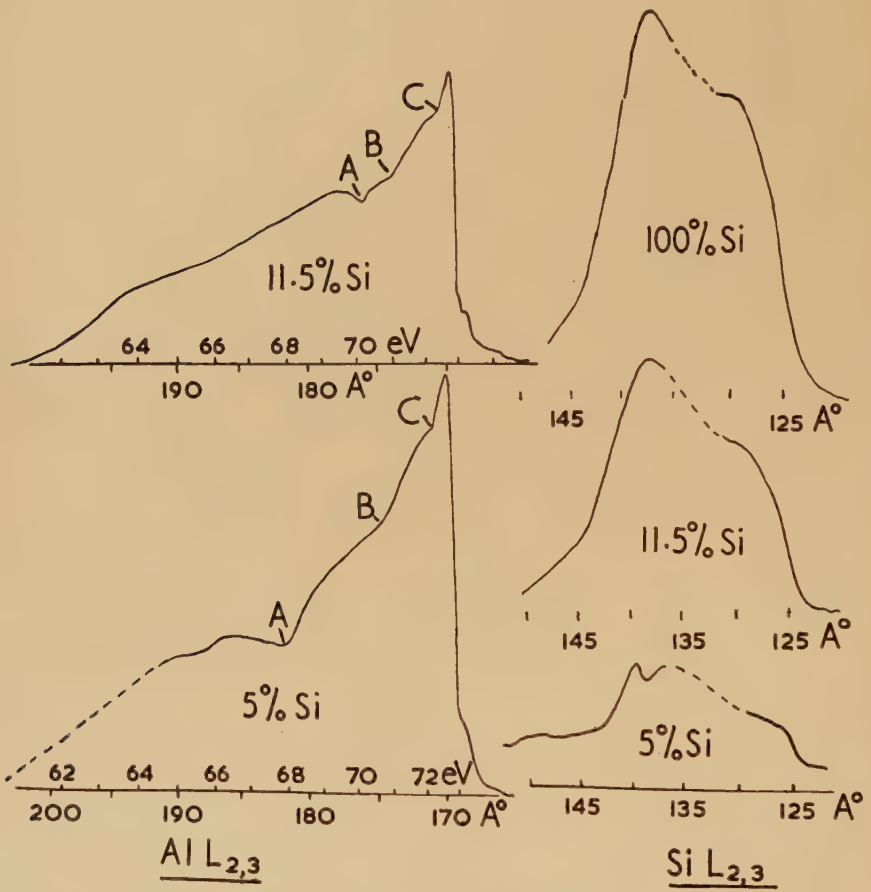

$L_{2,3}$ spectra from Al–Si alloys.

The Si band also appears to show structural changes in the case of the 5% alloy. The band widths of both Al and Si seem little affected by the alloying, even though the percentages of Si are low. Our curve is not suitable for finding the exact value of the Si band width, but Skinner (1940) gives 18·2 volts, and the Al bands are definitely considerably narrower than this. The solubility limit of Al in Si is $2\frac{1}{2}$% and there is practically no solubility of Si in Al.

3.3. Mg–Si *Alloys*

Three alloys were investigated which were prepared by the method (1) of simultaneous evaporation, followed by heat treatment on the target. The proportions of Mg and Si could roughly be estimated from

the relative intensities of the respective L bands. The results are shown in fig. 3. The 50% alloy may perhaps show an additional kink in the Mg band at C, though this is not certain. The weak alloy gave only a faint trace, and the results are perhaps not to be relied upon. But as far as the evidence goes, a considerable extension of the band towards low energies is indicated. It may be that there we have an example of the equalization of the band-widths of the two component metals in the case of a weak alloy. However, the solubility limit of Mg in Si is very small.

The Si band, in the alloy of 50% Si seems to show a definite structural change from that obtained with pure Si.

Fig. 3

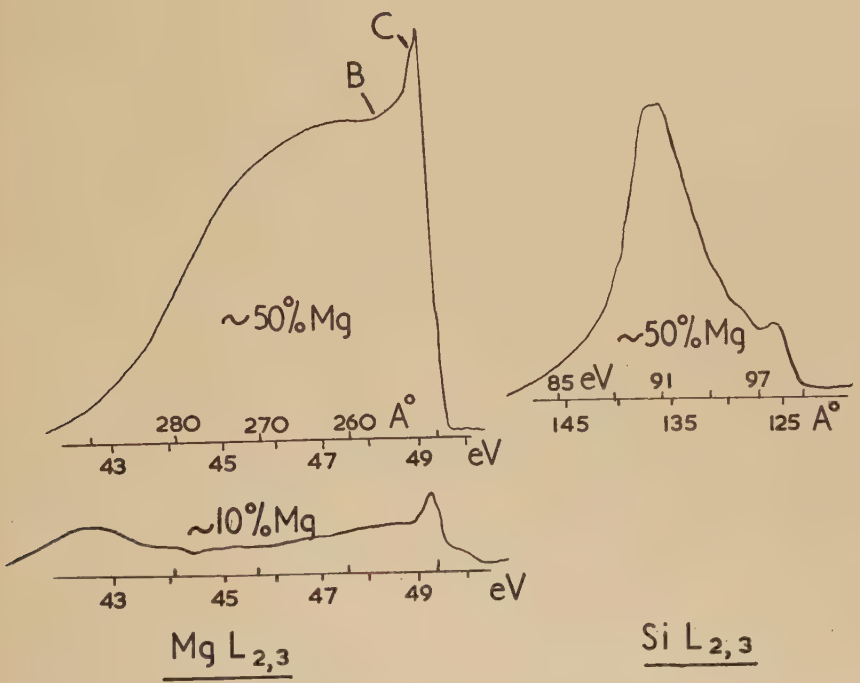

$L_{2,3}$ spectra from Mg–Si alloys.

§ 4. Conclusions

It seems clear that there is no one generally applicable picture of the effects of alloying on the soft x-ray bands. Three types of cases have to be considered :—

(1) There is some evidence by previous authors that in the case of genuine solid solutions, the edge of the band of the dilute constituent disappears completely. In these cases, there are apparently no electrons which take part in conductivity in the neighbourhood of the atoms of the dilute constituent. These atoms may perhaps act as 'donors' of electrons to the conduction band of the other atoms.

(2) There is the evidence of Farineau that in the case of the intermetallic compounds Mg_2Al_3 and Mg_3Al_2 the K-bands of both constituents are identical in shape and width. Although we have not worked with alloys of these definite compositions, in the case of the L-spectra we have not been able to find any signs of a similar case. Further work is needed to confirm Farineau's conclusion.

(3) There remain the rather nondescript set of ordinary alloys to which most of the present work applied. These consist of arbitrary proportions of the constituents and in these cases it may be that heat treatments, etc. are important factors. We have shown that in one case at least (Al–Mg alloy) the band-width of the Al is probably slightly diminished, though in the other cases the evidence is not good enough to draw any conclusion. We have also shown that the bands undergo structural changes on alloying, and that the edge-widths are broadened. These alloys must of course be expected to consist of mixtures of different phases and the results could be interpreted on the assumption that the alloys exist in the form of clusters of atoms of each type with a proportion of atoms of the other type included, rather than as a uniform mixture of both types of atom.

The authors acknowledge gratefully the interest taken in this work by Professor H. W. B. Skinner, F.R.S., who suggested it and was also partly responsible for writing up the results.

References

Das Gupta, K., 1946, *Ind. Journ. Phys.*, **20**, 226.
Farineau, J., 1938, *Ann. de Physique*, **10**, 20.
Skinner, H. W. B., 1940, *Phil. Trans. Roy. Soc.* A, **239**, 95.
Skinner, H. W. B., and Johnston, J. E., 1937, *Proc. Camb. Phil. Soc.* **34**, Pt. 1, 109.
Yoshida, S., 1935, *Scientific Papers, Tokyo*, **28**, 243.

XIII. *Point Defects and the Release of Energy from Deformed Nickel*

By J. F. Nicholas
Division of Tribophysics, C.S.I.R.O., University of Melbourne, Australia*

[Received October 25, 1954]

Summary

A plastically deformed specimen of nickel is assumed to consist of an assembly of spherical ' grains ' each of which contains a uniform distribution of point defects. On this model, a calculation is made of the rate of evolution of energy when such a specimen is heated at a uniform rate. The result is compared with experimental data given by Clarebrough, Hargreaves and West and it is shown that the model adequately explains a part of the evolution of energy at low temperatures. The activation energy for migration of the defects is calculated to be 1·0 ev (23 kcal/mole). It is suggested that the defects are probably vacancies but the possibilities that they are interstitials or vacancy pairs are not excluded. On the vacancy hypothesis, the energy stored per vacancy is about 1·6 ev and the size of the ' grains ' is of the same order as the size of the particles described by Gay and Kelly.

§ 1. Introduction

When a plastically deformed specimen of nickel is heated at a uniform rate, a considerable fraction of the energy stored during the deformation is released before recrystallization. A typical curve for the rate of release of energy as a function of temperature, as obtained by Clarebrough, Hargreaves and West (1953), is shown in fig. 1. There are two distinct

Fig. 1

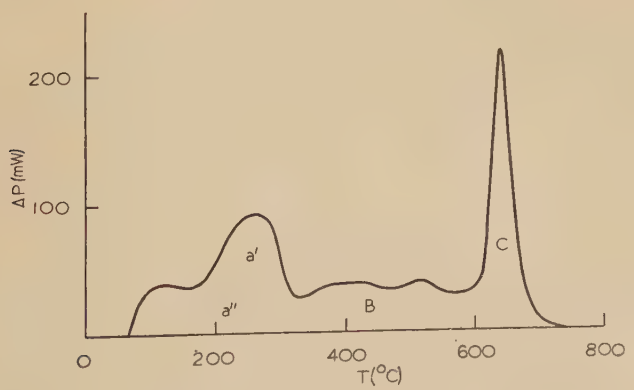

Typical result for the rate of evolution of energy from a specimen of deformed nickel as a function of temperature. The deformation used was 20 turns in torsion on a gauge length of 8 in. length and $\frac{3}{4}$ in. diameter. $\alpha = 0{\cdot}10°$C/sec.

* Communicated by W. Boas.

peaks, one at about 250°C and the other at about 600°C. These authors suggested that the release of energy represented by the peak at the lower temperature arises from the disappearance of vacancies created during the deformation. In the present paper this suggestion is put on a quantitative basis and it is shown that this peak can be explained as being due to the disappearance of an originally uniform array of point defects and that these defects are probably vacancies. It is further shown that the peak at the higher temperature cannot be explained on the same mathematically simple model.

§ 2. Theory

As a basis for calculation, the following assumptions are made :

(1) A deformed specimen of nickel consists of an assembly of spherical ' grains ' of radius a ;

(2) after deformation, but before heating, each ' grain ' contains a uniform distribution of point defects, their concentration being c_0 ;

(3) the defects move independently of each other by a diffusion-controlled process having energy of activation, Q, and frequency factor, D_0 ; and

(4) the ' grain boundaries ' act as infinite sinks for the defects and an energy, E, is evolved whenever a defect reaches a boundary.

If the whole volume, V, of the specimen is occupied by these ' grains ', we have $3V/4\pi a^3$ ' grains ' and the rate of evolution of energy, ΔP, is given by

$$\Delta P = -\frac{3V}{4\pi a^3} \cdot E \cdot \frac{dN}{dt},$$

where $N(t)$ is the total number of defects within a ' grain ' at time t. Further,

$$N = 4\pi \int_0^a r^2 c(r, t)\, dr,$$

where r is a radial co-ordinate within any ' grain ' and $c(r, t)$ is the concentration of defects at a point within a ' grain '.

Therefore, we can write

$$\Delta P = -\frac{3EV}{a^3} \int_0^a r^2 \frac{\partial c}{\partial t} dr \qquad \ldots\ldots (1)$$

and $c(r, t)$ must satisfy the equation

$$\frac{1}{D(t)} \frac{\partial c}{\partial t} = \nabla^2 c = \frac{1}{r^2} \frac{\partial}{\partial r}\left(r^2 \frac{\partial c}{\partial r}\right), \qquad \ldots\ldots (2)$$

where $D(t) = D_0 \exp(-Q/RT(t))$, $T(t)$ being the absolute temperature.

The solution of (2) subject to the appropriate initial and boundary conditions, viz. $c(a, t) = 0$ for $t > 0$ and $c(r, 0) = c_0$ for $0 \leqslant r < a$, is

$$c = -\frac{2ac_0}{\pi r} \sum_{n=1}^{\infty} \frac{(-1)^n}{n} \sin \frac{n\pi r}{a} \exp\left[-\frac{n^2\pi^2}{a^2} \int_0^t D(\tau)\, d\tau\right] \qquad \ldots (3)$$

(cf. eqn. (95) on p. 29 of Barrer (1941) where the r in the denominator before the Σ has been inadvertently omitted).

By substitution from (2) we can simplify (1) to the form

$$\Delta P = -\frac{3EV}{a^3} D(t) \left[r^2 \frac{\partial c}{\partial r} \right]_{r=a}, \quad \ldots \quad (4)$$

and on substituting (3) into (4) we obtain finally

$$\Delta P = \frac{6EVc_0}{a^2} D(t) \sum_{n=1}^{\infty} \exp \left[-\frac{n^2\pi^2}{a^2} \int_0^t D(\tau)\, d\tau \right]. \quad \ldots \quad (5)$$

Therefore, provided we know the dependence of T on t, we can in principle calculate ΔP as a function of time.

In the work of Clarebrough *et al.* the temperature is raised at a uniform rate, α, so that we can write

$$T(t) = T_0 + \alpha t. \quad \ldots \quad (6)$$

Using (6) and introducing a new variable $u(t) = Q/RT$, the integral in (5) can be written

$$\int_0^t D_0 \exp\left[-Q/R(T_0+\alpha\tau)\right] d\tau = -\frac{D_0 Q}{\alpha R} \int_{Q/RT_0}^{u} \frac{e^{-x}}{x^2}\, dx$$

$$= \frac{D_0 Q}{\alpha R} \left[\beta(u) - \beta(Q/RT_0)\right], \quad \ldots \quad (7)$$

where $\beta(u) = \mathrm{Ei}\,(-u) + \exp(-u)/u$.

Then, defining $\Delta P' = 6EVc_0 D_0/a^2$ and $K = \pi^2 D_0 Q/a^2 \alpha R$, we obtain finally,

$$\Delta P = \Delta P' \exp(-u) \sum_{n=1}^{\infty} \exp\left[-n^2 K(\beta - \beta_0)\right], \quad \ldots \quad (8)$$

where β_0 is the value of β for $T = T_0$, i.e., at zero time. Thus, for given Q and K the problem of plotting $\Delta P/\Delta P'$ as a function of t can be reduced to the evaluation of β and then the summation of the series

$$\sum_{n=1}^{\infty} \exp(-n^2\gamma),$$

where $$\gamma = K(\beta - \beta_0).$$

The evaluation of β can be carried out by use of the tables and formulae given by Coulson and Duncanson (1942) or by use of the asymptotic series

$$\beta(u) = \mathrm{Ei}(-u) + e^{-u}/u = (e^{-u}/u^2)\left(1 - \frac{2}{u} + \frac{6}{u^2} - \ldots\right). \quad \ldots \quad (9)$$

It is clear that β is a rapidly decreasing function of u so that, provided T is not very close to T_0, β_0 can be neglected in comparison to β.

In order to obtain 1% accuracy in the summation of the series, it is necessary to consider only the first term if $\gamma > 1{\cdot}535$ while two terms suffice for $\gamma > 0{\cdot}57$. However, for smaller values of γ, corresponding to lower temperatures, the series converges only slowly and it is convenient to transform it according to the relation (Whittaker and Watson 1946)

$$\sum_{n=1}^{\infty} \exp(-n^2\gamma) = \frac{1}{2}\left\{\left(\frac{\pi}{\gamma}\right)^{1/2} - 1\right\} + \left(\frac{\pi}{\gamma}\right)^{1/2} \sum_{n=1}^{\infty} \exp\left(-\frac{n^2\pi^2}{\gamma}\right). \quad \ldots \quad (10)$$

If only 1% accuracy is required the series on the right-hand side of (10) can be neglected in comparison with the first bracket for any $\gamma<1{\cdot}49$. Thus it is simple to evaluate $\Delta P/\Delta P'$ over any range of u.

By differentiating the first term of (8), we find that this expression has one maximum, this occurring at a value of u for which $K\beta<1$ i.e. at a point where this term is not a good approximation to $\Delta P/\Delta P'$. However, on substituting the first bracket of (10) for the series in (8) and differentiating, we find that this expression also has one maximum value which occurs when

$$K(\beta-\beta_0)^3=\pi\{(\beta-\beta_0)^2-\tfrac{1}{2}\,\mathrm{e}^{-u}/u^2\}^2 \quad . \quad . \quad . \quad . \quad . \quad (11)$$

By neglecting β_0 and using the asymptotic series (9) for β, (11) reduces to

$$K=\frac{\pi}{4}u^2\,\mathrm{e}^u\left(1-\frac{2}{u}-\frac{2}{u^2}+\frac{8}{u^3}\cdots\right). \quad . \quad . \quad . \quad . \quad (12)$$

From (12) and (9) it is clear that, at this maximum, $K\beta\sim\pi/4<1{\cdot}49$. Therefore, $\Delta P/\Delta P'$ should have a maximum at this value of u and, from the discussion above, this should be the only maximum of $\Delta P/\Delta P'$.

Finally, by taking logarithms of both sides of (12) and substituting for K and u, we obtain

$$\ln\frac{4\pi D_0R}{a^2Q}-\frac{Q}{RT^*}=\ln\left[\frac{\alpha}{T^{*2}}\left(1-\frac{2RT^*}{Q}-\frac{2R^2T^{*2}}{Q^2}+\cdots\right)\right] \quad . \quad (13)$$

where T^* is the temperature at which ΔP is a maximum.

Therefore, from a series of values of α and T^*, i.e., of heating rate and temperature for maximum ΔP, we can plot $\ln(\alpha/T^{*2})$ against $1/T^*$ and hence obtain a first approximation to Q/R by calculating the slope by the method of least squares. The method of successive approximations can then be used to refine this value and to evaluate D_0/a^2, the linearity of the final relationship giving a check on the validity of the theory. When we have values of Q/R and D_0/a^2 we can use the procedure outlined above to plot $\Delta P/\Delta P'$ as a function of T (or of t) and this curve can be compared with that determined experimentally. From the maximum value of ΔP_{expt}, $\Delta P'$ can be calculated and hence a value obtained for Ec_0.

One relaxation of the basic assumptions can be made. Instead of assuming that all the ' grains ' have the same radius, a, we may suppose that their radii form a statistical distribution of fairly narrow width about some mean value. A recalculation on the basis of this model leaves the whole theory unaltered except that the a appearing in the definition of K must be interpreted as the ratio

$$\frac{\text{second moment (about zero) of the grain radii}}{\text{first} \quad ,, \quad (\quad ,, \quad ,, \quad) \quad ,, \quad ,, \quad ,, \quad ,,}$$

while the a^2 in the definition of $\Delta P'$ must be interpreted as

$$\frac{\text{third moment (about zero) of the grain radii}}{\text{first} \quad ,, \quad (\quad ,, \quad ,, \quad) \quad ,, \quad ,, \quad ,, \quad ,,}.$$

Therefore, the determinations of Q and K and of the shape of the final curve will remain unaltered. Further, provided the distribution of radii is not too skew, only small errors will be introduced by treating the grain radius as having a unique value, a, equal to the mean value of the distribution. This result suggests furthermore that the shape of the calculated $\Delta P - T$ curve will be insensitive to the shape of the ' grains ' considered.

It is formally possible to make calculations, analogous to those above, for metals containing uniformly distributed arrays of line defects (e.g. dislocations) or of plane defects (e.g. grain boundaries). In each case, an expression similar to (8) is found except that (i) the expressions for K and $\Delta P'$ are slightly modified to take account of the different geometry and (ii) in the summand, n is replaced by δ_n for line defects and by $(2n-1)$ for plane defects, δ_n being the ratio of the nth to the first zero of $J_0(x)$. Further, expressions can be found for the variation of T^* with α so that, provided an experimental value for this variation is known, Q/R and K can be calculated and thence $\Delta P/\Delta P'$ plotted as a function of T. An example is given in fig. 4 of the shapes predicted by the three different assumptions about the nature of the defects for the same set of experimental results. Clearly, on changing from point to line to plane defects the width of the peak is decreased but the general shape of the curve is not greatly affected. In no case has it been possible to distinguish definitely between the three theoretical curves on the basis of agreement with experiment. However, on physical grounds, while it seems reasonable to consider an originally uniform array of point defects moving independently, arrays of line or plane defects will form networks and the movements of the various parts will be interdependent. For this reason, the equations for line and plane defects are not set out in detail here.

§ 3. Application to Experimental Results

In this section, the experimental results of Clarebrough *et al.* (to be published) are used to determine a series of corresponding values of α and T^*. From these, Q and D_0/a^2 are evaluated and $\Delta P - T$ curves plotted. The shapes of the calculated curves are then compared with the shapes determined experimentally and good agreement is found in the case of the low-temperature peaks in nickel.

Heating rate, α (°K/sec)	Temperature of first peak, T^* (°K)	Maximum of ΔP_{expt} (mw)
0·10	532	61
0·067	522	42
0·033	508	25

The table lists the values of α, T^*, and maximum ΔP that are used in the calculations, the data being taken from the experimental curves for a set of nickel specimens cut from one bar that had been deformed in torsion (see fig. 2). When these values are substituted into eqn. (13) and the constants adjusted by the methods of least squares and successive approximations (as described in the paragraph below eqn. (13)), the results are

found to fit a straight line, as shown in fig. 3, the final values for the constants being

$$Q = 22{\cdot}6 \text{ kcal/mole} = 0{\cdot}98 \text{ ev/defect}$$

and

$$D_0/a^2 = 5{\cdot}467 \times 10^5 \text{ sec}^{-1}.$$

Fig. 2

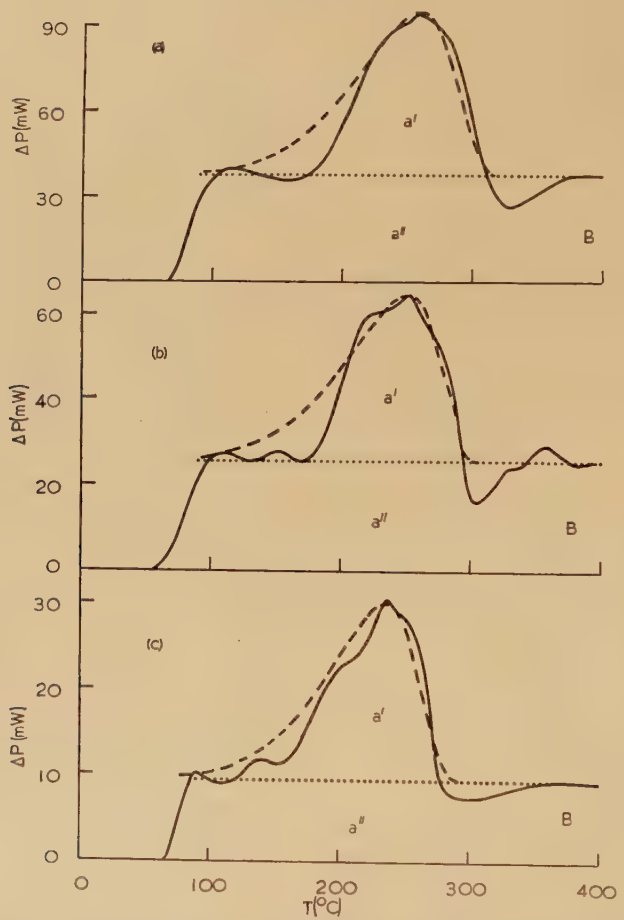

Solid lines show the low-temperature parts of experimental $\Delta P - T$ curves for nickel deformed as described in the legend to fig. 1. Heating rates were (*a*) 0·10°c/sec, (*b*) 0·07°c/sec, and (*c*) 0·03°c/sec. The dashed lines are the calculated curves for these cases relative to the dotted horizontal line which represents the backward extrapolation of part B of the experimental curve.

Since there are only three points to which the line is fitted, no great accuracy can be expected for these figures. However, using the deviations from linearity to provide an estimate of the errors involved, Q is found to have a standard deviation of $\pm 1{\cdot}0$ kcal/mole while D_0/a^2 is accurate to

within a factor of 2·8, the large variation in this latter value arising because eqn. (13) involves only ln (D_0/a^2). The constants are quoted here to more figures than are justifiable since these values were used in the calculations to maintain consistency.

At this stage it should be noted that, for this value of Q, the value of u at the maximum of $\Delta P/\Delta P'$ is approximately 20 so that the use of the asymptotic series (9) and (12) is justified.

By use of (8) and (10), $\Delta P/\Delta P'$ can now be plotted as a function of T but, in order to compare the results with experiment, we must determine a value for $\Delta P'$ by comparing the maximum values of ΔP_{expt} and $(\Delta P/\Delta P')_{\text{calc}}$. There are two possibilities here depending on whether the whole or only a part of the experimental rate of evolution of energy at the temperatures involved is ascribed to the movement of the point defects.

Fig. 3

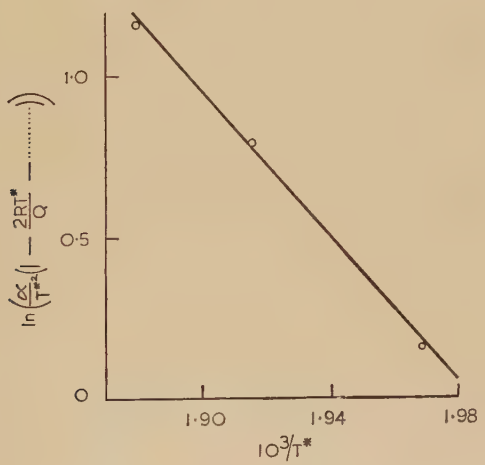

Plot of ln $\{\alpha/T^{*2}(1-2RT^*/Q-\ldots)\}$ against $1/T^*$ from the data of fig. 2.

If the total rate of evolution at T^* is used, then the calculated ΔP curves are much narrower than the experimental curves. Therefore, it will be assumed that the almost ' horizontal ' part, B, of the experimental curve (see fig. 1) can be produced back to lower temperatures and that only the energy represented by the area, a', lying above this line should be ascribed to the movement of the point defects. Use of the corresponding values of the maximum of ΔP_{expt} (see table) leads to slightly different values for $\Delta P'$ in each case. Therefore, a weighted mean value for $\Delta P'$ was determined using weights of 3, 2, and 1 respectively for the runs as set out in the table. This mean value corresponds to $Ec_0 = 1{\cdot}22$ cal/cm^3. The dotted curves in fig. 2 show the final plots of ΔP against T and the agreement between theory and experiment is seen to be reasonable.

In all this calculation there is some uncertainty about what value to use for T_0, but a consideration of the experimental work suggests that it lies between room temperature and 70°C, this latter temperature being

that at which the first evolution of energy occurs. In the curves plotted in fig. 2, T_0 has been taken as equal to 70°C (343°K). The choice of $T_0=273$°K would have reduced all the ΔP values at low temperatures but since the decreases range from 25% at 80°C to less than 1% at 120°C, the effect on the general shape of the curve is negligible.

Experimental data for the change in temperature for a peak with heating rate is also available for two other cases viz. the high-temperature peak in the curves for nickel deformed in torsion (part C in fig. 1) and the single peak in the curves for copper deformed in tension. From this data, values of Q and K have been calculated and curves for ΔP_{calc} plotted on the assumptions of point, line, and plane defects. In fig. 4 a typical set of calculated and experimental curves are plotted and it is clear that the

Fig. 4

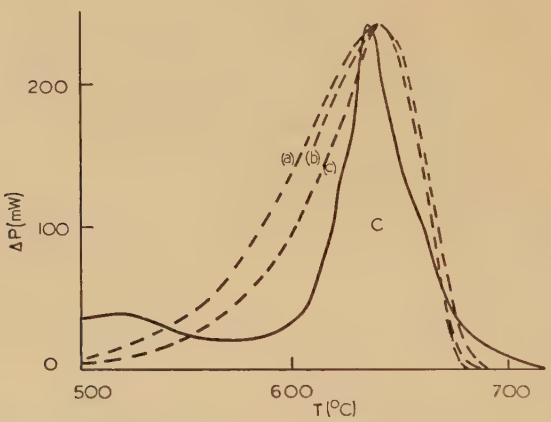

High-temperature part of the curve in fig. 1 in comparison with curves (dashed) calculated on the assumptions of (*a*) point, (*b*) line, and (*c*) plane defects. Curve (*b*) has not been computed for small values of T but it must lie between curves (*a*) and (*c*).

experimental curve has a much narrower peak than any of the calculated curves, a result which is true for both the sets of peaks discussed in this paragraph. This lack of agreement is not altogether surprising since both these sets of peaks are associated with recrystallization and the present model of defects originally distributed uniformly and moving independently is clearly not applicable to a metal during recrystallization.

§ 4. Discussion

In this section, only the peaks occurring at the lower temperature in the curves for nickel will be considered and it will be assumed that they are due to the movement of point defects. The nature of these point defects has been immaterial up to this stage but the assumption will now be made that they are vacancies. Later on, the modifications consequent on the alternative assumptions that they are interstitials or vacancy pairs will be pointed out.

In order to calculate the energy, E, released per defect, an estimate of the initial concentration, c_0, is required. There is a marked increase in density at about the same temperature as T^* and it seems logical to associate the two phenomena. We therefore ascribe the whole density change when a sample of the deformed metal is annealed at, say (T^*+50)°K, to the disappearance of the vacancies present in the deformed material. The measurements of Clarebrough *et al.* (to be published) then give $c_0=2{\cdot}0\times10^{19}$ vacancies/cm^3 from which we deduce that

$$E=37 \text{ kcal/mole}=1{\cdot}6 \text{ ev/vacancy}.$$

The total energy $E+Q=60$ kcal/mole should be of the order of the activation energy for self-diffusion and although this has not been measured directly, Le Claire (1953) gives two empirical methods of estimating it, viz. $39\times$(melting temperature in °K) and $0{\cdot}66\times$(latent heat of sublimation). For nickel, these estimates give 67 and 54 kcal/mole. This excellent agreement may be fortuitous since, if we use Le Claire's theoretical arguments (based on the assumption that diffusion in a face-centred cubic metal occurs by the movement of vacancies) to compute the components of the activation energy of self-diffusion, these do not agree nearly so well with the values of E and Q. Using Le Claire's formulae, the activation energy for formation of a vacancy in nickel, ΔH_1, should be 17·3 kcal/mole and the activation energy for movement, ΔH_2, should be 54·8 kcal/mole. These discrepancies will be discussed below.

Le Claire's work also gives us a means of estimating the order of magnitude of D_0. It should be noted that, in the notation of the present paper. D_0 is the frequency factor for diffusion of vacancies *already present in the lattice* and not the frequency factor for self-diffusion by a vacancy mechanism since this latter quantity involves the entropy of *formation* of the vacancies. Then, from Le Claire, we have

$$D_0=\nu b^2 \exp(\Delta S/R) \text{ and } \Delta S=-Q(\mu'-\rho'), \quad . \quad . \quad . \quad . \quad (14)$$

where ν=frequency of vibration of an atom next to a vacancy, b=lattice parameter, ΔS=entropy of activation for the migration of a vacancy, and μ', ρ' are the temperature coefficients of an appropriate elastic modulus and the density at the absolute zero of temperature. Using (14), with ν equal to half the Debye frequency and Young's modulus as the appropriate elastic modulus, D_0 can be calculated and hence the value of 'grain' radius determined as $a=3{\cdot}4\times10^{-4}$ cm.

In view of the possible errors in the value of D_0/a^2 and in view of the assumptions made in deriving and applying eqn. (14), it seems unwise to attach too much weight to this value of a. However, this 'grain size' of 7μ is more comparable with the limits of 'particle size', viz. 1·9μ to 0·04μ, found by Gay and Kelly (1953) in nickel rolled 33% than with the crystal size of approximately 100μ that Clarebrough *et al.* have found by microscopic examination of their specimens. On this basis the 'grains' of the present theory will be tentatively identified with the

' particles ' of Gay and Kelly and it will therefore be assumed that most of the vacancies disappear by absorption onto the edge dislocations which exist in the ' particle ' boundaries (Gay, Hirsch and Kelly 1954).

On this interpretation of the results, E becomes a measure of the mean energy evolved when a vacancy is absorbed onto an edge dislocation in a particle boundary and this should not be identical with the ΔH_1 of Le Claire's theory since this latter is the energy for formation of a vacancy in a perfect lattice. A discussion of the relative magnitudes of E and ΔH_1 is pointless since the value of E depends directly on the value assumed for c_0 i.e. on the assumptions made about the relationship between overall density change and number of vacancies originally present.

The discrepancy between Q and the theoretical estimate of ΔH_2 is more serious since both purport to be measures of the same quantity, viz. the activation energy for migration of a vacancy in nickel. This is not strictly true since Q has been determined from measurements on a deformed metal and the work of Gay *et al.* has shown that even within the ' particles ' there is still a certain amount of strain. Thus, we might expect Q to be less than the value ΔH_2 found from work on annealed metals. Furthermore, Le Claire's formula for ΔH_2 contains two possible sources of error viz. (i) a numerical factor calculated from diffusion data on other metals and (ii) an uncertainty in the choice of an appropriate elastic modulus. In this connection, it is interesting to note that Le Claire's formula gives ΔH_2 for copper equal to 36 kcal/mole. This is considerably higher than the theoretical value of about 22 kcal/mole given by Huntington and Seitz (1942) or Bartlett and Dienes (1953).

Let us now consider the possibilities that the moving defects are either interstitials or vacancy pairs. There are no theoretical values for the activation energies of migration for either of these defects in nickel but for copper, Huntington (1953) estimates 0·25 ev for the energy of migration of an interstitial atom while Bartlett and Dienes (1953) estimate 0·34 ev for the energy of migration of a vacancy pair, both values being considerably less than Q. While Huntington's work cannot easily be extended to nickel, substitution of the appropriate figures for nickel into the formulae of Bartlett and Dienes causes very little change from the copper results. Thus the measured value of Q provides strong support for the suggestion that the defects are vacancies.

A further argument against the postulate of interstitials causing the peak is provided by the measurements of density. On the same assumption as before, i.e. that the first increase in density is associated with the peak in the ΔP curve, this implies that the disappearance of an interstitial atom *increases* the density. While this seems unlikely at first sight, it is not impossible since the removal of an interstitial atom does allow the lattice to become more close-packed. However, since atoms are not hard spheres, the elastic forces will almost certainly ensure that any density increase due to the removal of an interstitial atom is less

than 10% of that associated with the removal of one vacancy. This would imply $E<0{\cdot}16$ ev per interstitial, a value that seems far too low to be the energy released on the disappearance of an interstitial atom. In the case of vacancy pairs, the density argument follows the same lines as for single vacancies and we find $E=3{\cdot}2$ ev per vacancy pair which is not unreasonable.

Therefore, it can be concluded that the assumptions set out in § 2 provide a model that gives a consistent description of part of the release of energy from deformed nickel. Furthermore, while it is not impossible that the defects involved are interstitials or vacancy pairs, the data deduced from the experiments can be interpreted most reasonably on the assumption that the defects are single vacancies.

Acknowledgments

The experimental work on which this paper is based has been carried out by L. M. Clarebrough, M. E. Hargreaves and G. W. West. The author would like to thank his colleagues for allowing him free use of their results before publication. Thanks are also due to Miss M. Thomson for assistance with some of the computations.

References

Barrer, R. M., 1941, *Diffusion in and through Solids* (Cambridge: University Press).
Bartlett, J. H., and Dienes, G. J., 1953, *Phys. Rev.*, **89**, 848.
Clarebrough, L. M., Hargreaves, M. E., and West, G. W., 1953, *Phil. Mag.*, **44**, 913.
Coulson, C. A., and Duncanson, W. E., 1942, *Phil. Mag.*, **33**, 754.
Gay, P., Hirsch, P. B., and Kelly, A., 1954, *Acta Cryst.*, **7**, 41.
Gay, P., and Kelly, A., 1953, *Acta Cryst.*, **6**, 165.
Huntington, H. B., 1953, *Phys. Rev.*, **91**, 1092.
Huntington, H. B., and Seitz, F., 1942, *Phys. Rev.*, **61**, 315.
Le Claire, A. D., 1953, *Acta Met.*, **1**, 438.
Whittaker, E. T., and Watson, G. N., 1946, *Modern Analysis* (Cambridge University Press), p. 124, Ex. 18.

XIV. CORRESPONDENCE

The Vibrations of a Stressed Framework

By H. C. Longuet-Higgins
The University Chemical Laboratory, Cambridge

[Received October 1, 1954]

In this note equations are derived for the normal modes of vibration of a system of massive particles connected in pairs by light springs. The case of interest is that in which the number of springs exceeds the number of internal degrees of freedom of the system; for then in equilibrium the springs will be under stress, and the vibrational modes will depend on the equilibrium stresses as well as on the force constants of the springs.

Let $\boldsymbol{r}_\alpha$ be the position vector of particle α in equilibrium, and denote $\boldsymbol{r}_\alpha - \boldsymbol{r}_\beta$ by $\boldsymbol{r}_{\alpha\beta}$. Then the force exerted on particle α by particle β in equilibrium is

$$\frac{-\phi_{\alpha\beta}\,\boldsymbol{r}_{\alpha\beta}}{r_{\alpha\beta}}$$

where $\phi_{\alpha\beta}$ is the equilibrium tension in the spring $\alpha\beta$.

Now let the system be distorted slightly from equilibrium, so that the position of α becomes $\boldsymbol{r}_\alpha + \boldsymbol{s}_\alpha$. The vector distance of α from β is now $\boldsymbol{r}_{\alpha\beta} + \boldsymbol{s}_{\alpha\beta}$, where $\boldsymbol{s}_{\alpha\beta} = \boldsymbol{s}_\alpha - \boldsymbol{s}_\beta$, and the scalar distance is $r_{\alpha\beta} + q_{\alpha\beta}$, where $r_{\alpha\beta}\, q_{\alpha\beta} = \boldsymbol{r}_{\alpha\beta} \cdot \boldsymbol{s}_{\alpha\beta}$. The tension in the spring $\alpha\beta$ may therefore be written $\phi_{\alpha\beta} + \psi_{\alpha\beta}\, q_{\alpha\beta}$, where $\psi_{\alpha\beta}$ is the force constant, and the force exerted on α by β is

$$\frac{-(\phi_{\alpha\beta} + \psi_{\alpha\beta}\, q_{\alpha\beta})(\boldsymbol{r}_{\alpha\beta} + \boldsymbol{s}_{\alpha\beta})}{r_{\alpha\beta} + q_{\alpha\beta}}$$

which, to the first order of small quantities, is equal to

$$-\left\{\chi_{\alpha\beta}\boldsymbol{r}_{\alpha\beta} + \frac{\omega_{\alpha\beta}\, q_{\alpha\beta}\, \boldsymbol{r}_{\alpha\beta}}{r_{\alpha\beta}} + \chi_{\alpha\beta}\, \boldsymbol{s}_{\alpha\beta}\right\}$$

where $\chi_{\alpha\beta} = \phi_{\alpha\beta}/r_{\alpha\beta}$, $\omega_{\alpha\beta} = \psi_{\alpha\beta} - \phi_{\alpha\beta}/r_{\alpha\beta}$.

Now in a normal mode of frequency ν, the total force on α must equal $-4\pi^2\nu^2 m_\alpha \boldsymbol{s}_\alpha$, where m_α denotes the mass of the particle. But $\sum_\beta^{\neq\alpha} \chi_{\alpha\beta}\, \boldsymbol{r}_{\alpha\beta} = 0$, since the total force vanishes in equilibrium. Hence, if $\lambda = 4\pi^2\nu^2$,

$$\lambda m_\alpha\, \boldsymbol{s}_\alpha = \sum_\beta^{\neq\alpha} \left\{\frac{\omega_{\alpha\beta}\, q_{\alpha\beta}\, \boldsymbol{r}_{\alpha\beta}}{r_{\alpha\beta}} + \chi_{\alpha\beta}\, \boldsymbol{s}_{\alpha\beta}\right\}.$$

Therefore

$$\lambda \boldsymbol{s}_{\alpha\gamma} = \lambda(\boldsymbol{s}_\alpha - \boldsymbol{s}_\gamma)$$

$$= \frac{1}{m_\alpha} \sum_\beta^{\neq\alpha} \left\{\frac{\omega_{\alpha\beta}\, q_{\alpha\beta}\, \boldsymbol{r}_{\alpha\beta}}{r_{\alpha\beta}} + \chi_{\alpha\beta}\, \boldsymbol{s}_{\alpha\beta}\right\} - \frac{1}{m_\gamma} \sum_\varepsilon^{\neq\gamma} \left\{\frac{\omega_{\gamma\varepsilon}\, q_{\gamma\varepsilon}\, \boldsymbol{r}_{\gamma\varepsilon}}{r_{\gamma\varepsilon}} + \chi_{\gamma\varepsilon}\, \boldsymbol{s}_{\gamma\varepsilon}\right\}.$$

Taking the scalar product of both sides with $\boldsymbol{r}_{\alpha\gamma}/r_{\alpha\gamma}$, one obtains

$$\lambda q_{\alpha\gamma}=\frac{1}{m_\alpha}\sum_{\beta}^{\neq\alpha}\left\{\omega_{\alpha\beta}\,c_{\gamma\alpha\beta}\,q_{\alpha\beta}+\chi_{\alpha\beta}\,\frac{\boldsymbol{r}_{\alpha\gamma}\cdot\boldsymbol{s}_{\alpha\beta}}{r_{\alpha\gamma}}\right\}+\frac{1}{m_\gamma}\sum_{\varepsilon}^{\neq\gamma}\left\{\omega_{\gamma\varepsilon}\,c_{\alpha\gamma\varepsilon}\,q_{\gamma\varepsilon}+\chi_{\varepsilon\gamma}\,\frac{\boldsymbol{r}_{\gamma\alpha}\cdot\boldsymbol{s}_{\gamma\varepsilon}}{r_{\gamma\alpha}}\right\},$$

where $c_{\gamma\alpha\beta}$ is the cosine of the angle $\gamma\alpha\beta$. Now

$$\begin{aligned}\boldsymbol{r}_{\alpha\gamma}\cdot\boldsymbol{s}_{\alpha\beta}&=(\boldsymbol{r}_{\alpha\beta}+\boldsymbol{r}_{\beta\gamma})\cdot\boldsymbol{s}_{\alpha\beta}\\&=r_{\alpha\beta}\,q_{\alpha\beta}+\boldsymbol{r}_{\beta\gamma}\cdot(\boldsymbol{s}_{\alpha\gamma}+\boldsymbol{s}_{\gamma\beta})\\&=r_{\alpha\beta}\,q_{\alpha\beta}+(\boldsymbol{r}_{\beta\alpha}+\boldsymbol{r}_{\alpha\gamma})\cdot\boldsymbol{s}_{\alpha\gamma}-r_{\beta\gamma}\,q_{\beta\gamma}\\&=r_{\alpha\beta}\,q_{\alpha\beta}-r_{\beta\gamma}\,q_{\beta\gamma}+r_{\alpha\gamma}\,q_{\alpha\gamma}+\boldsymbol{r}_{\alpha\beta}\cdot\boldsymbol{s}_{\gamma\alpha}.\end{aligned}$$

Using again the fact that $\sum_{\beta}^{\neq\alpha}\chi_{\alpha\beta}\,\boldsymbol{r}_{\alpha\beta}=0$, we obtain finally

$$\begin{aligned}\lambda q_{\alpha\gamma}=&\frac{1}{m_\alpha}\sum_{\beta}^{\neq\alpha}\left\{\omega_{\alpha\beta}\,c_{\gamma\alpha\beta}\,q_{\alpha\beta}+\chi_{\alpha\beta}\left(\frac{r_{\alpha\beta}}{r_{\alpha\gamma}}q_{\alpha\beta}-\frac{r_{\gamma\beta}}{r_{\alpha\gamma}}q_{\beta\gamma}+q_{\alpha\gamma}\right)\right\}\\&+\frac{1}{m_\gamma}\sum_{\varepsilon}^{\neq\gamma}\left\{\omega_{\gamma\varepsilon}\,c_{\alpha\gamma\varepsilon}\,q_{\gamma\varepsilon}+\chi_{\gamma\varepsilon}\left(\frac{r_{\gamma\varepsilon}}{r_{\gamma\alpha}}q_{\gamma\varepsilon}-\frac{r_{\varepsilon\alpha}}{r_{\gamma\alpha}}q_{\varepsilon\alpha}+q_{\gamma\alpha}\right)\right\}.\end{aligned}$$

This is a set of homogeneous linear equations of the form

$$\sum_j A_{ij}\,q_j=\lambda q_i,$$

where i and j denote pairs of particles. If i and j refer to the same pair of particles (α,γ), then

$$A_{ii}=\frac{1}{m_\alpha}\left(\psi_{\alpha\gamma}+\sum_{\beta}^{\neq\alpha}\chi_{\alpha\beta}\right)+\frac{1}{m_\gamma}\left(\psi_{\alpha\gamma}+\sum_{\varepsilon}^{\neq\gamma}\chi_{\gamma\varepsilon}\right).$$

If i denotes the pair (α,γ) and j the pair (α,β) then

$$A_{ij}=\frac{1}{m_\alpha}\left(\omega_{\alpha\gamma}\,c_{\beta\alpha\gamma}+\chi_{\alpha\beta}\frac{r_{\alpha\beta}}{r_{\alpha\gamma}}\right)-\frac{1}{m_\gamma}\chi_{\beta\gamma}\frac{r_{\alpha\beta}}{r_{\alpha\gamma}};$$

and if i and j have no common member then $A_{ij}=0$.

If there are n particles, there will be $\frac{1}{2}n(n-1)$ equations altogether, determining $3n-6$ modes of vibration, if the system is non-planar. The difference between these two numbers is the number of geometrical relations between the q_i. For there to be permanent stresses in the system this number must be positive, which implies $n>4$. However, if the equilibrium configuration is planar (or linear) the equations give only the *in*-plane (or *in*-line) vibrations. This is because the out-of-plane or out-of-line vibrations do not alter the distances between particles to the first order. In the absence of permanent stresses these vibrations would consequently have zero frequency ; but in the presence of stresses this is not so, as the following argument shows.

Suppose the equilibrium configuration is planar, and consider a distortion in which every particle moves a small distance perpendicular to the plane. The extensions $q_{\alpha\beta}$ vanish to the first order, and so the force on α reduces to

$$\sum_{\beta}^{\neq\alpha}\chi_{\alpha\beta}\,\boldsymbol{s}_{\alpha\beta},$$

where $\mathbf{s}_{\alpha\beta}$ is perpendicular to the equilibrium plane. Therefore

$$\lambda \mathbf{s}_{\alpha\gamma} = \frac{1}{m_\alpha} \sum_{\beta}^{\neq\alpha} \chi_{\alpha\beta}\, \mathbf{s}_{\alpha\beta} - \frac{1}{m_\gamma} \sum_{\varepsilon}^{\neq\gamma} \chi_{\gamma\varepsilon}\, \mathbf{s}_{\gamma\varepsilon} ;$$

taking the scalar product of both sides with $\mathbf{s}_{\alpha\gamma}/s_{\alpha\gamma}$, one obtains

$$\lambda s_{\alpha\gamma} = \frac{1}{m_\alpha} \sum_{\beta}^{\neq\alpha} \chi_{\alpha\beta}\, s_{\alpha\beta} + \frac{1}{m_\gamma} \sum_{\varepsilon}^{\neq\gamma} \chi_{\gamma}\, s_{\gamma\varepsilon}$$

which is a set of equations of the form

$$\sum_j \beta_{ij}\, s_j = \lambda s_i,$$

like the equations for the *in*-plane modes. A necessary condition for the out-of-plane frequencies to be finite is therefore that the permanent stresses shall not all vanish.

Angular Correlation in the Reaction ^{14}N (d, $\alpha\gamma\gamma$) ^{12}C

By J. Seed
Cavendish Laboratory, Cambridge

[Received November 8, 1954]

An alpha-particle group in the reaction ^{14}N (d, α) ^{12}C, corresponding to a level in carbon-12 at 7·5 Mev, was first reported by Holloway and Moore (1940); recently the existence of the alpha-group has been confirmed by the more accurate work of Dunbar *et al.* (1953), who assign an energy of 7·68 Mev to the ^{12}C level.

Evidence for the existence of this level has also accumulated from studies of the reaction ^{9}Be (α, n) ^{12}C. Using polonium alpha particles, Harries and Davies (1952) observed electron–positron pairs of total energy 7 Mev in a cloud chamber. No gamma rays of energy around 7 Mev have been observed, although Beghian *et al.* (1953) and Uebergang (1954) have reported 3 Mev gamma rays in coincidence with the 4·5 Mev gamma rays from the first excited state of carbon-12. The above evidence alone might lead one to conclude tentatively that the 7·68 Mev level has spin either zero or $\geqslant 4$.

In the present author's experiments, the angular correlation between 3 Mev and 4·5 Mev gamma rays has been measured in the reaction ^{14}N (d, $\alpha\gamma\gamma$) ^{12}C. Targets of tantalum nitride, made by heating tantalum metal in dry ammonia, were bombarded by a 1 μA beam of 630 kev deuterons. Gamma rays emitted by the target were detected by two sodium iodide scintillation counters, the angle between which could be varied in the plane perpendicular to the incident deuterons. The output of the one counter was fed into a single-channel kicksorter adjusted to select pulses corresponding to the energy of 4·5 Mev gamma rays less two annihilation quanta; the output of the other counter was fed through a

gate into a 60-channel pulse height analyser (Hutchinson and Scarrott (1951)). The gate operated when a fast coincidence from the two γ-counters was accompanied by a pulse from the output of the single-channel kicksorter. The coincidence resolving time was $3{\cdot}5\times10^{-8}$ sec using a circuit of the type described by Bell, Graham and Petch (1952).

In the experiments, coincidence γ-ray spectra were observed on the 60-channel pulse analyser for five different angles between the gamma-counters. At each angle, peaks at approximately 2·5 MeV and 2 MeV appeared, corresponding to the one-escape and two-escape annihilation peaks of a 3 MeV gamma ray in coincidence with the 4·5 MeV gamma ray. These peaks were superimposed on a background chiefly due to 1·5 MeV and 2 MeV gamma ray coincidences with the 5 MeV gamma rays in the reaction ^{14}N (d, p$\gamma\gamma$) ^{15}N. For the purposes of the correlation, the intensity of the 3 MeV gamma ray was estimated at each angle from the strength of the ' one-escape ' peak, monitored on the number of gating pulses applied to the 60-channel analyser. At all angles this number was much greater than the number of ' one-escape ' pulses, owing to the presence of the background coincidences from ^{14}N (d, p$\gamma\gamma$) ^{15}N.

In order to check that the 2·5 MeV peak arose solely from coincidences with the 4·5 MeV gamma ray, a second experiment was performed in which the single channel kicksorter in series with the one counter was adjusted to detect only gamma rays of energy greater than 4·5 MeV. No pulses at 2·5 MeV were observed in this experiment, although a small peak at 2 MeV was still evident, corresponding to the total capture energy of a 2 MeV gamma ray in ^{14}N (d, p$\gamma\gamma$) ^{15}N.

The results of the coincidence measurements (about 200 hours' running time) are shown in fig. 1. The full curve represents

$$I(\theta)=1-3\cos^2\theta+4\cos^4\theta$$

corrected for the finite solid angles of the counters, and it is seen that within the limits of accuracy of the experiment the curve is a reasonable fit to the experimental points. This curve would result if the 7·68 MeV level had spin and parity (0+), giving a pure $0+\rightarrow 2+\rightarrow 0+$ transition involving two electric quadrupole gamma rays. Odd parity for the level would give a similar result, however, and higher spins such as 3+ or $4\pm$ cannot be definitely ruled out.

It has been pointed out (Salpeter 1953, Öpik 1952) that, in stars that have largely exhausted their central hydrogen, oxygen and carbon can be produced via the reactions

$$^4\mathrm{He}+{}^4\mathrm{He}\rightarrow{}^8\mathrm{Be}$$
$$^8\mathrm{Be}+{}^4\mathrm{He}\rightarrow{}^{12}\mathrm{C}$$
$$^{12}\mathrm{C}+{}^4\mathrm{He}\rightarrow{}^{16}\mathrm{O}$$

Hoyle (1954) has concluded from the observed cosmic abundance ratios of the elements that the latter reaction should have a resonance at 0·31 MeV, corresponding to a level in carbon-12 at 7·68 MeV. If the level has *odd* parity with zero spin, however, the reaction ^{8}Be + ^{4}He $\rightarrow$ ^{12}C cannot take place.

Fig. 1

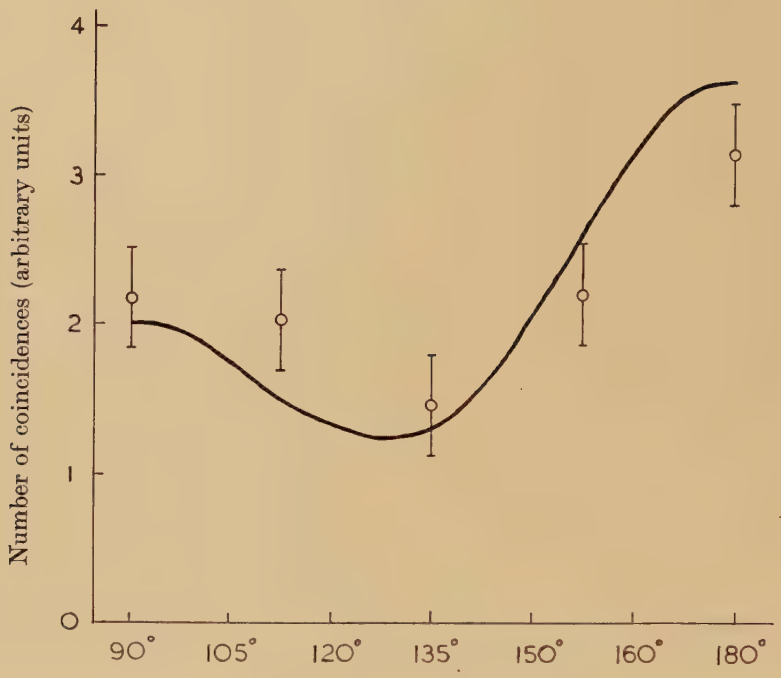

(γ, γ) angular correlation in the reaction $^{14}N(d, \alpha\gamma\gamma)^{12}C$.

I wish to thank Mr. S. D. Charter for much assistance with the operation of the High Tension Set. I am also indebted to the Department of Scientific and Industrial Research for a Senior Research Award.

References

Beghian, L. E., Halban, H. H., Husain, T., and Sanders, L. G., 1953, *Phys. Rev.*, **90**, 1129.

Bell, R. E., Graham, R. L., and Petch, H. E., 1952, *Canad. Journ. Phys.*, **30**, 35.

Dunbar, D. N. F., Pixley, R. E., Wenzel, W. A., and Whaling, W., 1953, *Phys. Rev.*, **92**, 649.

Harries, G., and Davies, W. T., 1952, *Proc. Phys. Soc.* A, **65**, 564.

Holloway, M. G., and Moore, B. L., 1940, *Phys. Rev.*, **58**, 847.

Hoyle, F., 1954, *Astrophys. Journ. Supp.*, **1**, 121.

Hutchinson, G. W., and Scarrott, G. G., 1951, *Phil. Mag.*, **42**, 792.

Öpic, E. J., 1952, *Proc. Roy. Irish Acad.* A, **54**, 49.

Salpeter, E. E., 1953, *Annual Review of Nuclear Science*, **2**, 41.

Uebergang, R. G., 1954, *Austral. Journ. Phys.*, **7**, 279.

An Estimate of the Mean Lifetime of the θ^0-particles

By D. I. Page*
The Physical Laboratories, The University, Manchester†

[Received October 15, 1954]

An estimate of the mean lifetime of the θ^0-particles has been made by a method similar to that previously used for the Λ^0-particles (Page 1954). From a sample of 357 V^0-decays obtained at the Jungfraujoch (3 580 m), 14 events were selected which satisfied the following criteria :

(*a*) The momentum of the positive secondary particle and the ionization density were consistent with the particle being a light meson and inconsistent with its being a proton,

(*b*) the dynamics of the decay were consistent with the scheme (Thompson 1954)

$$\theta^0 \rightarrow \pi^+ + \pi^- + 214 \text{ Mev.}$$

It is estimated that less than 10% of these events are due to the decay of particles other than θ^0-particles (Discussion at the Bagnères de Bigorre Conference, 1953). In all cases the potential path length of each decaying particle was limited by the length of the positive secondary track which must be allowed for the momentum of the particle to be determined. This in turn was limited by the maximum detectable momentum measureable in the chamber.

An analysis of the actual and potential times of flight of the particles (Bartlett 1953) gives the lifetime as

$$\tau = (0{\cdot}7^{+0{\cdot}3}_{-0{\cdot}2}) \times 10^{-10} \text{ sec.}$$

Combining this value with all the previously published results (Gayther 1954) the weighted mean value for the lifetime becomes

$$\tau = (1{\cdot}5^{+0.4}_{-0.3}) \times 10^{-10} \text{ sec.}$$

I am grateful to the administration of the Hochalpine Forschungsstation, Jungfraujoch, for providing research facilities at the Jungfraujoch and to the Department of Scientific and Industrial Research for a maintenance grant.

References

Bartlett, M. S., 1953, *Phil. Mag.*, **44**, 249.
Gaythér, D. B., 1954, *Phil. Mag.*, **45**, 570.
Page, D. I., 1954, *Phil. Mag.*, **45**, 863.
Thompson, R. W., 1954, *Bull. Am. Phys. Soc.*, **29**, 73.

---

* Communicated by G. D. Rochester.
† Now at the Atomic Energy Research Establishment, Harwell.

Reversible Generation of Temperature Waves ('Second Sound') in Liquid Helium II

By N. Kurti and J. McIntosh
Clarendon Laboratory, Oxford

[Received December 10, 1954]

The existence of temperature waves in liquid helium II was first postulated by Tisza (1938). Landau (1941), on the basis of his quantum hydrodynamical treatment of liquid helium, proposed the existence of a phenomenon which he called the 'second sound'. An unsuccessful attempt to detect this effect by an acoustic method, namely by the beats in standing waves radiated by an oscillating piezo electric quartz crystal was made by Shalnikov and Sokolov (quoted by Peshkov 1947). An analysis of this negative result led Lifshitz (1944) to predict the essentially thermal nature of 'second sound'. Peshkov (1944), using thermal generation succeeded in demonstrating the existence of 'second sound' which is identical with the temperature waves proposed by Tisza. Since then many experiments have been done on these temperature waves, but with the exception of Peshkov's (1948) method of 'filtration of the superfluid' they appear to have been always generated by irreversible Joule heating. In this method there is a net heat flow and heat dissipation in the liquid helium and this might affect the results especially at the lowest temperatures.

The temperature oscillations of a suitable paramagnetic salt placed in an alternating magnetic field provide a method 'par excellence' for producing second sound reversibly.* This method should compare favourably with the filtration of the superfluid method which becomes ineffective at low temperatures. We have therefore carried out some experiments between 1·3°K and the λ-point in order to prove the feasibility of generating second sound by means of a paramagnetic salt.

Standing waves of second sound were produced in a resonant cavity of 2 cm diameter and 2·3 cm length. A carbon resistance thermometer which served as detector formed one end of the cavity while the other end was formed by the smooth end-face of a cylindrical pill of compressed ferric ammonium alum powder. An alternating magnetizing field of up to 120 gauss at frequencies between 150 and 1200 cycles per second was produced by a small external coil cooled in liquid hydrogen. The unwanted signal produced in the thermometer circuit by the stray field of this coil was compensated by injecting in the thermometer circuit a voltage of suitable phase and amplitude. To obtain maximum sensitivity and to eliminate the effect of any residual pickup, the output of the

* This method was probably first considered in the autumn of 1938 when possible experiments to demonstrate his temperature waves were discussed with Professor Tisza.

amplifier, normally displayed on a cathode ray oscilloscope, could be coupled to a phase sensitive detector and the amplitude of the signal measured on a meter.

The results may be summarized as follows. Standing waves were observed with the fundamental frequency and up to the third harmonic. By measuring the resonance frequency at selected temperatures the temperature dependence of the velocity of ' second sound ' was also determined. The values found agreed within the limit of experimental accuracy with those of previous authors. The temperature excursions as measured on the carbon resistance thermometer were only of the order of $10^{-4}°$, although the temperature amplitudes of the spin system of the paramagnetic salt were of the order of $10^{-2}°$. This is due partly to the effect of the spin lattice relaxation time but chiefly to the relatively large specific heat of the liquid helium in this temperature range. It is worth pointing out that with a Joule heater a power input of the order of 10^{-2} watts would be required to obtain temperature amplitudes of $10^{-4}°$ in liquid helium.

Experiments were also carried out in a superimposed constant magnetic field of 600 gauss so as to increase the temperature amplitude for a given a.c. field. This method has, however, the slight disadvantage that the frequency of the second sound is now the same as that of the a.c. field which makes it more difficult to distinguish spurious effects from genuine resonance. With no superimposed steady field the second sound frequency is twice that of the a.c. field frequency.

Our experiments have shown that the efficacy of this method of generating ' second sound ' increases with decreasing temperature. In other words, any decrease in amplitude due to increasing spin lattice relaxation time is outweighed by the decrease of specific heat of liquid helium. Moreover it should be possible to find substances with shorter spin lattice relaxation times than that of ferric ammonium alum. It seems therefore that this method will be suitable for the temperature range below 1°K. Experiments with only very small heat dissipation might well help towards a better understanding of the exact nature of ' second sound ' in this temperature range. The paramagnetic method could also be used for the pulse technique and it will thus be possible to generate ' cold ' pulses as well as ' heat ' pulses.

This work was done during J. McIntosh's tenure of a Berry Scholarship of the University of St. Andrews for which grateful acknowledgement is made.

References

Landau, L., 1941, *J. Phys., U.S.S.R.*, **5**, 71.
Lifshitz, E., 1944, *J. Phys., U.S.S.R.*, **8**, 110.
Peshkov, V. P., 1944, *J. Phys., U.S.S.R.*, **8**, 381 ; 1947, *Rep. Intern. Conf. Cambridge, Phys. Soc.*, Vol. II, 19 ; 1948, *J. Exp. Theor. Phys., U.S.S.R.*, **18**, 867.
Tisza, L., 1938, *Comptes Rendus, Paris*, **207**, 1035, 1186.

Spin Orbit Coupling and the Mesonic Lamb Shift

By E. W. Laing
Department of Natural Philosophy, University of Glasgow

[Received November 18, 1954]

It has recently been shown by Chisholm and Touschek (1953) that the self-energy corrections for a nucleon moving in a scalar potential well $U(r)$ lead to a strong spin orbit coupling for pseudoscalar mesons with pseudoscalar coupling. Assuming charge symmetric meson theory, these authors obtain a spin orbit coupling

$$\Delta U^{S.O.}=3(g/4\pi M)^2 \frac{1}{r}\frac{dU}{dr}\,\boldsymbol{\sigma}.\mathbf{L},\quad \mathbf{L}=\mathbf{r}\times\mathbf{p}. \qquad \ldots \quad (1)$$

This is of the right order of magnitude, but of the wrong sign, for application to the nuclear shell model.

It is the purpose of this note to show that a more detailed investigation of the total matrix element reveals contributions to the spin orbit coupling from the small components of the initial and final spinor wave functions. These contributions are such that they reverse the sign of the spin orbit coupling, while leaving its magnitude unchanged.

We shall employ the usual Feynman–Dyson prescription for evaluating the S-matrix element $\Lambda(p_2, p_1)$ in momentum space. The only second order graph which contributes is shown in the figure.

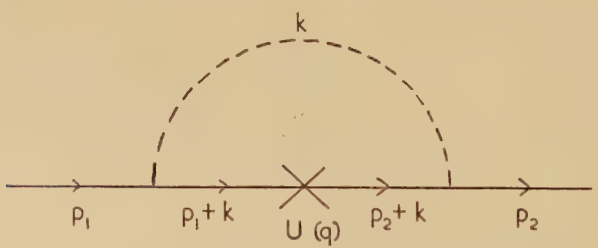

This leads to the following expression for the matrix element

$$\Lambda(p_2, p_1)=\frac{3ig^2}{(2\pi)^4}\int d^4k\,\frac{\overline{\psi}(p_2)\gamma_5[i\gamma.(p_2+k)-M]U(q)[i\gamma.(p_1+k)-M]\gamma_5\psi(p_1)}{(k^2+\mu^2)[(p_2+k)^2+M^2][(p_1+k)^2+M^2]} \qquad \ldots \quad (2)$$

where

$$U(r)=\int d^3q\, e^{i\mathbf{q}.\mathbf{r}}\, U(q).$$

$\Lambda(p_2, p_1)$ is logarithmically divergent. By the usual renormalization procedure, $\Lambda_0=\Lambda(p_0, p_0)$ is subtracted from $\Lambda(p_2, p_1)$. (p_0 in Λ_0 is a free particle momentum.)

The finite part $\Lambda_c = \Lambda - \Lambda_0$ contains four terms which contribute to the spin orbit coupling, namely :

$$\left.\begin{aligned}
\Lambda_1 &= A_1\,\overline{\psi}(p_2)\,\gamma_i\gamma_j p_{2i} p_{1j}\,\psi(p_1)\,U(q),\\
\Lambda_2 &= A_2\,\overline{\psi}(p_2)\,\gamma_4\gamma_i\,P_{2i}\,\psi(p_1)\,U(q),\\
\Lambda_3 &= A_3\,\overline{\psi}(p_2)\,\gamma_i P_{3i}\,\psi(p_1)\,U(q),\\
\Lambda_4 &= A_4\,\overline{\psi}(p_2)\,\psi(p_1)\,U(q),
\end{aligned}\right\}, \quad . \quad . \quad . \quad (3)$$

where $i, j = 1, 2, 3$ and summation is implied. Here P_{ki} is a linear combination of p_{1i} and p_{2i}, say $a_k p_{1i} + b_k p_{2i}$, $k = 2, 3$. The constants $A_1, A_2, A_3, A_4, a_k, b_k$ are easily obtained by standard methods.

The $\Lambda_\mu (\mu = 1, 2, 3, 4)$ contain the following terms, Λ_μ', on reduction to two-component spinors χ in the non-relativistic limit,

$$\left.\begin{aligned}
\Lambda_1' &= iA_1\chi^+\boldsymbol{\sigma} \cdot (\mathbf{p}_2 \times \mathbf{p}_1)\,U(q)\chi\\
&= iA_1 S, \text{ say}\\
\Lambda_2' &= (b_2 - a_2)\,A_2 S/2M,\\
\Lambda_3' &= (a_3 + b_3)\,A_3 S/2M,\\
\Lambda_4' &= -i/(2M)^2\,A_4 S,
\end{aligned}\right\} \quad . \quad . \quad . \quad . \quad . \quad (4)$$

$$iS = \frac{1}{r}\frac{dU}{dr}\,\boldsymbol{\sigma} \cdot \mathbf{L}, \text{ in configuration space.}$$

The results obtained are as follows :—

$$\left.\begin{aligned}
\Lambda_1' &= 3(g/4\pi M)^2\,\frac{1}{r}\frac{dU}{dr}\,\boldsymbol{\sigma} \cdot \mathbf{L},\\
\Lambda_2' &= \Lambda_3' = -\Lambda_1'.
\end{aligned}\right\} \quad . \quad . \quad . \quad . \quad . \quad . \quad (5)$$

Λ_4' is negligible, since, to the order considered, calculations show that the static radiative correction amounts to only 6% of $U(r)$.

Thus, the total contribution to the spin orbit coupling is

$$-3(g/4\pi M)^2\,\frac{1}{r}\frac{dU}{dr}\,\boldsymbol{\sigma} \cdot \mathbf{L}. \quad . \quad . \quad . \quad . \quad . \quad . \quad (6)$$

This is just a change of sign from the previous work by Chisholm and Touschek, referred to above, which reported the contribution of the term Λ_1' alone.

The results obtained are encouraging insofar as they afford a possible field theoretical picture for the nuclear shell model. One must bear in mind, however, that a systematic search for spin orbit coupling from all possible sources should be made and that only the total contribution should be compared with the experimentally observed spin orbit coupling. For example, Klein (1953) obtains a spin orbit coupling of the wrong sign for the shell model as a velocity dependent correction to fourth order two-body forces. Further work is being done by the author along the lines indicated above.

In conclusion the author wishes to extend grateful thanks to Professor J. C. Gunn and Dr. J. S. R. Chisholm, under whose guidance this work was performed.

References

Chisholm, J. S. R., and Touschek, B. F. X., 1953, *Phys. Rev.*, **90**, 763.
Klein, A., 1953, *Phys. Rev.*, **90**, 1101.

ERRATA

On the Evaluation of Characteristic Temperatures for Cubic Crystals, by A. B. Bhatia and G. E. Tauber, 1954, *Phil. Mag.*, **45**, 1211.

(1) In eqn. (3) read $4\pi\alpha_0 K_0$ instead of $4\pi\alpha_0$.

(2) Multiply the right-hand side of (5) by $(\rho)^{3/2}$, where ρ is the density of the substance. (The Θ-values given in the table were, however, calculated with the correct formula.)

XV. REVIEWS OF BOOKS

Atlas of Typical Expansion Chamber Photographs. By W. Gentner, H. Maier-Leibnitz and W. Bothe. [Pp. 199.] (Pergamon Press Limited.) Price £5 5*s*. 0*d*.

This volume forms a completely new and up-to-date version of the 'Atlas typischer Nebelkammerbilder' published by the same authors in 1940. An impressive selection of photographs, many as yet unpublished, illustrates the numerous contributions made by cloud chamber observations to the field of nuclear physics. The subjects covered include natural and artificial radioactivity, nuclear transmutations, and the properties of the various types of fundamental particles and radiations. The atlas is completed by a small but representative collection of cosmic-ray events—these having already been comprehensively surveyed in 'Cloud Chamber Photographs of the Cosmic Radiation' by Rochester and Wilson.

The quality of reproduction of the photographs is excellent. They are adequately explained by legends in English, French and German, and supplemented by some thirty useful diagrams and tables. Not only will this volume be invaluable to the student of nuclear physics, but it will appeal also to the non-specialist, for the photographs display in a straight-forward and vivid manner the fundamental processes resulting from interactions in the atomic nucleus.

D. H. P.

Rocket Exploration of the Upper Atmosphere. Edited by Dr. R. L. F. Boyd and Dr. M. J. Seaton in consultation with Prof. H. S. W. Massey, F.R.S. (London: Pergamon Press Ltd.) [Pp. viii+376.] Price 75*s*.

Workers in America have opened up a new method of attack on the problems of upper atmospheric physics by the use of rockets, of the type devised by the Germans during the war of 1939–45. The papers presented in this volume constitute a good survey of the results obtained up to August 1953. The greatest height reached seems to have been about 400 km, while a height of 150 km was reached several times.

There is always some doubt about deductions made in a very tenuous atmosphere from a rocket which inevitably carries some gas with it, and which is moving at a velocity comparable with the gas kinetic velocity of the molecules, and some of the deductions are still open to doubt. In spite of that doubt the results have already made a considerable difference to the theory of the ionosphere. The most direct measurements are those of the intensity of solar x-radiation at different heights. Less direct, but very important, are those in which the density and temperature of the atmosphere are measured. The results of these experiments have already revolutionized our thinking about the radiations responsible for ionizing the E layer, and about the air density in the F region.

In studies of the composition of the upper atmosphere the techniques have included direct sampling, and the use of a mass spectrograph in the rocket. Direct measurements of electron and ion density in the ionosphere have been attempted. All these experiments are very difficult and we cannot yet be certain that the results are unambiguous.

In one of the most direct, and important, experiments the earth's magnetic field was measured at different heights and the results seem to show that the currents of the 'atmospheric dynamo' theory of geomagnetism flow at a height of about 90 km.

This book will be of great value to all students of the upper atmosphere, particularly because much of the American work has up to now only appeared in progress reports and has not found its way into acknowledged literature.

J. A. R.

Quantum Mechanics. By F. Mandl. (Butterworths Scientific Publications.) [Pp. 232.] Price 35*s*.

Non-relativistic quantum mechanics seems here to stay, and most physicists must understand it in the same way that engineers understand dynamics; that is, they must know how to calculate with it to solve specific problems. Dr. Mandl's treatment is in this spirit. All the usual topics are included (except field theory), but only up to the degree of complexity necessary to demonstrate an important principle or technique: the reader can work the heavier algebra for himself, in numerous examples with detailed hints. The author writes: "Apart from classical physics, calculus, and vector analysis, the reader is assumed to be familiar with the qualitative concepts of quantum theory, such as the wave nature of matter, and their experimental basis". The special virtue of the book is that without attempting real mathematical and metaphysical rigour (although there is an illuminating note on the Dirac δ function), it sets forth clearly and concisely the various viewpoints, formulations, and notations of such men as Schrödinger, Heisenberg, von Neumann and Dirac in a logical whole, so that the student will have knowledge and experience of all the different techniques when he comes to read and to write original research papers. This eclectic, up-to-date account (it even shows how group theory stems naturally from atomic physics) should make a most useful textbook, suitable for good students in their third year and for all post-graduate students, whether they specialize on experimental or theoretical physics.

Transactions of Symposia on Applied Mathematics, Vol. I. [Pp. 243.] (Interscience Publishers.) Price $5.

This volume contains a collection of papers delivered at a symposium on fluid mechanics and computing held at New York University in April 1953 and sponsored by the American Mathematical Society and the U.S. Army Office of Ordnance Research.

In all there are 14 papers by various well-known scientists. They consist of a paper on the theory of homogeneous turbulence, by G. Birkhoff, a critical discussion of approximation techniques used in boundary layer problems, by G. F. Carrier, four papers on computational methods by J. H. Giese, M. Lotkin, P. D. Lax and L. H. Thomas, and eight papers on compressible flow by M. J. Lighthill, G. S. S. Ludford and M. H. Martin, L. Bers, A. Weinstein, P. Germain, R. von Mises, G. E. Hudson and H. Schardin.

Of particular interest are the four papers on the problem of transonic flow, which give a good picture of the present state of knowledge on this difficult problem, and contain some interesting speculations. W. C.

BOOK NOTICES

Probability and Information Theory with Applications to Radar. By P. M. Woodward. (London: Pergamon Press Ltd.) [Pp. 128.] Price 21*s*.

The Atmospheric Lunar Tides. By Ryukicei Sawada. (New York: University Press.) Price $1.50.

British Journal for the Philosophy of Science. Vol. V, No. 19. (Edinburgh: Thomas Nelson and Sons Ltd.) Price 7*s*. 6*d*.

Nuclear Species. By H. E. Huntley. (London: Macmillan & Co. Ltd.) [Pp. 193.] Price 21*s*.

[*The Editors do not hold themselves responsible for the views expressed by their correspondents.*]